

**Multisensory Smartphone Applications in Vibration-Based Structural
Health Monitoring**

Ekin Ozer

Submitted in partial fulfillment of the
requirements for the degree
of Doctor of Philosophy
in the Graduate School of Arts and Sciences

COLUMBIA UNIVERSITY

2016

©2016
Ekin Ozer
All rights reserved

ABSTRACT

Multisensory Smartphone Applications in Vibration-Based Structural Health Monitoring

Ekin Ozer

Advances in sensor technology and computer science in the last three decades have boosted the importance of system identification and vibration-based structural health monitoring (SHM) in civil infrastructure safety and integrity assessment. On the other hand, practical and financial issues in system instrumentation, maintenance, and operation have remained as fundamental problems obstructing the widespread use of SHM applications. For this reason, to reduce system costs and improve practicality as well as sustainability, researchers have been working on emerging methods such as wireless, distributed, mobile, remote, smart, multisensory, and heterogeneous sensing systems.

Smartphones with built-in batteries, processor units, and a variety of sensors, have stood as a promising hardware and software environment that can be used as SHM components. Communication capabilities with the web, enable them to compose a smart and participatory sensor network of outnumbered individuals. Besides, crowdsourcing power offered by citizens, sets a decentralized and self-governing SHM framework which can even be pertained by very limited equipment and labor resources.

Yet, citizen engagement in an SHM framework brings numerous challenges as well as opportunities. In a citizen-induced SHM scenario, the system administrators have limited or no control over the sensor instrumentation and the operation schedule, and the acquired data is subjected change depending on the measurement conditions. The citizen-induced errors can stem from spatial, temporal, and directional uncertainties since the sensor configuration relies on smartphone users' decisions and actions. Moreover, the sensor-structure coupling may be unavailable where the smartphone is carried by the user, and as a consequence, the vibration features measured by smartphones can be modified due to the human biomechanical system. In addition, in contrast with the conventional

high fidelity sensors, smartphone sensors are of limited quality and are subjected to high noise levels.

This dissertation utilizes multisensory smartphone features to solve citizen-induced uncertainties and develops a smartphone-based SHM methodology which enables a cyber-physical system through mobile crowdsourcing. Using smartphone computational and communicational power, combined with a variety of embedded sensors such as accelerometer, gyroscope, magnetometer and camera, spatiotemporal and biomechanical citizen-induced uncertainties can be eliminated from the crowdsourced smartphone data, and eventually, structural vibrations collected from numerous buildings and bridges can be collected on a single cloud server. Therefore, unlike the conventional platforms designed and implemented for a particular structure, citizen-engaged and smartphone-based SHM can serve as intelligent, scalable, fully autonomous, cost-free, and durable cyber-physical systems drastically changing the forthcoming trends in civil infrastructure monitoring.

In this dissertation, iOS is used as the application development platform to produce a smartphone-based SHM prototype, namely Citizen Sensors for SHM. In addition, a web-based software is developed and cloud services are implemented to connect individual smartphones to an administrator base and automate data submission and processing procedure accordingly. Finally, solutions to citizen-induced problems are provided through numerous laboratory and field test applications to prove the feasibility of smartphone-based SHM with real life examples. Through collaborative use of the software, principles and methodologies presented in this dissertation, smartphones can be the core component of futuristic smart, resilient, and sustainable city and infrastructure systems. And this study lays down an innovative and integrated foundation empowering citizens to achieve these goals.

Table of Contents

List of Figures	iv
List of Tables	vii
Acknowledgments.....	viii
Chapter 1: Introduction.....	1
1.1 Dissertation Outline	3
Chapter 2: Smartphone Accelerometer Tests	4
2.1 Introduction	4
2.2 Smartphone accelerometer properties	6
2.3 Small-scale shaking table tests	7
2.4 Large-scale shaking table tests	9
2.4.1 Operational vibration tests	10
2.4.2 White noise excitation tests	12
2.4.3 Earthquake excitation tests	13
2.4.4 Comparison of identified natural frequencies.....	15
2.5 Field tests of a bridge	16
2.5.1 Ambient vibration tests.....	17
2.5.2 Random dynamic tests	18
2.5.3 Synchronized dynamic tests.....	19
2.5.4 Comparison of identified natural frequencies.....	21
2.6 Conclusions	21
Chapter 3: Crowdsourcing Platform Development.....	24
3.1 Introduction	24
3.2 Multilayered computer platform	26
3.2.1 User-side sensing and acquisition.....	27
3.2.2 Server-side processing and database.....	29

3.3	Crowdsourcing	31
3.3.1	Sensors	34
3.3.2	Data wisdom, contribution quality, web extension.....	34
3.3.3	Human skill and incentives.....	34
3.3.4	Involvement	35
3.4	Pedestrian link bridge case study	36
3.4.1	Measurement, data processing, modal identification.....	37
3.4.2	Uncertainties associated with citizen participation.....	39
3.5	Conclusions	49
Chapter 4: Citizen-Induced Uncertainties.....		52
4.1	Orientation effects	52
4.1.1	Introduction.....	52
4.1.2	SHM-focused smartphone features.....	54
4.1.2.1	Smartphone sensor components.....	55
4.1.2.2	iOS and core frameworks.....	57
4.1.2.3	Data heterogeneity	60
4.1.3	Coordinate system transformation	62
4.1.3.1	Coordinate system transformation fundamentals.....	64
4.1.3.2	Coordinate systems in smartphone-based SHM	66
4.1.4	On campus applications	70
4.1.4.1	Sampling rate and tilt corrections of a 2DOF model	71
4.1.4.2	Pedestrian bridge example	74
4.1.5	Transformation procedure on landmark bridges.....	79
4.1.6	Conclusions.....	82
4.2	Spatiotemporal effects	84
4.2.1	Introduction.....	84
4.2.2	Sensor position and node identification.....	86
4.2.3	Energy normalization.....	89
4.2.4	Multichannel data synthesis and modal parameters.....	91
4.2.5	Field tests	92

4.2.6	Results and discussion	98
4.2.7	Conclusions.....	101
4.3	Human biomechanical effects	103
4.3.1	Introduction.....	103
4.3.2	Methodology and framework.....	105
4.3.2.1	Biomechanical models	106
4.3.2.2	Walk-induced vibrations.....	108
4.3.2.3	Transfer functions	109
4.3.2.4	Field tests	114
4.3.3	Results and discussion	117
4.3.3.1	Estimating pedestrian forces	118
4.3.3.2	Isolating biomechanical effects and modal identification	120
4.3.4	Conclusions.....	123
Chapter 5: Integration with SHM and Reliability.....		126
5.1	Introduction	126
5.2	Materials and methods.....	128
5.2.1	Testbed structure.....	129
5.2.2	Cyber-physical systems	130
5.2.3	Finite element model updating.....	132
5.2.4	Structural reliability estimation.....	133
5.3	Results and discussion.....	134
5.3.1	Objective function minimization	134
5.3.2	Simulating probabilistic seismic response	138
5.4	Conclusions	141
Chapter 6: Conclusions and Future Work.....		143
6.1	Summary	143
6.2	Main contributions and concluding remarks	145
6.3	Future research directions	147
Bibliography		151

List of Figures

Figure 2.1: Sine wave shaking table test setup	8
Figure 2.2: Sine wave time histories of different frequencies	8
Figure 2.3: Masonry column model and shaking table setup	10
Figure 2.4: Time history of impact and operational vibration response	11
Figure 2.5: Spectral density of impact and operational vibration response	11
Figure 2.6: Time history of white noise excitation response	12
Figure 2.7: Spectral density of white noise excitation response	12
Figure 2.8: Time history of targeted and achieved earthquake input ground motion	14
Figure 2.9: Time history of earthquake response.....	14
Figure 2.10: Spectral density of earthquake excitation measurements	15
Figure 2.11: The pedestrian bridge in Princeton, NJ	17
Figure 2.12: Time history of ambient vibration response	18
Figure 2.13: Spectral density of ambient vibration response.....	18
Figure 2.14: Time history of random dynamic tests	19
Figure 2.15: Spectral density of random dynamic tests	19
Figure 2.16: Time history of synchronized dynamic tests	20
Figure 2.17: Spectral density of synchronized dynamic tests.....	20
Figure 3.1: Integration scheme of system platforms.....	27
Figure 3.2: User login, recording, and submission screenshots.....	28
Figure 3.3: Server-side digital signal processing operations	29
Figure 3.4: Screenshot from the web interface showing the SHM results page	31
Figure 3.5: Bridge views, dimensions, and sensor layout.....	37
Figure 3.6: Modal frequencies and mode shapes identified by reference accelerometers.....	38

Figure 3.7: Time histories and Fourier spectra samples from Test 3 and Test 6.....	42
Figure 3.8: Fourier spectra from the average of 40 samples for Test 1-6.....	43
Figure 3.9: Identified frequencies obtained from different samples.....	44
Figure 3.10: Energies obtained from different samples.....	46
Figure 3.11: Modal identification results from Test 1-6 and crowdsourcing.....	47
Figure 3.12: Time histories and Fourier spectra samples during pedestrian pass.....	49
Figure 4.1: Shaking table test setup and different smartphone orientations.....	59
Figure 4.2: Multisensorial time histories of a distorted smartphone.....	59
Figure 4.3: Logic diagram showing sensor data usage in iOS frameworks.....	61
Figure 4.4: Relation between initial and final axes, attitude data, and device orientation.....	64
Figure 4.5: Local to global measurement coordinate system scales.....	67
Figure 4.6: Block diagram for overall coordinate system transformation.....	69
Figure 4.7: Setup, drawings, and rotationally distorted device positions.....	71
Figure 4.8: Rotationally distorted and corrected accelerometer data.....	72
Figure 4.9: Structural and sensorial coordinate systems of Test 1-4.....	75
Figure 4.10: Reference and smartphone sensor configuration and application interface.....	75
Figure 4.11: Coordinate estimations by smartphone geolocation services.....	76
Figure 4.12: Time histories of Test 1-4.....	77
Figure 4.13: Spectral densities of Test 1-4.....	77
Figure 4.14: Coordinate systems and aerial views of Golden Gate Bridge.....	80
Figure 4.15: Time histories from Golden Gate Bridge.....	81
Figure 4.16: Fourier spectra from Golden Gate Bridge.....	81
Figure 4.17: Procedural framework.....	92
Figure 4.18: Satellite, outer, inner views of Mudd-Schapiro Bridge.....	93
Figure 4.19: Identified modal frequencies and mode shapes from FDD.....	93
Figure 4.20: Node configuration of Mudd-Schapiro Bridge.....	94
Figure 4.21: Node identification using geolocation estimations.....	96
Figure 4.22: QR code instrumentation from 1 st to 8 th node.....	96
Figure 4.23: Test timeline.....	97

Figure 4.24: STFTs obtained from Test 1-8	99
Figure 4.25: Sample energies from Test 1-8.....	99
Figure 4.26: Averaged spectra from Test 1-8	99
Figure 4.27: Envelope spectra from Test 1-8.....	100
Figure 4.28: Identified mode shapes	101
Figure 4.29: Exemplary citizen postures and activities	106
Figure 4.30: Human biomechanical models of different detailing	107
Figure 4.31: Walk-induced pedestrian force models	109
Figure 4.32: Transfer functions based on biomechanical models of different subjects.....	111
Figure 4.33: Signal flowchart through the vibration source and the sensor data.....	112
Figure 4.34: Bridge and pedestrian instrumentation.....	114
Figure 4.35: Time histories and Fourier spectra for Case 1-8	118
Figure 4.36: Walk-induced forces identified by pedestrian’s smartphone	119
Figure 4.37: Scheme for isolation of biomechanical features through transfer functions	121
Figure 4.38: Biomechanical effect isolation process for phone in pedestrian’s bag	122
Figure 4.39: Biomechanical effect isolation process for phone in pedestrian’s pocket.....	122
Figure 4.40: Fourier spectra for output-only cases (no pedestrian interference).....	122
Figure 5.1: Cyber-physical processes of CS4SHM system	129
Figure 5.2: Mudd-Shapiro Link Bridge	129
Figure 5.3: Conceptual CPS scheme for smartphone-based SHM	131
Figure 5.4: Exemplary crowdsourced time histories and Fourier spectra	131
Figure 5.5: Finite element modeling uncertainties	132
Figure 5.6: Frequency error surfaces for fixed-fixed, fixed-pinned, fixed-roller BCs	136
Figure 5.7: Updated modal parameters for fixed-fixed, fixed-pinned, fixed-roller BCs	137
Figure 5.8: Exemplary input ground motion and simulated structural response	139
Figure 5.9: Peak responses indexed according to the strong motion parameters	139
Figure 5.10: Maximum displacement demands based on Northridge Earthquake records ..	140

List of Tables

Table 2.1: Reference and smartphone sensor properties	7
Table 2.2: Peak horizontal acceleration error	9
Table 2.3: Comparison of natural frequencies	16
Table 2.4: Comparison of natural frequencies	21
Table 3.1: Mobile crowdsourcing taxonomy	36
Table 3.2: Field measurement with different sensor locations and coupling conditions	40
Table 3.3: Identified modal frequencies	45
Table 3.4: Statistical values of peak vertical acceleration and energy.....	48
Table 4.1: Accelerometer, gyroscope, and magnetometer properties.....	57
Table 4.2: Heterogeneous smartphone sensor features.....	62
Table 4.3: Dominant modal parameters and accelerations in x-direction	73
Table 4.4: Pedestrian bridge test properties and smartphone configurations	74
Table 4.5: Test 3 dominant modal parameters and bridge accelerations in z-direction	78
Table 4.6: Test 4 dominant modal parameters and bridge accelerations in z-direction	79
Table 4.7: Identification results of Golden Gate Bridge.....	82
Table 4.8: Relationship between the node identities and the node locations.....	94
Table 4.9: Sources of uncertainties in pedestrian-extracted structural vibration data	115
Table 4.10: Test descriptions	116
Table 5.1: Optimal models for different BCs	137

Acknowledgments

First of all, I would like to express my sincere thanks to Professor Maria Q. Feng for her long-lasting support and advisory during my PhD studies. Thanks to her valuable guidance, I was able to accomplish my research goals and complete this dissertation with joy and excitement. It was a wonderful experience and a great honor to work under her supervision which I am truly thankful for.

I also would like to acknowledge my dissertation committee members Professor George Deodatis, Professor Raimondo Betti, Professor Sharon Di, and Professor John Wright, for their outstanding contribution to my dissertation and taking part in my defense, as well as everything they have taught me throughout my studies.

I would like to thank Liming Li, Eric Sporer, Adrian Brügger, Travis Simmons and all other researchers in Carleton Laboratory for their valuable collaboration throughout my experimental studies. I also would like to thank Michael Smith, Scott Kelly, Elaine Macdonald, and Nathalie Rodriguez for their diligent help and support, and my colleagues Alessandro Sabato, Andrea Zampieri, Dongming Feng, Longxi Luo, Oscar Ortiz, and Samuel Valdez for their kind cooperation. Besides, I would like to thank Professor William Hart and Professor Julius Chang for being tremendously supportive throughout my teaching duties. Other than these, I appreciate Professor Andrew Smyth's, Professor Shiho Kawashima's, Professor Ali Ashrafi's, and Professor Richard Longman's contributions to my coursework. What is more, I would like to acknowledge all Columbia staff including Yaniv Phillips, Ngozi Okezie, Colleen Eng, and Anissa Timothy-Caesar.

Friends I would like to thank is a long list including Undrakh Sisunton, Maura Torres, Shengduo Du, Priyadarshika Vidayakumar, Qi Sun, Debapriya Das, Olga Brudastova, Wenting Luo, Adele Scampoli, Siyang Pan, Ziyun Xiao, Mostafa Mobasher, Bethany Doran, Tze Phei Poh, Yuwei Zhang, Christine Tse, Thanh Xuan, Zhuoshi Xie, Djordje Vuckovic, Feifei Kong, and all

Moy Yee members. As time goes on, I will personally keep thanking to those whom I haphazardly skipped to acknowledge here.

Finally and the foremost, I would like to thank my sister, my father, and my mother, Ürün, Şeref, and Emel Özer, and my grandparents, Ali and Mukaddes Bal, Cemal and Aliye Özer, for everything they have brought into my life from the very first day. Together they portrayed the entire past, present, and future with thousands of beautiful memories.

This dissertation is dedicated

to my family

Chapter 1

Introduction

This chapter presents an introduction to the vibration-based SHM, emerging SHM technologies, smartphone potential, and the objective of this study along with the outline of the dissertation.

Industrialization and urbanization in the last two centuries have tremendously increased the building stocks in cities. Aging, fatigue, natural and man-made disasters have resulted in structural deterioration, damage, and sometimes failure in the long run. Unpredictability and uncertainty in structural demand as well as capacity, in most cases, forced engineering design to take the reasonable risk and compromise between safety and economy. For these reasons, assessment of serviceability and safety measures has become of utmost importance to use these building stocks efficiently. Performance evaluation of existing structures via static and dynamic analysis methods has appeared as a pre-event prediction and post-event assessment methodology in structural engineering codes and regulations. However, these methodologies solely rely on analytical models but not experimental data representing the actual characteristics of the structure. At this stage, adopting the state-of-the-art theoretical models as well as field test results from sensor signals, vibration-based SHM have risen as an indispensable practice that can combine the analytical and the experimental information.

Advances in sensor technology and computational power have led vibration-based SHM to become one of the hot topics in civil infrastructure engineering in the last few decades. Adopting system identification methods on a comparative basis, one can monitor changes in structural vibration characteristics to evaluate structural safety and integrity of buildings, bridges, dams, etc. Other than that, updating finite element models with monitoring results offers a suitable framework to verify, validate, and calibrate models with real world data and increase accuracy in analyses. As

the digital and physical representations of civil infrastructure get more and more interconnected; the decision-making processes regarding existing civil infrastructure investments can be pursued in a more intelligent way. Continuation of these advancements leads to an upcoming technology revolution, where the knowledge, gathered from automated processors and connected sensors, is used to construct cyber-physical civil infrastructure systems.

Despite all of the aforementioned advantages of vibration-based SHM, in practice; instrumentation, operation, and maintenance of monitoring systems require substantial time, cost, and labor. Sensor and cable installation on a civil infrastructure takes long durations, and sometimes can be difficult, dangerous, or even inapplicable. To tackle with these practical problems, researchers have been working on emerging methodologies such as non-contact vision sensing, laser interferometer, GPS displacement, and more. Likewise, for the cases where the sensor-structure integration is essential; e.g. accelerometers, strain gauges, and tiltmeters; novel technologies such as mobile, wireless, and smart sensor networks are deployed to have remote access to the sensor. Besides, integrating different kinds of sensors either on a single acquisition platform or decentralized distributed platforms, various structural response parameters such as acceleration, displacement, tilt, strain, and more can be obtained through a heterogeneous, but unified system.

Concurrent with these developments in measurement science and engineering, smartphones have become an outstanding technological boom in communication industry in the last decade. Their embedded batteries, internal hard-drive, processor, and sensors have the potential to compose standalone vibration monitoring instruments which are, by default, mobile, intelligent, sustainable, and ubiquitous. Soon after the release of the first generations, they have been introduced as seismic sensor network components, and afterwards as explained throughout this dissertation, they have been adopted by vibration-based SHM systems.

In spite of all of the advantages inherited from the emerging technologies, SHM using smartphones brought numerous challenges due to the errors and uncertainties stemming from citizen participation. Unlike typical monitoring systems, the platform developer have no control over the sensor instrumentation and the operation schedule. Instead, citizens take the initiative to measure vibrations on a structure under the conditions depending on citizens' decisions and actions. Self-governance and auto-control in the vibration sensing platform has brought new dimensions

to the SHM-related uncertainties. Discovering the sources of these uncertainties, and finding solutions through multisensory smartphone technology, is therefore, the main goal of this dissertation. To begin with, the following subchapter presents the dissertation outline with a brief overview of each chapter's major focus.

1.1 Dissertation Outline

To derive solutions to the fundamental issues discussed above; (1) smartphone accelerometer performance, (2) crowdsourcing initiation and citizen-engaged vibration monitoring, (3) the effects of rotational and translational variation in sensor position as well as duration uncertainties, and biomechanical effects are progressively discussed in this dissertation. In addition, (4) the mobile cyber-physical system implementation aspects are examined. Each particular problem explained herein is a milestone in smartphone-based SHM in terms of how it differentiates from the conventional monitoring practices.

In this dissertation, the key aspects of smartphone-based SHM systems are discussed through 6 chapters. As presented, Chapter 1 proposes a brief introduction to SHM and the recent trends, then, introduces the use of smartphones as SHM instruments. Chapter 2 discusses the performance of smartphone accelerometers as structural response measurement devices, through reference datasheets, laboratory, and field tests. Chapter 3 implements a crowdsourcing-based modal identification platform through mobile (iOS) and web (PHP and MySQL) software development, and presents the first participatory sensing results collected by citizens. Chapter 4 proposes potential citizen-induced errors and uncertainties in smartphone-based SHM, and formulates solutions that can tackle with spatiotemporal, directional, and biomechanical effects. Chapter 5 uses the crowdsourcing-based modal identification results to follow an SHM-integrated performance assessment process which is an early prototype of a mobile cyber-physical system. Finally, Chapter 6 presents the summary and the conclusions, and proposes further research directions for the future work.

Chapter 2

Smartphone Accelerometer Tests

This chapter presents the early laboratory and field tests, and evaluates different smartphone accelerometers' performance as SHM instruments. This chapter is reproduced from the paper coauthored with Maria Q. Feng, Yoshio Fukuda, and Masato Mizuta, published in the journal Sensors [1].

2.1 Introduction

With the rapid advances in computer and sensor technologies in the last three decades, structural health monitoring (SHM), mostly based on structural vibration, has become an important research field in civil engineering [2, 3]. Implementation of SHM in civil engineering structures, however, has practical difficulties and financial burdens associated with instrumentation and monitoring. Conventional sensors have high hardware, installation, and maintenance costs, as well as remote monitoring and cabling issues. Although wireless sensors aim to solve some of these issues, additional issues are then introduced regarding power consumption, data acquisition and networking. These issues have hindered practical implementation of SHM methodologies on massive scales such as networks of highway bridges and urban areas with large stocks of buildings. To address these issues, many emerging sensor technologies are being developed, including those proposed by the authors' team (e.g. [4, 5]).

On the other hand, the Internet, smartphones, and mobile networks have given rise to citizen participation for crowdsourcing applications and producing valuable data. A number of seismology and earthquake engineering projects have shown the benefits of such data. In Southern California, citizens reported experiences to a seismology network after the 1999 7.1-magnitude Hector Mine Earthquake, taking part in mapping the intensity of the earthquake in a project called ShakeMap [6]. "Did you feel it?" the online seismic intensity database, received more than 750,000

responses by 2007, and was able to generate intensity maps in an automated fashion [7, 8]. “The Quake Catcher Network” introduced a rapidly deployable seismic network that aimed to increase the number of seismic stations extensively with minimal cost based on inexpensive MEMS sensors and volunteers [9–12]. “Community Seismic Network” is a seismic network which is supported by low-cost accelerometers connected to personal computers or sensors embedded in mobile devices, and uses data fusion techniques to distinguish earthquake-induced vibrations from false alarms [13–15]. “iShake” is the proposed framework for using smartphones as seismographs, and studies [16–18] investigated the reliability of ground motion data obtained from the smartphone sensors. “Community Seismic Network” and “The Quake Catcher Network” are utilized to simulate structural response based on the Timoshenko beam theory [19]. These studies show the potential of using smartphones to measure vibrations.

Encouraged by the recent development and the enthusiasm of citizens to participate, the authors propose a smartphone-based Citizen Sensor network to collect structural integrity data at low cost. This network enables a crowdsourcing platform where smartphones act as mobile sensors and provide structural vibration data (pre-processed by the phones) and GPS location data to a cloud server. The long-term vibration measurement data and the subsequently identified structural vibration characteristics will establish a baseline database for the structure for the purposes of structural health monitoring and damage detection, as demonstrated in prior research (which is beyond the scope of this chapter). Engaging the crowd will allow efficient monitoring of a large number of structures in an urban setting, which can be particularly useful for rapid assessment of structural damage of buildings and urban infrastructure after a major event such as an earthquake.

This chapter represents the first step toward the envisioned Citizen Sensor network by investigating the feasibility of using smartphone accelerometers to monitor structural vibration under normal and extreme loads. A number of shaking table tests are conducted to compare smartphone sensor performance with high-quality accelerometers for measuring vibration of different frequencies. Furthermore, input ground motion and response of a column model, subjected to operational loads, white noise and earthquake excitations throughout shaking table tests, are monitored using smartphone and high-quality accelerometers. Finally the smartphone sensor was used to measure ambient and forced vibrations of a bridge.

It is noted that the coupling between the smartphone and the structure can affect the vibration

measurement [20]. In this study, the smartphones are fixed on the structures using double-sided tapes to ensure that no local vibration would affect the quality of the structural vibration measurement. In reality, smartphone users would need to place their phones on rigid holders that are permanently fixed on building floors or columns/walls while taking the vibration measurement. The measurement could be automatically triggered by an event (such as an earthquake) when the phones are placed in such holders.

2.2 Smartphone accelerometer properties

The most widely used brands and generations of smartphones, referred to as Smartphone 1, Smartphone 2 and Smartphone 3, are tested in this study. They were carefully selected in order to consider the factors that might have an influence on the smartphone sensors' measurement performance. These factors could be related to hardware such as the accelerometer and processor embedded in the phone, as well as the material and geometrical properties of the phone case. A detailed study on the effects of such physical properties on smartphone seismometer data quality was conducted by applying different coupling conditions and can be found in [16-18]. Software including the measurement application and the phone's operating system might also affect the measurement performance.

Over the last few years, smartphone technology has made significant advances. The phone central processing unit (CPU) and random-access memory (RAM) capabilities have increased significantly while the phone size and weight have decreased [21]. Furthermore, Smartphone 1 and Smartphone 2, two generations of the same smartphone, are embedded with different microelectromechanical systems (MEMS) accelerometers, the LIS331DLH [22] and LIS331DL [23], respectively. The accelerometer properties are listed in Table 2.1, in comparison with high-quality piezoelectric sensors used in this study as reference sensors [24]. In addition, another widely available new generation smartphone, Smartphone 3, was also tested [25]. Several available smartphone applications were tested and the "Seismometer" application was chosen for the vibration measurements in this study. Due to the limitations of the application, the sampling rate is set to 100 Hz for both smartphone sensors, leading to a Nyquist frequency of 50 Hz.

Table 2.1: Reference and smartphone sensor properties

Property	Reference	Smartphone 1	Smartphone 2	Smartphone 3
Sensor maker	PCB Piezotronics	ST Micro- electronics	ST Micro- electronics	Bosch Sensortec
Sensor model	393B04	LIS331DL	LIS331DLH	SMB380
Phone maker, model & Operating System (OS)/Data Acquisition (DAQ) model	NI SCXI- 1531	iPhone 3GS, iOS	iPhone 5, iOS	Samsung Galaxy S4, Android
Type	Piezoelectric	MEMS	MEMS	MEMS
Sensitivity ± 2 g	1000 mV/g	18 mg/digit	1 mg/digit	3.9 mg/digit
Measurement range	5 g	2 g	2 g	2 g
Output data rate/Frequency range	0.05–750	100, 400	0.5–1000	3000
Noise density ($mg\sqrt{Hz}$)	0.00004	N/A	0.218	0.5

2.3 Small-scale shaking table tests

Although sensor datasheets provide extensive information regarding smartphone accelerometers, accelerometers' performance can be influenced by a number of external effects such as phone hardware, embedded filters, and phone geometry. In other words, bare accelerometer performance might be different than an accelerometer embedded in a smartphone. Therefore, in order to investigate the smartphone sensors' capabilities of measuring vibration of different frequencies and amplitudes, small-scale shaking table tests are carried out. As shown in Figure 2.1, smartphone sensors are fixed on an electromagnetic shaking table, together with two of the high-quality piezoelectric reference accelerometers.

The shaking table is excited with sinusoidal motions of different frequencies including 0.5, 0.8, 1, 2, 5, 10 and 20 Hz. Due to the limitations of the shaking table, low-frequency content sinusoidal wave amplitudes are relatively small compared with high-frequency content sinusoidal waves. As a result, the maximum acceleration amplitudes range from 0.05 g to 0.2 g.

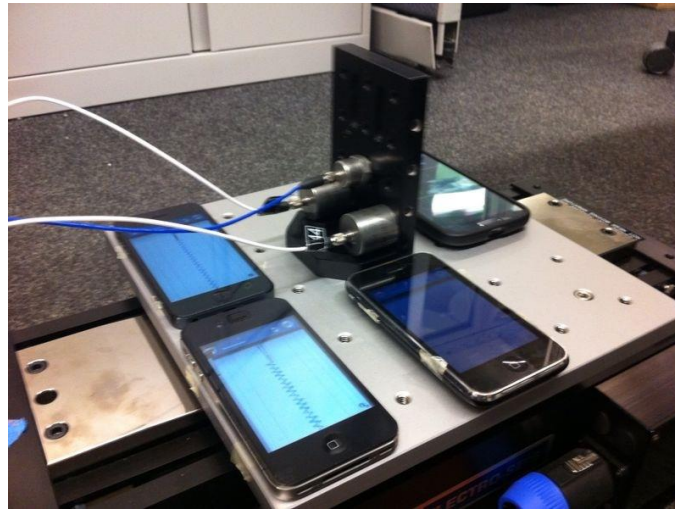


Figure 2.1: Sine wave shaking table test setup

Figure 2.2 illustrates the acceleration time histories measured by the reference and smartphone accelerometers under sinusoidal excitations of different frequencies. The measured peak amplitudes by the smartphone sensors agree well with those by the reference sensors, although the smartphone sensors tend to slightly overestimate the amplitude (which is in correlation with Arias Intensity results presented in [18]). It is noted that the reference and the smartphone sensor data are acquired by different data acquisition systems and thus not perfectly synchronized. There are slight differences among the clocks in the smartphones and in the reference sensor data acquisition system, resulting in the slight phase differences in the measured acceleration time histories.

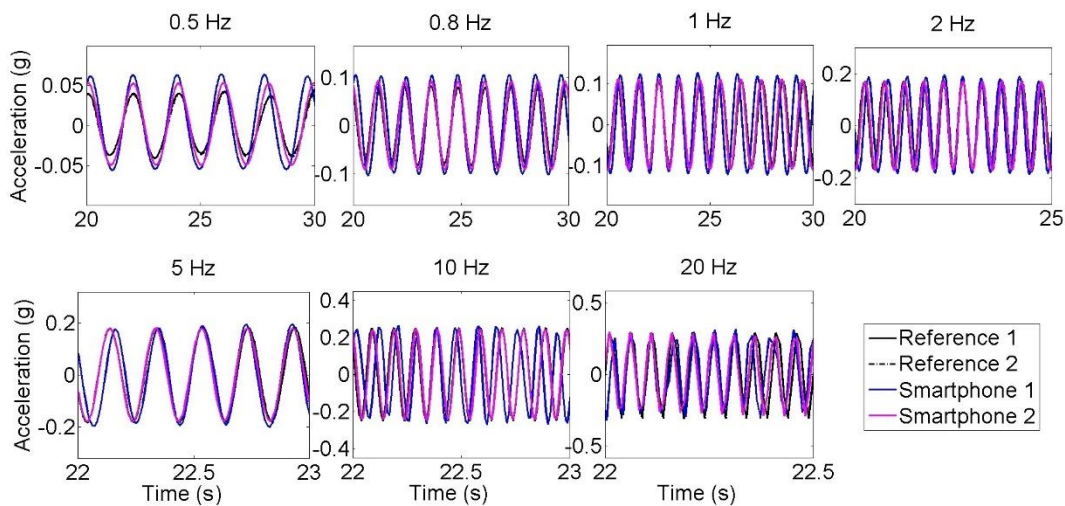


Figure 2.2: Sine wave time histories of different frequencies

Table 2.2 summarizes the frequency and the amplitude errors between the reference and the smartphone sensors. It is observed that the new generation smartphone (Smartphone 2) is significantly more accurate than the old generation smartphone (Smartphone 1). For instance, for the 1 Hz excitation, the error between peak horizontal accelerations decreases from 17.5% (Smartphone 1) to 3.10% (Smartphone 2). Similarly, new smartphone sensors are capable of obtaining the dominant frequency of the signal with an error up to 0.96% whereas old generation smartphone errors are significantly large, ranging between 4% and 5%. Although accuracy in frequency slightly changes with different tests, the accuracy in amplitude decreases as peak horizontal acceleration decreases. In conclusion, the error results in Table 2.2 show that the new generation smartphone (Smartphone 2) is reasonably accurate for measuring vibration in the frequency range relevant to most of the civil engineering structures.

Table 2.2: Peak horizontal acceleration error

Frequency (Hz)		0.5	0.8	1	2	5	10	20
Error	Smartphone 1	4.57	4.58	5.04	5.03	4.73	4.96	4.01
(%)	Smartphone 2	0.92	0.95	0.92	0.92	0.95	0.92	0.96
Amplitude (g)		0.04	0.08	0.11	0.17	0.18	0.25	0.29
Error	Smartphone 1	43.9	25.6	17.5	8.19	15.3	17.3	25.7
(%)	Smartphone 2	17.4	8.51	3.10	4.97	1.14	0.45	3.82

2.4 Large-scale shaking table tests

In order to examine the capabilities of smartphone sensors for measuring different types of vibration at different amplitudes, large-scale seismic shaking table tests are performed on a masonry column model, as shown in Figure 2.3, involving operational, white noise and earthquake excitation inputs. Further details about the experiment can be found in [26, 27]. The smartphone and reference accelerometers are installed on the top of the model, while another smartphone is installed on the top of the shaking table near the foot of the model. The visual inspections before and after the tests show no crack or other types of damage, and thus the structure is assumed to be

a linear time invariant system throughout the tests. In previous studies, the same assumption is used by the authors in [28, 29], and the crack-damage relationship can be observed from the shaking table test data as shown in [30, 31]. The vibration measurements are used to identify modal characteristics of the structure. In order to determine modal frequencies, power spectral densities are used. Prior to computation of power spectral densities, operational, white-noise, and earthquake excitation test time histories are subjected to zero-padding to smoothen the spectral curves. Therefore, actual spectral resolutions, 0.0100, 0.0142, and 0.0142 Hz, respectively, are converted into 0.0015 Hz as a result of zero-padding the original time signals.

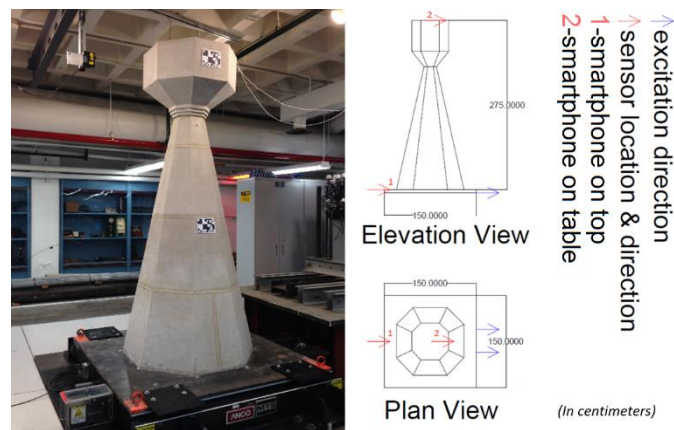


Figure 2.3: Masonry column model and shaking table setup

2.4.1 Operational vibration tests

First, the seismic shaking table is locked and the responses of the column model to environmental vibrations and to hammer impact loading on top are measured. Figure 2.4 shows the acceleration time history responses measured at the top of the column by the reference and smartphone sensors under the hammer impact loading and under the operational vibrations respectively. The plots corresponding to reference and smartphone sensors are plotted separately because that the measurements are not synchronized, yet the time histories show the similarities between the two measurements. Likewise, error is not quantified as a function of time since samples obtained from reference and smartphone sensors refer to different time instants. Cross-correlation or GPS synchronization can be addressed to deal with this problem, which can be addressed in the future. The peak response to the impact load is approximately 0.02 g, while the

operational vibration amplitude is less than 0.004 g. It is observed that smartphone measurements agree well with the reference measurements in terms of amplitude characteristics. Figure 2.5 shows the power spectral densities of the vibration responses measured by the reference and smartphone sensors, demonstrating frequency characteristics of the measured responses are significantly close to each other. In other words, Figure 2.5 reflects the spectra of the response to the initial impact followed by operational vibrations.

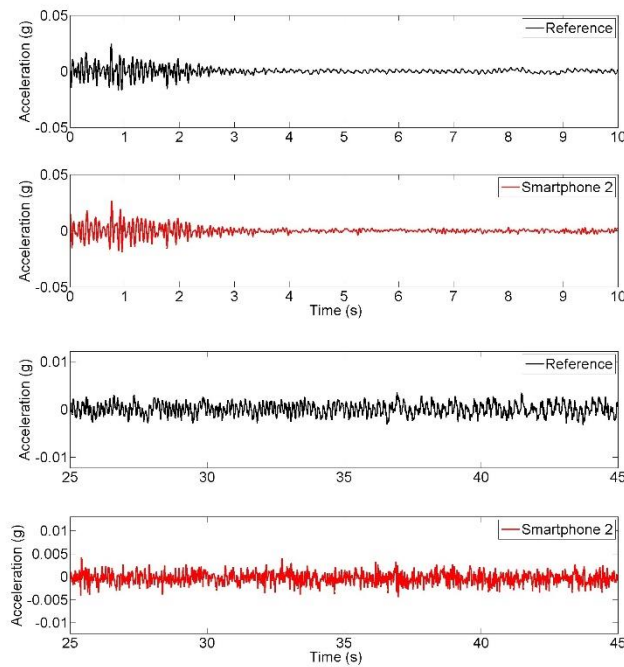


Figure 2.4: Time history of impact and operational vibration response measurements

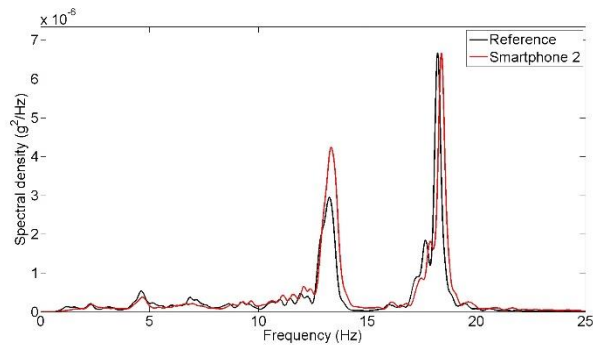


Figure 2.5: Spectral density of impact and operational vibration response

2.4.2 White noise excitation tests

The seismic shaking table is excited by white-noise ground motion input and the smartphone and reference sensors measure the response of the column model. Figure 2.6 compares the time history responses obtained from the reference and smartphone sensors. Figure 2.7 shows the power spectral densities of reference and smartphone measurements. Significant agreement is observed in both the time and frequency domains.

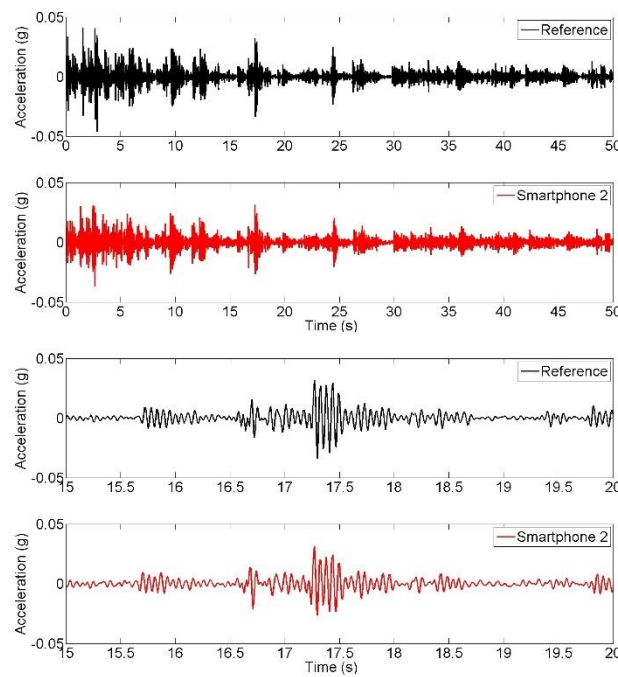


Figure 2.6: Time history of white noise excitation response

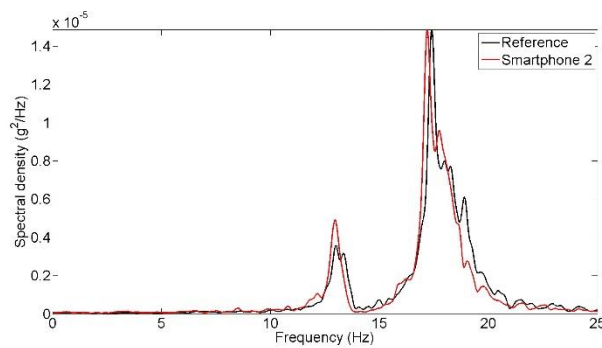


Figure 2.7: Spectral density of white noise excitation response

2.4.3 Earthquake excitation tests

Finally, seismic input ground motion and response measurements are made in order to evaluate the smartphone performance in measuring seismic strong motion and structural response. Figure 2.8 show the input ground motion time histories targeted by shaking table controller (Reference), and the ones measured by Smartphone 2 and Smartphone 3. The bottom three plots in the figure are the enlarged portions (between 15 s to 20 s) to show more details. It is noted that the shaking table acceleration (the input) was not measured by the reference sensor. The “Reference” in Figure 2.8 refers to the input seismic acceleration generated by the controller of the seismic shaking table. The reference sensor was used for measuring the structural response in this seismic excitation experiment. An excellent agreement is observed between the measurements made by the two different smartphones. A considerable difference is observed between the target time history and the measurements by the smartphone sensors, due to the fact that a seismic shaking table has physical limitations of generating targeted motion [32]. Figure 2.9 shows the acceleration response time histories measured at the top of the model by the reference sensor and Smartphone 2. Similarly, portions of the top two plots are enlarged in the bottom two plots to show more details. An excellent agreement is observed between the responses measured by the smartphone and the reference sensor.

Power spectral densities are obtained from the targeted input, measured input and response acceleration time histories and plotted in Figure 2.10, based on which the transfer function is developed and plotted in the same figure. Again, the spectral densities of the responses measured by the reference and the smartphone sensors agree well. Although the ground motions of two different smartphones have significant difference with the target input motion applied to the shaking table, they agree very well in the frequency domain as well.

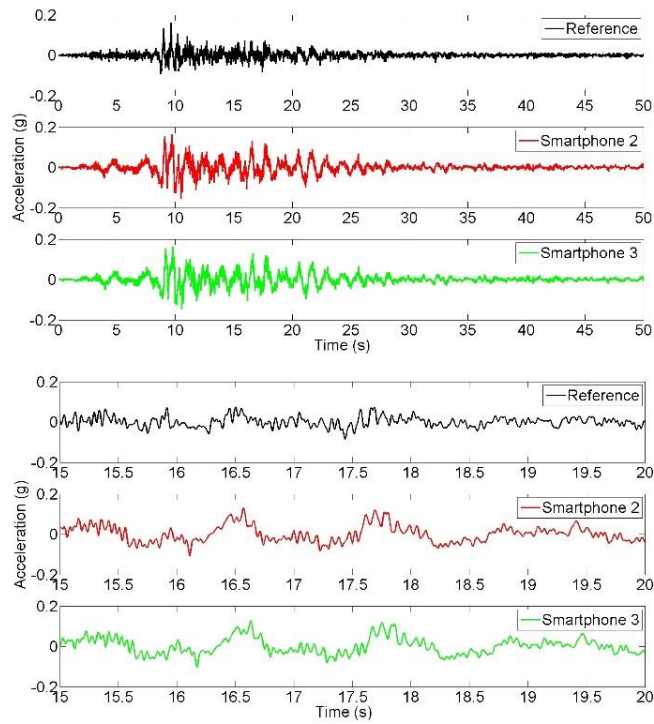


Figure 2.8: Time history of targeted and achieved earthquake input ground motion

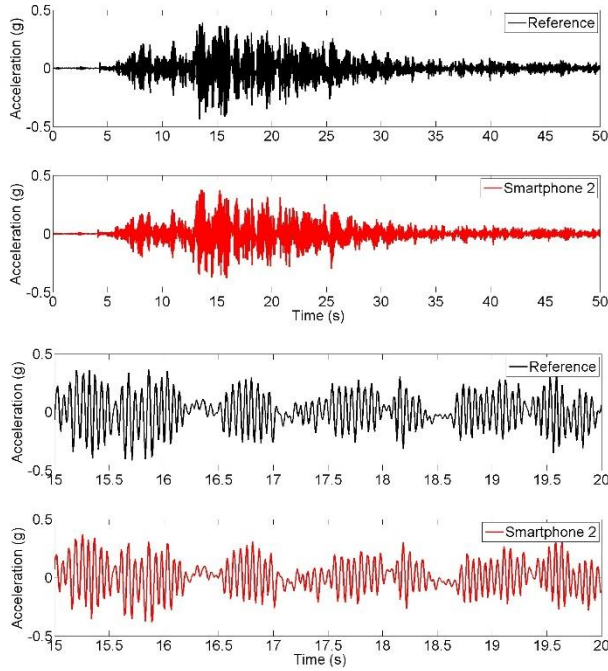


Figure 2.9: Time history of earthquake response

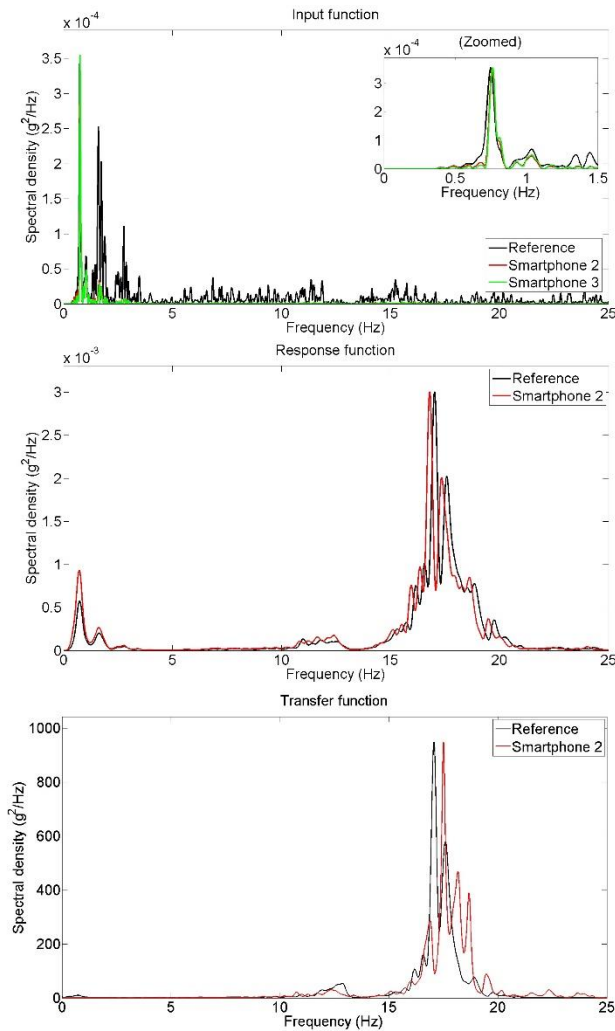


Figure 2.10: Spectral density of earthquake excitation measurements

2.4.4 Comparison of identified natural frequencies

Natural frequencies of the masonry column model are identified based on the measurements made in the seismic shaking table tests involving the different types of excitations. The peak picking method is applied to extract the natural frequencies from the power spectral densities of the response acceleration under the operational and white-noise excitations shown in Figure 2.5 and Figure 2.7. For the seismic excitation, the natural frequencies are identified from the spectral density function plot in Figure 2.10. The identified fundamental frequency values are summarized in Table 2.3. From the measurements made by the reference sensor, the fundamental frequency of the column model is identified as 18.2, 17.4, and 17.1 Hz respectively under the operational, white

noise, and earthquake excitations. Their counterparts measured by the smartphone sensor are 18.4, 17.2, and 17.5 Hz. The frequency values measured by the smartphone sensor and the reference sensors are highly comparable, demonstrating the capability of the smartphone sensor in measuring a structure’s natural frequencies.

Furthermore, it is observed that the fundamental frequency of the structural model decreases as its vibration amplitude increases. This phenomenon has been confirmed by many other studies [33–35] and further analysis is beyond the scope of this chapter.

Table 2.3: Comparison of natural frequencies

Excitation Type		Ambient	White Noise	Earthquake
Natural frequency	Reference	18.2	17.4	17.1
(Hz)	Smartphone	18.4	17.2	17.5
Error (%)		1.10	1.15	2.34

2.5 Field tests of a bridge

In order to investigate the performance of smartphone sensors on actual structures, a series of field tests are conducted on a pre-stressed reinforced concrete pedestrian bridge located in Princeton (NJ, USA) shown in Figure 2.11. Smartphone 2 and the reference sensor are fixed by double-sided adhesive tapes in the mid-span of the bridge deck to measure its ambient vibration and response to dynamic loading. Two sets of dynamic loading tests are carried out. First, a group of participants runs randomly on the bridge with different speeds, rhythms and directions to generate dynamic loads of broader frequency content. Second the same group jumps synchronically at 3 Hz, which is close to the estimated natural frequency of the bridge, to excite the first mode of vibration. Similar to the previous tests, in ambient vibration, random dynamic, and synchronized dynamic test time histories, zero-padding is applied. Therefore, actual spectral

resolutions, 0.0142, 0.0067, and 0.0033 Hz, respectively, are converted into 0.0015 Hz as a result.

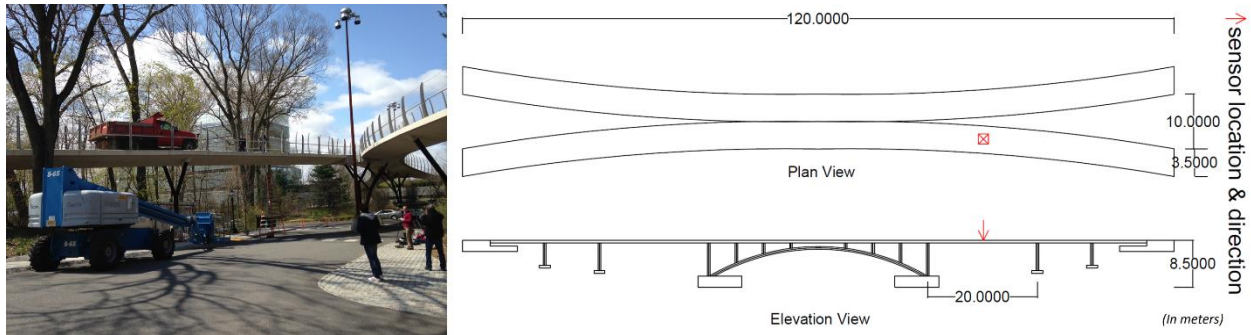


Figure 2.11: The pedestrian bridge in Princeton, NJ

2.5.1 Ambient vibration tests

Ambient vibration of the bridge, resulting from the environmental vibration caused by pedestrians and vehicles passing under the bridge, are measured using the smartphone and reference accelerometers located at the mid-span. Figure 2.12 compares the time histories obtained from the reference and smartphone accelerometers. The bottom two plots are enlarged portions to show more details. First, the amplitude of the vibration is less than 0.005 g. At this low amplitude, the smartphone sensor is not as sensitive as the high-quality reference sensor, and as a result some differences between the two measurements are observed in the time histories. However, the frequency domain characteristics measured the two sensors match quite well, as shown in the power spectral density plots in Figure 2.13. For example, the fundamental frequency of the bridge identified from the reference sensor measurement is 3.13 Hz compared with 3.16 Hz by the smartphone measurement. The error is less than 1%. The higher modes by the two measurements also agree well. Moreover, measurements include smartphone sensors positioned without fixing, which also resulted in the same accuracy. In other words, the smartphone sensors are free to move on the structure, yet coupled by the friction between the phone surface and the bridge surface. This implies the practicality of smartphone sensors for vibration measurement. A detailed study, considering different coupling conditions and targeting the effect of fixity on smartphone sensors as seismic instruments is conducted in [16, 18].

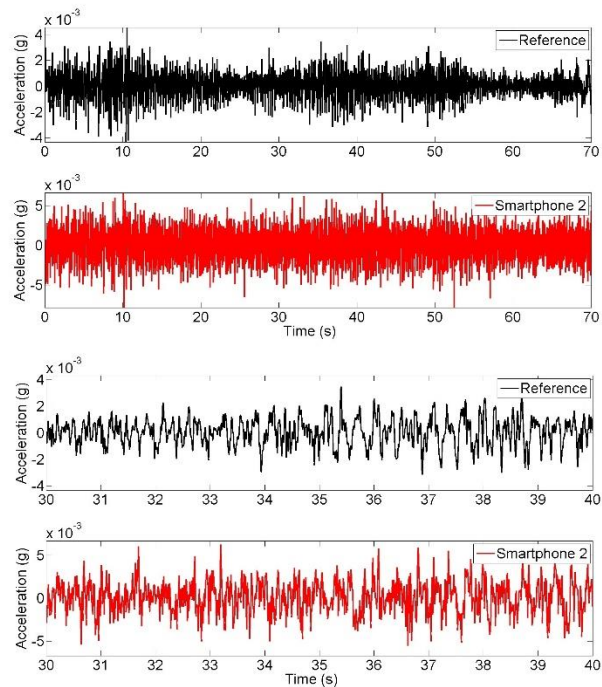


Figure 2.12: Time history of ambient vibration response

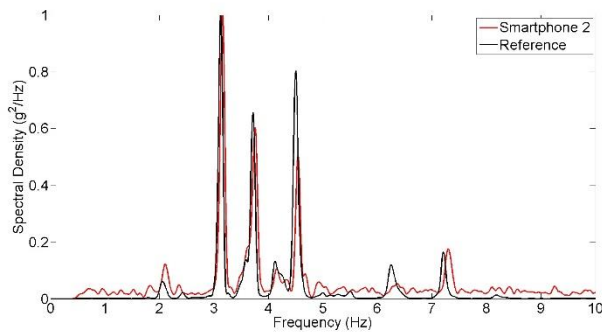


Figure 2.13: Spectral density of ambient vibration response

2.5.2 Random dynamic tests

In order to apply dynamic loads with broadband frequency content to the bridge, a group of pedestrians run on the bridge deck randomly with different, varying speeds, rhythms and directions without any particular pattern. Figure 2.14 shows that the smartphone measurement agrees much better with the reference sensor measurement than it does in the ambient vibration case (shown in Figure 2.13). This is because of the increased vibration amplitude; in fact the random running-

induced vibration is ten times higher than the ambient vibration. From the power spectral density plots in Figure 2.15, natural frequency of bridge is estimated as 3.08 Hz and 3.11 Hz respectively from reference and smartphone sensor measurements, resulting in an error less than 1%.

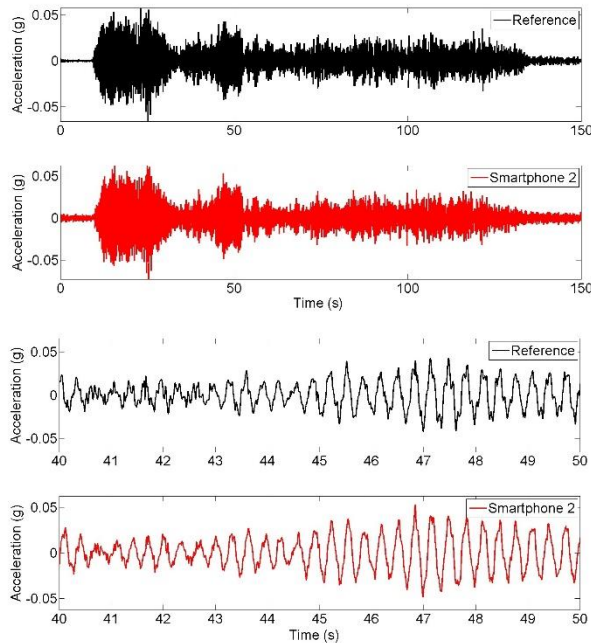


Figure 2.14: Time history of random dynamic tests

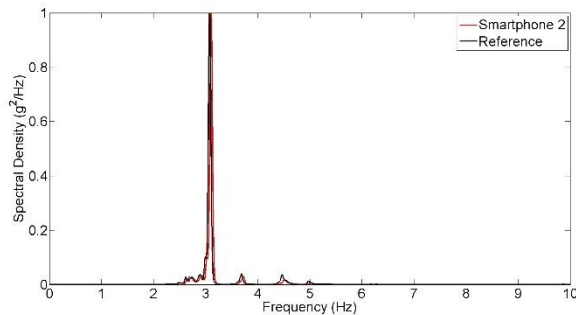


Figure 2.15: Spectral density of random dynamic tests

2.5.3 Synchronized dynamic tests

Finally, in order to maximize the dynamic load effect, the pedestrian participants jump on the mid-span of the bridge deck synchronically at a frequency of 3 Hz, which is close to the estimated

natural frequency of the bridge. Figure 2.16 plots the time histories obtained from the reference and smartphone accelerometers. Due to the dynamic amplification, the bridge response acceleration exceeds 0.1 g. As the vibration amplitude increases, the measurement error of smartphone sensor (with respect to the reference sensor) becomes insignificant. The power spectral densities based on the smartphone and reference measurements, as plotted shown in Figure 2.17, show their excellent agreement. This synchronized jumping excited only the first mode, which is 3.00 Hz (by the reference sensor) and 3.03 Hz (by the smartphone sensor). Likewise, the error is less than 1%.

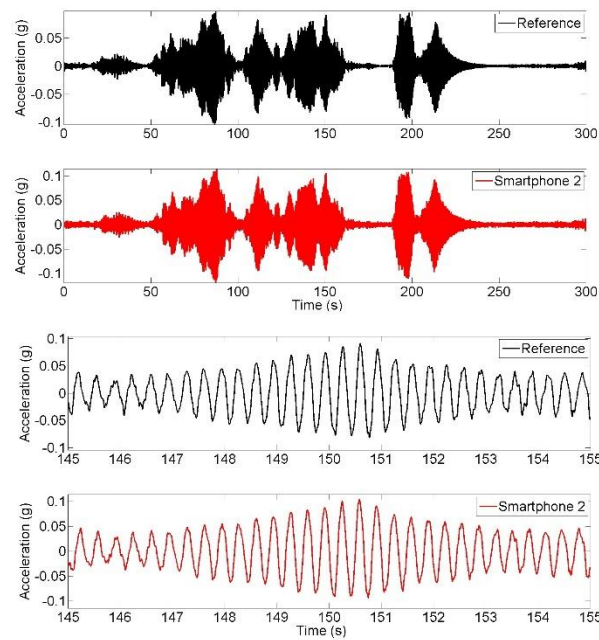


Figure 2.16: Time history of synchronized dynamic tests

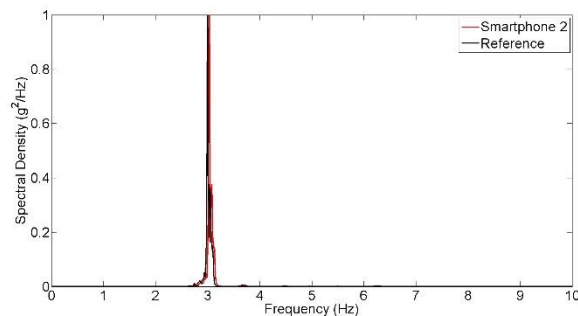


Figure 2.17: Spectral density of synchronized dynamic tests

2.5.4 Comparison of identified natural frequencies

Natural frequencies of the bridge are identified based on the measurements made in the field tests. The peak picking method is applied to extract the natural frequencies from the power spectral densities of the response acceleration under the ambient, random and synchronized excitations shown in Figure 2.13, Figure 2.15, and Figure 2.17. Table 2.4 compares the identified fundamental frequency values. From the measurements made by the reference sensor, the fundamental frequency of the bridge is identified as 3.13, 3.08, and 3.00 Hz respectively under the ambient vibration, and the random and synchronized dynamic loading tests, while their counterparts made by the smartphone sensor are 3.16, 3.11, and 3.03 Hz. Again, frequency values measured by the smartphone sensor and the reference sensors are highly comparable, demonstrating the capability of the smartphone sensor in measuring a structure’s natural frequencies. Like the observation made in the seismic shaking table tests, the fundamental frequency of the bridge decreases as its vibration amplitude increases.

Table 2.4: Comparison of natural frequencies

Excitation Type		Ambient	Random	Synch
Natural frequencies	Reference	3.13	3.08	3.00
(Hz)	Smartphone	3.16	3.11	3.03
Error (%)		0.96	0.97	1.00

2.6 Conclusions

A comprehensive experimental study, involving seismic shaking table tests and bridge field tests, was carried out to investigate the performance of smartphone accelerometers in measuring structural response to dynamic loading ranging from low-amplitude ambient to high-amplitude seismic excitations, as well as sinusoidal excitations. Three widely-used smartphones embedded with different accelerometers and a high-quality reference sensor are tested on a small shaking table, a structural model on a large seismic shaking table, and an actual bridge. All the

measurement results are compared in both time and frequency domains. The following conclusions can be drawn from this study:

(1) The small-scale shaking table tests confirm that the smartphone sensors are capable of accurately measuring sinusoidal vibration of 0.5 Hz through 20 Hz, a frequency range relevant to most civil engineering structures. The measurement error in terms of the vibration amplitude, when compared with the high-quality reference sensor, is less than 5% for vibration higher than 1 Hz, but increases as the peak horizontal acceleration decreases. The measurement error in terms of vibration frequency is 1% and 5% respectively for the new and the old generation smartphone sensors.

(2) The large-scale seismic shaking table tests of the structural model and the field dynamic tests of the bridge demonstrate the capabilities of smartphone sensors in measuring structural responses to a variety of dynamic loads of different amplitude as well as frequency characteristics. Despite the measurement error of the structural response in the time domain under the low-amplitude (less than 0.005 g) ambient vibration, it is possible to extract the structures' fundamental frequencies with remarkably small error of less than 1%.

(3) The two types of the widely-used smartphones with different operating systems and different accelerometers show comparable performance. The accelerometer in the newer generation smartphone is significantly more accurate than that in the old generation smartphone. The quality of the sensors embedded in smartphones is expected to continue to improve in the future.

(4) The laboratory and field tests show advantages of the smartphone sensors over the conventional sensor, such as the ease of installation and data acquisition as well as wireless transmission.

It is noted that many issues are yet to be solved such as the on-phone signal pre-processing, power-efficient signal transmission and practical phone-structure couplings. Nevertheless, this study demonstrates the feasibility of using smartphone accelerometers for measurement of structural vibration characteristics, from which structural health can be diagnosed as shown in prior research. Encouraged by the results of this study, the authors are exploring the potential of forming a smartphone-based low-cost Citizen Sensor network for structural health monitoring and post-event damage assessment in structure- and city-scales, by developing frameworks of citizen

engagement, online database and crowdsourcing data analytics.

Chapter 3

Crowdsourcing Platform Development

This chapter presents the software platforms developed for smartphone-based SHM and presents the first crowdsourced modal identification results acquired from citizens through the web integration. This chapter is reproduced from the paper coauthored with Maria Q. Feng and Dongming Feng, published in the journal Sensors [36].

3.1 Introduction

Structural health monitoring (SHM) has attracted significant attention as the computational and technological environment matures. Vibration-based SHM has been explored for damage detection, model updating, performance assessment, and reliability estimation of civil engineering structures such as buildings and bridges (e.g. [3, 28, 29, 33, 34, 37, 38]), bringing new solutions to cope with aging and deteriorating urban infrastructure. Besides, the exponential growth of internet and smartphones has brought novel solutions to civil and earthquake engineering problems with citizen engagement [8, 10, 14, 18]. Likewise, the widespread use of smartphones has produced a new potential source for vibration monitoring of civil infrastructure. State-of-the-art smartphone technology takes advantage of multiple embedded sensors to maximize the user experience and device productivity. Moreover, its advanced communication and networking capabilities enable the users to connect with each other or the web. A number of studies have discussed the possibility of using smartphones and citizen collaboration for SHM purposes [19, 39, 40].

Crowdsourcing has become popular over the last few years [41–47]. By definition, crowdsourcing is a collaborative problem-solving process with help from the community and volunteer participation, leading to a new understanding to Von Hippel’s user-oriented innovation

concept [48]. In particular, with the rise of civic participation in a variety of platforms, innovative organizations have initiated new projects to make use of crowdsourcing as a low-cost or no-cost labor. Successful examples include commercial entrepreneurship such as Amazon's Mechanical Turk, InnoCentive or nonprofit organizations such as Wikipedia. For instance, software engineering platforms use crowdsourcing as an access to technological progress [49–55]. Moreover, a wide range of research areas have benefitted from sourcing the crowd for environmental [56, 57], geospatial [58-60], seismicity [61], and finally SHM studies [62]. In spite of the advantages offered by crowdsourcing, the data quality and accuracy need to be validated [63, 64]. Likewise, machine learning methods might be utilized to detect false vibration measurements such as falling or defected phones and discard the flawed data accordingly [65].

These advancements have inspired the authors to develop a novel crowdsourcing-based Citizen Sensor System for SHM, which utilizes smartphone-embedded sensors for measuring structural vibration and defining sensor locations. In their previous study, the authors investigated the performance of smartphone accelerometers through a number of laboratory and field tests on civil engineering structures, and confirmed the usefulness of these sensors [1]. As a further step, this study aims at developing a novel crowdsourcing platform, which enables citizens to use their smartphones to measure structural vibration, transmit the data to an online server and process the data into a database automatically. The crowd incentives can be established through contests and rewards [66, 67]. For example, the best identification results or participation above a certain sampling number could be rewarded to increase citizen encouragement. Another possibility is to utilize gamification strategies to convert the identification problem into an entertainment medium [68, 69]. What is more, because the modal identification results may reveal post-event structural damage due to extreme events or aging, integrity and safety of urban infrastructure itself is a fundamental incentive that can mobilize people for crowdsourcing-based SHM. Pedestrians for bridges and occupants for office and residential buildings can be the target group for citizen sensors.

The proposed system includes a multilayered structure integrating mobile sensing and web platforms. An iOS (iPhone Operating System) smartphone application provides citizens with a tool for measuring structural vibration and submitting data wirelessly to a central server. The web-based server receives the citizen submissions, processes the vibration data and stores the processed data such as the identified modal properties (frequencies, damping ratios and mode shapes) as well

as the vibration time history data. In this study, a crowdsourcing review is conducted to effectively formulate citizen experience and contribution. The platform developed in this study is then tested through field measurements on a bridge structure. A number of low-amplitude ambient vibration measurements with varied phone locations and coupling conditions are made to evaluate sources of uncertainties associated with citizen participation. Short-term individual data are collected to generate large-sized data and are averaged to compensate short measurement duration which is uncommon for SHM under ambient vibration. The results show that a smartphone-based system can produce valuable SHM information even with uncertainties associated with the citizen participation. What is more, integration with the web server enables modal identification in an online and automated manner.

This study lays a technical foundation for crowdsourcing-based, citizen-engaged SHM applications. Therefore, the case presented in this chapter is a small-scale crowdsourcing problem discussing the issues related to citizen participation. The progress of Citizen Sensors for SHM will lead to a unique crowdsourcing example, because of its transitional descriptions due to the existing taxonomies. In other words, the presented platform will be the initial stage of a complex system which utilizes crowd participation, mobile sensing, and web services in a hybrid framework.

3.2 Multilayered computer platform

The goal of the computer platform developed in this study is to connect citizens with their smartphone sensors and a web-based server. The platform has a multilayered structure including the user, communication, and server layers, while each layer can be designed, implemented, and tested independently.

The user-side platform is based on the mobile devices used by the citizen participants. A smartphone application is developed to enable citizens to collect data with the smartphone-embedded sensors and transmit sensor data. Data transmission between the citizens and the server uses an existing cellular network or Wi-Fi and will not be discussed in this study.

The server-side platform receives, processes, and stores the measured vibration time-history data and processed results. The documents regarding system architecture scheme, requirements analysis can be found in [70]. Similarly, collaboration diagrams describing architectural design, class diagrams describing database design can be found in [71]. What is more, the software

components and database tables are provided in [72]. Figure 3.1 shows the integrated, multilayered platform and its components. Details regarding user-side and server-side platforms are discussed within the following subchapters.

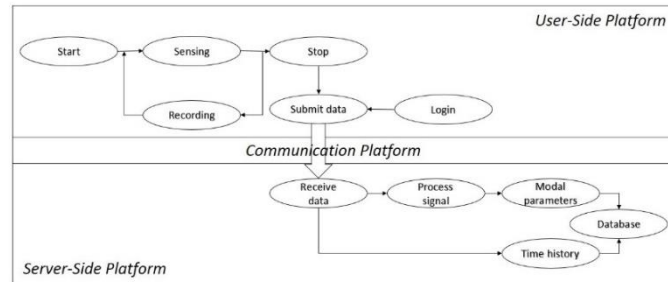


Figure 3.1: Integration scheme of system platforms

3.2.1 User-side sensing and acquisition

An iOS application named Citizen Sensors for SHM was developed as part of this study to enable citizens to measure vibration with their iPhone-embedded accelerometers and to submit the data to the server on Internet via a cellular network or WiFi connected to the Internet. Xcode Version 6.1.1 is used for coding the application. Objective-C is used to develop the header and implementation files of the application. Cocoa Touch is the user interface framework which provides a wide set of classes for application development. The iOS application development is logically divided into three categories such as model-view-controller (MVC). With this approach, it is possible to build the computational background, design a user layout and connect these separate aspects with modular principles. In other words, MVC separates the application components in a modular way. In MVC approach, “Model” is involved in application data and methods, whereas “View” provides the user with interaction widgets. The third component, “Controller”, isolates the other two components from each other, controls the connection between them and updates both components based on received actions from “View” and data from “Model” [73].

In order to provide users with a simple interface, a single view application is chosen as the project template. The interface building element storyboard is utilized to set up interface objects, header (ViewController.h) and implementation (ViewController.m) file scripts are developed after

interface objects and scripts are connected via the assistant editor. Basically, four interface objects are introduced to show the application status, activation button, acceleration time history column and the gateway to the server. Being generated by predefined object types such as UILabel, UIButton, UITextView, and UIWebView, these objects are introduced to the model via outlets and actions to display smartphone sensor data and receive user commands. Once the user touches the activation button object, the application requests acceleration data from the phone's accelerometers at a sampling rate (such as 100 Hz, which is sampling frequency's upper limit for old generation iOS devices [74]). This means that the application is capable of identifying modal frequencies up to Nyquist frequency, 50 Hz, which is equal to the half of sampling frequency. The acquired data are accumulated in a temporary variable and transferred to the acceleration time history column once the button is repressed. The user simply logs in and uploads the acceleration time history data to the server via the web view object. Figure 3.2 shows three screenshots of the iOS application interface, which enables the users to interact with the smartphone sensors and the server. The application Citizen Sensors for SHM is currently available at the iTunes Store [75]. Further sources regarding the iOS application development can be found in [76, 77]. This application is developed for iOS, and can be extended to different mobile operating systems such as Android, Windows Mobile, and Blackberry 10 in the future, provided that smartphone models have embedded accelerometers.

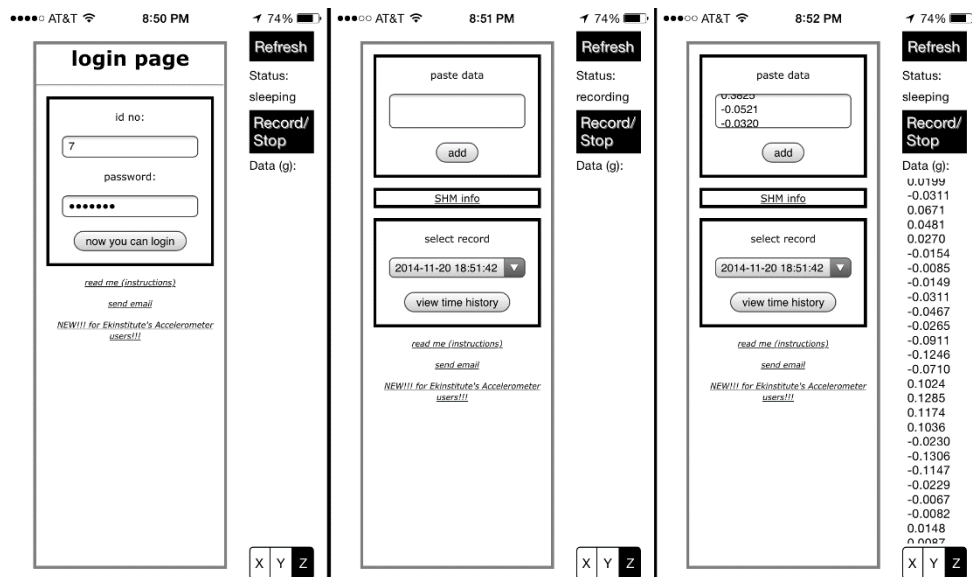


Figure 3.2: User login, recording, and submission screenshots

3.2.2 Server-side processing and database

The web-based server-side platform receives the acceleration time history data measured by the citizens at a structure, processes the data to identify the modal properties of the structure (such as the modal frequencies) which are correlated with the structural health conditions as shown in previous studies, and stores the results as well as the raw data. An administrator may be granted with an online access to the data in the server. A number of computer languages are used to build the platform. PHP (formerly Personal Home Page, recently PHP: Hypertext Preprocessor) is used as the main scripting language throughout webpage development process. The database is constructed with MySQL (SQL: Structured Query Language), and automatically updated by MySQL codes embedded in PHP scripts. In order to produce a web interface with a user friendly design, HTML (HyperText Markup Language) and CSS (Cascading Style Sheets) scripts are developed. A web platform was built on a server hosted by a commercial web-hosting service and is accessible online [78].

The system is designed to provide an online SHM environment which is capable of being used by multiple users and multiple structures at the same time. The system receives the acceleration time history from the users, conducts discrete Fourier transform (DFT) analysis, determines peak frequency and stores the input and the output data with the submission details such as measurement date, record number, and user identification number. Figure 3.3 summarizes the digital signal processing applications implemented in server-side to apply band-pass filter to the acquired raw data and compute the natural frequency based on the DFT results [79].

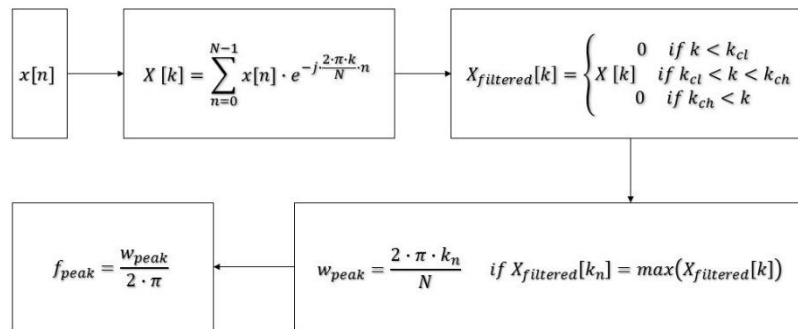
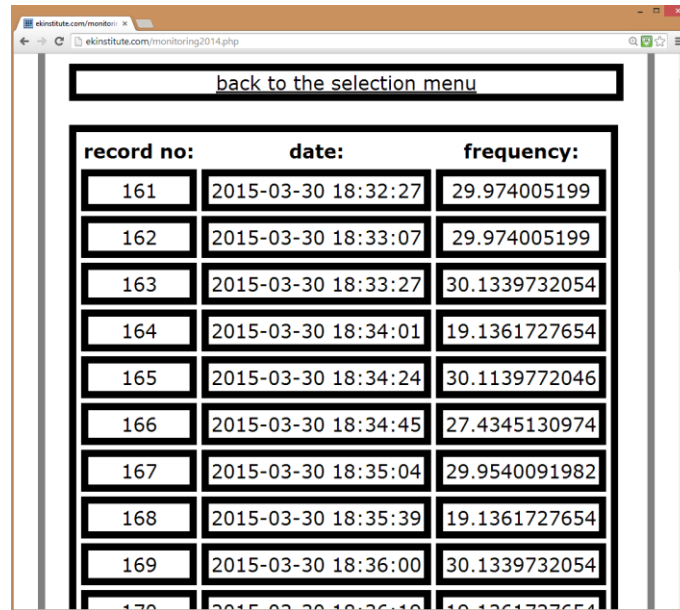


Figure 3.3: Server-side digital signal processing operations

The web users are divided into two categories, citizens and administrators. Citizen accounts are created, managed and given access to records by the administrator and do not have permission to modify database except vibration data submission. Other than that, citizens have access to view the information related to their account. A new account is created with an automatically generated identification number. Similarly, once the platform is ready to be used at massive scales, citizens will be provided with randomly generated passwords. In other words, the platform will not store any personal information until privacy, anonymity, and security issues are comprehensively dealt with. Furthermore, volunteers will be offered to opt-out to avoid violation of privacy. Administrators can activate or deactivate citizen accounts, have access to the data provided by citizens such as analysis results or vibration time history records either for a specific structure or multiple structures. This ability provides the potential to develop a further relationship between long-term monitoring records and reveal correlations between common environment-induced parameters (e.g., wind, temperature changes, earthquakes) to generate big data. However, because the proposed platform has recently been initiated, big data analytics is a long term goal and is not addressed in this study.

The web platform is built on PHP scripts referencing each other according to the submission or monitoring process. The hierarchical script reference order for a user starts with the index as the first step, login as the second step, view of user's own monitoring results and previously submitted data, or addition of new data as the third and the last step. Viewing one's own monitoring results on landmark structures (e.g., Eiffel Tower, Golden Gate Bridge) can be one of the incentives that motivate citizens to participate as crowdsourcers. The administrator account has the same hierarchy except its access is extended to the entire database, and can delete or assign new user accounts. Further details regarding PHP-MySQL integrated web development are referred to [80]. Figure 3.4 is an example of the interface showing the overall measurement results at a specific structure, including the record number, measurement date and the structure's natural frequency in Hz identified from the vibration measured at the structure system



record no:	date:	frequency:
161	2015-03-30 18:32:27	29.974005199
162	2015-03-30 18:33:07	29.974005199
163	2015-03-30 18:33:27	30.1339732054
164	2015-03-30 18:34:01	19.1361727654
165	2015-03-30 18:34:24	30.1139772046
166	2015-03-30 18:34:45	27.4345130974
167	2015-03-30 18:35:04	29.9540091982
168	2015-03-30 18:35:39	19.1361727654
169	2015-03-30 18:36:00	30.1339732054
170	2015-03-30 18:36:16	19.1361727654

Figure 3.4: Screenshot from the web interface showing the SHM results page

3.3 Crowdsourcing

Another important component of Citizen Sensors for SHM is citizens, therefore utilizing citizens' enthusiasm for problem solving is crucial. In other words, crowdsourcing, basically collaborating with citizens, has an important role in system performance as well as the computer platform. For the purpose of understanding current crowdsourcing methodologies, a number of different approaches are evaluated.

Howe was the first to diagnose upcoming low-cost labor and production model for the industry, society and more [41]. Crowdsourcing, as a problem solving paradigm, was one of the actors replacing conventional, static, individual approaches with a novel, online, distributed model [42]. Like, the Internet, open source, and others, crowdsourcing—a virtual community—was one of the collaboration models identified by Albors et al. [43], and it was able to “create value for the general public [44]” even without a profit incentive.

Stemming from multiple theoretical foundations such as value chain, auction, motivation crowding, organizational learning, cognitive evaluation, transaction cost, strategic management, innovation and game theory [42], a mutual agreement regarding crowdsourcing definition still has not been established. Albors et al [43] presented a taxonomy which classifies collaboration alternatives according to social and information connectivity. Schenk and Guittard [46]

distinguished crowdsourcing from related concepts such as open innovation, user innovation and open source software, classified different crowdsourcing practices, and discussed a number of opportunities and threats. Eventually, Estelles-Arolas and Gonzalez-Ladron-de-Guevara collected 32 different definitions, investigated their commonly-agreed aspects, and came up with a comprehensive definition based on the trend of existing studies [47]:

“Crowdsourcing is a type of participative online activity in which an individual, an institution, or company proposes to a group of individuals of varying knowledge, homogeneity and number, via a flexible open call, the voluntary undertaking of a task. The undertaking of the task, of variable complexity and modularity, and in which the crowd should participate bringing their work, money, knowledge and/or experience, always entails mutual benefit. The user will receive the satisfaction of a given type of need, be it economic, social recognition, self-esteem, or the development of individual skills, while the crowdsourcer will obtain and utilize to their advantage what the user has brought to the venture, whose form will depend on the type of activity undertaken.”

Based on the preexisting crowdsourcing definitions and classifications, the authors attempted to develop an SHM-oriented crowdsourcing model to receive smartphone sensor data via citizen contribution. A crowdsourcing model can be prepared by setting the proper actors and their corresponding actions. A robust classification defines crowdsourcing actors as “the crowd”, “the initiator”, and “the process” [47]. “The crowd” element is defined by (1) “who forms it”, (2) “what it has to do”, and (3) “what it gets in return” [47]. Similarly “the initiator” description must reveal (1) “who it is”, and (2) “what it gets in return” [47]. Finally, “the process” refers to “the type of process, the type of call, and the medium used” [47]. Likewise, crowdsourcing actors can be distributed into three groups: individuals as crowd participants, beneficiary company/institute, and the platform connecting individuals and beneficiaries [46]. Crowdsourcing tasks can be divided into three groups: “cognitive dimension”, “nature of incentives” and “benefits of crowdsourcing” [46]. What is more, based on the individual value’s importance with respect to the community, crowdsourcing can be either “integration-based” or “selection-based” [46]. Similarly, crowdsourcing dimensions can be described by agents such as “provider”, “mode”, “ownership”, and “motivation and incentive” [45]. In addition, crowdsourcing can be divided into elements such as “components”, “processes”, and “actions” [45]. Finally, the future crowdsourcing problem will evolve due to different perspectives such as “participant”, “organization”, and “system” [45].

Based on these foundations, the authors formulated the proposed crowdsourcing model with three actors [47], groups [46], or perspectives [45]: citizens, administrators, and web platform. Citizens herein are described as people who are motivated to take measurements of structures (such as buildings and bridges) and submit the data with their smartphones. Likewise, administrators' motivation is to collect the best available vibration data and maximize structural system identification efficiency and accuracy. Finally, the process will involve mobile sensing, submission, server acquisition, digital signal processing, and database storage. The proposed system can be constructed on a combination of "integration-based" and "selection-based" crowdsourcing, since every participant is likely to have a different contribution accuracy, yet compose a strong, integrated platform when combined together [45–47].

In order to apply these crowdsourcing concepts to citizen-engaged smartphone-based structural health monitoring, a number of uncertainties causing variation in measurement results must be studied. Basically, these can be divided into (1) user-related; (2) hardware-related; and (3) structure-related uncertainties. User-related uncertainties can stem from a variety of different issues including users' understanding of the crowdsourcing problem and platform, third-party accessories attached to their smartphones, and the time and quality of their measurement. Hardware-related uncertainties are mainly due to the model/performance of the sensors and CPU's embedded in the users' smartphones.

Structure-related uncertainties can be caused by different vibration loading patterns including ambient vibration, operational vibration and extreme events (such as earthquakes). Considering these uncertainties, the authors specified crowdsourcing parameters including the vibration loading type, the smartphone model, the phone-structure coupling, the phone position, and measurement duration.

Finally, to provide the connection between citizen sensors and crowdsourcing, it is essential to understand the potential of smartphone sensors, with an emphasis on participatory sensing and mobile crowdsourcing aspects. For this purpose, a taxonomy discussing mobile crowdsourcing applications is taken as a reference, which defines a crowdsourcing solution in terms of its web-extension, involvement, data wisdom, contribution quality, incentives, human skill, sensors, and location [81]. The mobile crowdsourcing taxonomy characteristics are discussed from a citizen-engaged SHM perspective below:

3.3.1 Sensors

Smartphone sensors may not only serve crowdsourcing-based SHM with sole vibration data, but also enable citizens to obtain “smarter” measurements. For example, orientation errors due to smartphone placement can be corrected instantaneously by utilizing smartphone gyroscope. GPS and magnetometer data provides the server with the measurement location and direction that can be used to match the phone position with the structure and avoid submissions from false locations. Server-side workload can be reduced, and signal processing speed can be extensively increased by using smartphone processors as components of a distributed computing platform. If applicable, structural nodes can be assigned information features (e.g., barcodes, matrix codes) and can be automatically detected by smartphone cameras. Nearby excitation sources such as vehicles can be detected with the microphones, and their effects can be classified accordingly. If the environment is rich in participants, the devices can be synchronized with Bluetooth or Wi-Fi connection, and simultaneous data can be gathered from multiple channels.

3.3.2 Data wisdom, contribution quality, web extension

Combining the mobile features [75] with the web server [78], it is possible to improve the crowdsourcing value by converting individual submissions into collective data as a means of data wisdom. In particular, averaging collective Fourier spectra will improve the individual results by discarding the noise. Thanks to a central platform with a structured database, heterogeneous and homogeneous vibration data can be organized, mined and structural features can be extracted even if the datasets involve high complexity.

3.3.3 Human skill and incentives

The way crowdsourcing-based SHM receives contributions is a mixture of labor and visual human skills which is ideally reduced as platform improvement progresses. These skills (adjusting device’s position, coupling conditions, sampling duration etc.) can be improved with motivation sources or educational tools (e.g., demos, instructions, user manuals). There is a wide variety of incentives that can be utilized such as receiving awards or safety (monetary, service), gamification (entertainment), and social responsibility (ethical). For example, the identification problem can be

gamified such that the most accurate citizen submission can be rewarded. Likewise, a threshold can be set, and the citizens who have significant contribution can be acknowledged and honored. The platform can be linked to social media for advertisement and can attract those attention who are likely to participate in a novel crowdsourcing platform.

3.3.4 Involvement

By nature, crowdsourcing-based SHM involves many challenges due to its complicated structure. The quality of the vibration data depends on citizen's intuition as well as the sensor quality. With the help of proper participatory sensing and mobile crowdsourcing strategies, though, citizen-induced error can be minimized. At this stage, Citizen Sensors for SHM resembles a hybrid crowdsourcing platform with participatory and opportunistic components. In other words, the participatory aspect is characterized by the smartphone user's skills, whereas the opportunistic aspect basically relies on computer and sensor properties. Using all of the hardware and software capabilities to the best extent, the mobile crowdsourcing problem can partially be reduced from participatory to opportunistic, which differs from classical crowdsourcing approaches by taking advantage of mobile crowdsourcing tools [81].

To summarize, the crowdsourcing-based SHM presented in this study is already capable of using accelerometers, can be provided with further sensor and location services, and has the web extension, which are some of the mobile crowdsourcing fundamentals. As the platform is improved with the new sensors, computational tools, and services, the majority of the human skills will be replaced with sensor data. Moreover, many different incentives can be created depending on society's and urban infrastructures' needs. In addition, the platform presents a unique crowdsourcing solution in the way it combines participatory and opportunistic involvement, individual and collective data wisdom, heterogeneous and homogeneous contributions in a transitive manner. Table 3.1 presents the prospective Citizen Sensors for SHM (CS4SHM)'s characteristics with the taxonomy and the examples provided by [81].

Table 3.1: Mobile crowdsourcing taxonomy

Application	Web	Involvement	Data	Contribution	Incentives	Skill	Sensors	Location
Gigwalk.com	Yes	Participatory	Individual	Heterogeneous	Monetary	Labor	Camera	Yes
CityExplorer	No	Participatory	Collective	Homogeneous	Entertainment	Visual	Camera	Yes
PotHole	No	Opportunistic	Collective	Homogeneous	Ethical	Non	Vibration	Yes
CS4SHM	Yes	Both	Both	Both	Multiple	Multiple	Multiple	Yes

3.4 Pedestrian link bridge case study

Field measurements are conducted in order to evaluate the capability of the Citizen Sensor system developed in this study. The purpose of these tests is to evaluate the integrated SHM system with firsthand experience. Moreover, the system is tested to see if it can produce valuable modal identification results for SHM purposes. In other words, accuracy of modal identification is important for SHM, since they are highly correlated with structural integrity. Finally, the citizen-induced uncertainties such as coupling, positioning, and duration are studied. Therefore, implementation of the proposed platforms is tested on a pedestrian bridge structure which is widely accessible by citizens.

The structure is an 11-m single span steel arch bridge, which serves as a passage between two multistory buildings. Because bridge flexibility is expected to be higher than adjacent reinforced concrete multistory buildings, dynamic effects due to these adjacent structures are not considered. Figure 3.5 shows the inner and outer views of the bridge structure, dimensions, and sensor layout for reference measurements.

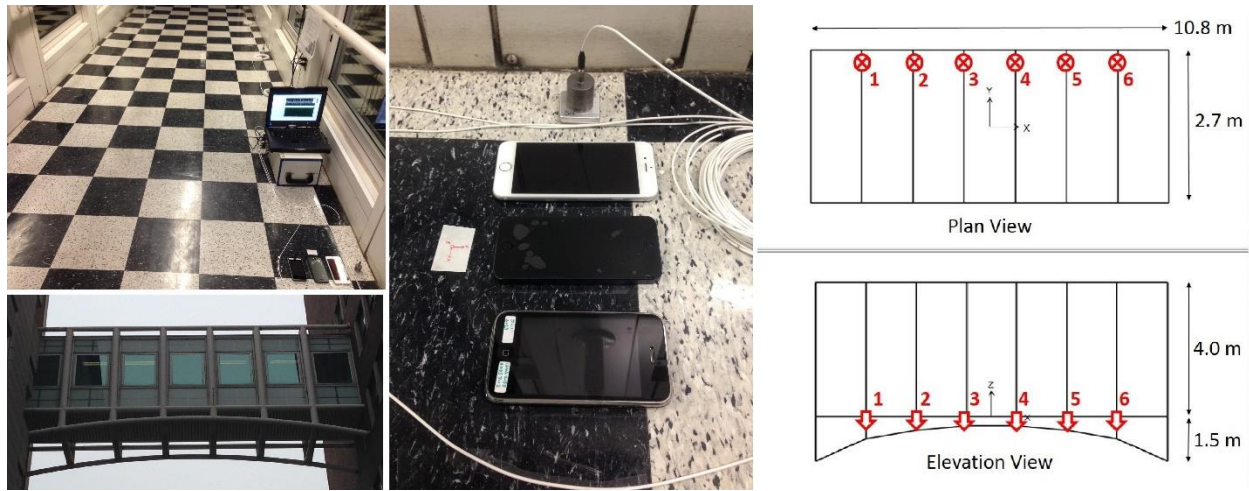


Figure 3.5: Bridge views, dimensions, and sensor layout

The bridge is instrumented with six high-quality reference piezoelectric accelerometers of model 393B04 PCB Piezotronics. The reference accelerometers are fixed via double-sided adhesive tape. The data is transmitted through cable connection, and acquired by a data acquisition system (National Instruments SCXI-1531) synchronously at a sampling rate of 100 Hz. The measurements are sequentially conducted at nighttime, to minimize passenger-induced vibrations and obstructions in the test procedure. In other words, the ambient vibration is dominated by low-amplitude environmental effects such as wind, rather than walking-induced structural input. Then, the Frequency Domain Decomposition (FDD) method is used to conduct modal identification and obtain modal frequencies and mode shapes as the reference. Afterwards, a number of tests with changing coupling conditions and sensor locations are conducted to compare smartphone measurements with reference measurements and evaluate smartphone sensor behavior under different citizen-induced conditions.

3.4.1 Measurement, data processing, modal identification

In order to determine modal characteristics of the bridge structure, high-quality, synchronous, multichannel vibration data is acquired and processed as the reference. The accelerometers are oriented in the vertical direction, and are equally spaced spanning the longitudinal direction, as shown in Figure 3.5. Therefore, acceleration time histories at six different locations are obtained under ambient vibration and processed with FDD method to determine modal frequencies and

mode shapes in vertical direction. By discretizing multi-channel vibration data in the frequency domain, arrays of spectral values are generated for each discrete frequency step. Singular value decomposition of these matrices will result in eigenvalues and eigenvectors, which corresponds to the singular values and modal displacements as a function of frequency. These functions are used to determine the modal frequencies and mode shapes. For brevity, the first three modes in vertical direction are considered, whereas lateral, longitudinal and torsional, and higher modes are not discussed. Further details regarding FDD method can be found in [82].

Figure 3.6 shows the singular value spectra obtained from FDD analysis. It is observed that the second and the third modes dominate the vibration characteristics, and spectral value due to first mode is relatively small. Accordingly, the first, second and third modal frequencies are identified as 8.46, 18.95, and 29.67 Hz, respectively. The mode shapes corresponding to the first, second and third modes are presented in Figure 3.6. According to these mode shapes, modal displacements due to the first, second, and third mode are maximized at Node 4, Node 3, and Node 2, respectively.

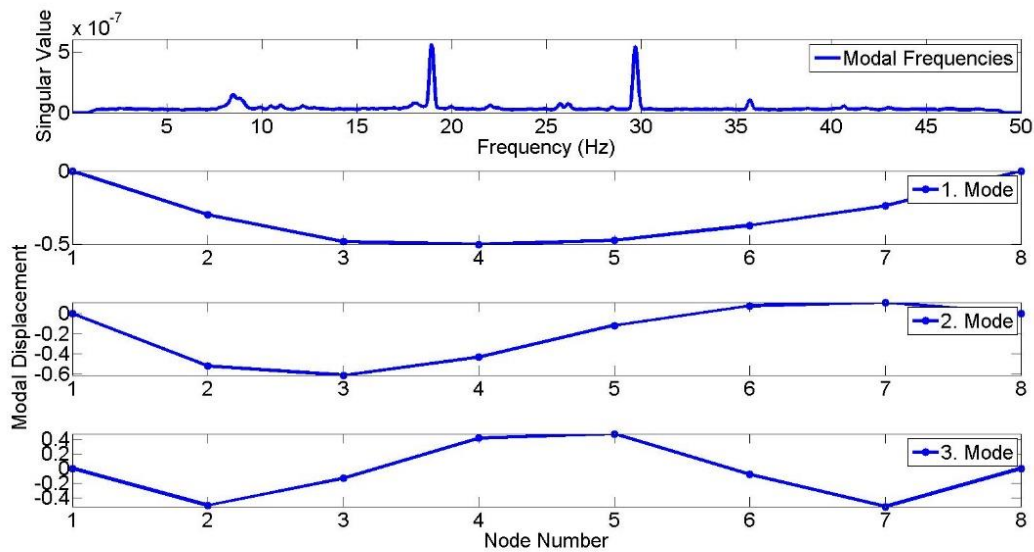


Figure 3.6: Modal frequencies and mode shapes identified by reference accelerometers

3.4.2 Uncertainties associated with citizen participation

After the system's dynamic characteristics are determined with the advanced reference system identification tools, smartphone measurements are taken to compare their performance with the reference results. Based on the crowdsourcing discussions presented in Chapter 3.3, a number of tests are conducted to characterize smartphone performance under changing user-related conditions. These conditions include different coupling conditions, as well as location effects. These parameters are evaluated for different smartphone generations such as Smartphone 1, Smartphone 2, and Smartphone 3 which corresponds to iPhone 3GS, iPhone 5, and iPhone 6, respectively. In keeping with the crowdsourcing discussions in Chapter 3.3, a number of principles are developed to maximize citizen engagement. These principles characterize the uncertainties and challenges of a potential crowdsourcing-based SHM methodology such as:

- (1) Smartphone location and orientation might change according to smartphone users' initiative.
- (2) Smartphone coupling conditions might vary according to external accessories or surrounding material.
- (3) Measurement duration can extensively vary according to the users' motivation.
- (4) Users should not be subjected to additional charges for data submission and therefore are allowed to prefer different communication platforms to submit data (wireless, cellular, etc.).

Considering these principles, a number of regulations are made to decrease the level of uncertainty. For instance, for this structure, unless external mounting instrumentation is used, the only convenient device orientation is the z-direction, with the phone's rear side facing the bridge deck surface. Therefore, other device orientation effects are not considered as influential parameters. For modes other than the vertical ones, the mobile application allows users to adjust the sensing direction. Moreover, to allow user benefit from smartphone communication capabilities in the preferred way, one can either submit data right after acquisition or keep the time history as a text file until preferred communication tools are available. What is more, citizens are not expected to spend a long time on the bridge; instead, they stop by for a limited amount of time, not more than a few minutes. Therefore, data submissions are received in small data packages and every one-minute data is presented as a sample. The strategy to take advantage of crowdsourcing presented herein is to keep citizen comfort high and receive large numbers of samples from a large-

sized community, rather than being dominated by few users. Eventually, the monitoring results will rely on the society as a whole rather than a small number of individuals.

In order to implement these principles into the developed platform, a number of different tests are conducted to evaluate these crowdsourcing effects on sensing performance. Table 3.2 presents the parameters of six different tests which vary in measurement location and coupling conditions. Test 1, Test 2, Test 3, and Test 4 compare smartphone sensor performance under different coupling conditions, whereas Test 3, Test 5, and Test 6 observe the difference between different sensor locations. Therefore, in Test 1, Test 2, Test 3, and Test 4, smartphones are either attached to the bridge floor with double-sided adhesive tapes, or set free to move with or without a smartphone case, or contained in a bag. Test 3, Test 5, and Test 6 keep the coupling conditions constant while sensor location is different such as mid-span, one-third span, and one-sixth span.

As mentioned before, to maintain citizen patience and motivation throughout measurements, duration of a sample is set equal to one minute. This is contradictory with the conventional ambient vibration measurement practice, because long-duration measurements are more reliable for removing random noise. While the measurement duration of each citizen is relatively short (i.e., one minute), a significant number of submissions from many citizens are expected to achieve reliable measurement results.

Table 3.2: Field measurement with different sensor locations and coupling conditions

Test No	Time (min)	Sensor Location	Coupling Conditions
1	40	Mid-span	Adhesive Taped
2	40	Mid-span	Free to Move–With Case
3	40	Mid-span	Free to Move–No Case
4	40	Mid-span	Free to Move–In Bag
5	40	One-third Span	Free to Move–No Case
6	40	One-sixth Span	Free to Move–No Case

In this study, it is observed that most of the smartphones measured the bridge's ambient vibration reasonably well. Figure 3.7 shows the time history and Fourier spectra of two samples obtained during Test 3 and Test 6. According to Figure 3.7, similar to the reference modal identification results, dominant peaks are located at 20 and 30 Hz whereas the first modal peak is less significant around 8.5 Hz. According to the time histories and Fourier spectra, it is seen that vibration signal amplitudes change according to the smartphone generation. For instance, it is seen that the reference sensor has the lowest amplitude, whereas amplitude increases as the smartphone model gets older. Likewise, it can be observed that Smartphone 1 measurements have very high amplitudes in the time domain, and high spectral values in the frequency domain. These coincide with the relatively low sensor quality of Smartphone 1 discussed in [1] and the measurements are corrupted due to high level of noise. In other words, there is a correlation between the measured amplitudes and the sensitivity levels of accelerometers which are 18, 1, and 0.24 mg/digit for Smartphone 1, Smartphone 2, and Smartphone 3, respectively. Detailed information for Smartphone 1, Smartphone 2, and Smartphone 3 sensors can be found from the datasheets of the accelerometers LIS331DL (ST Microelectronics), LIS331DLH (ST Microelectronics), and BMA280 (Bosch Sensortec), respectively.

Another way to observe noise effects is that the Fourier spectra of Smartphone 1 are extremely broad-band, which resembles a typical white noise spectra and does not reflect structural vibration characteristics. Looking at the newer smartphone generations, Smartphone 2 and Smartphone 3, the smartphone signal amplitude is greatly reduced as the noise level reduces and the structural peaks become more significant as the smartphone generation gets younger. A similar pattern can be observed by evaluating the Arias intensity of acceleration signals which is a measure of signal energy [18, 83] and is correlated with the area under the vibration signal.

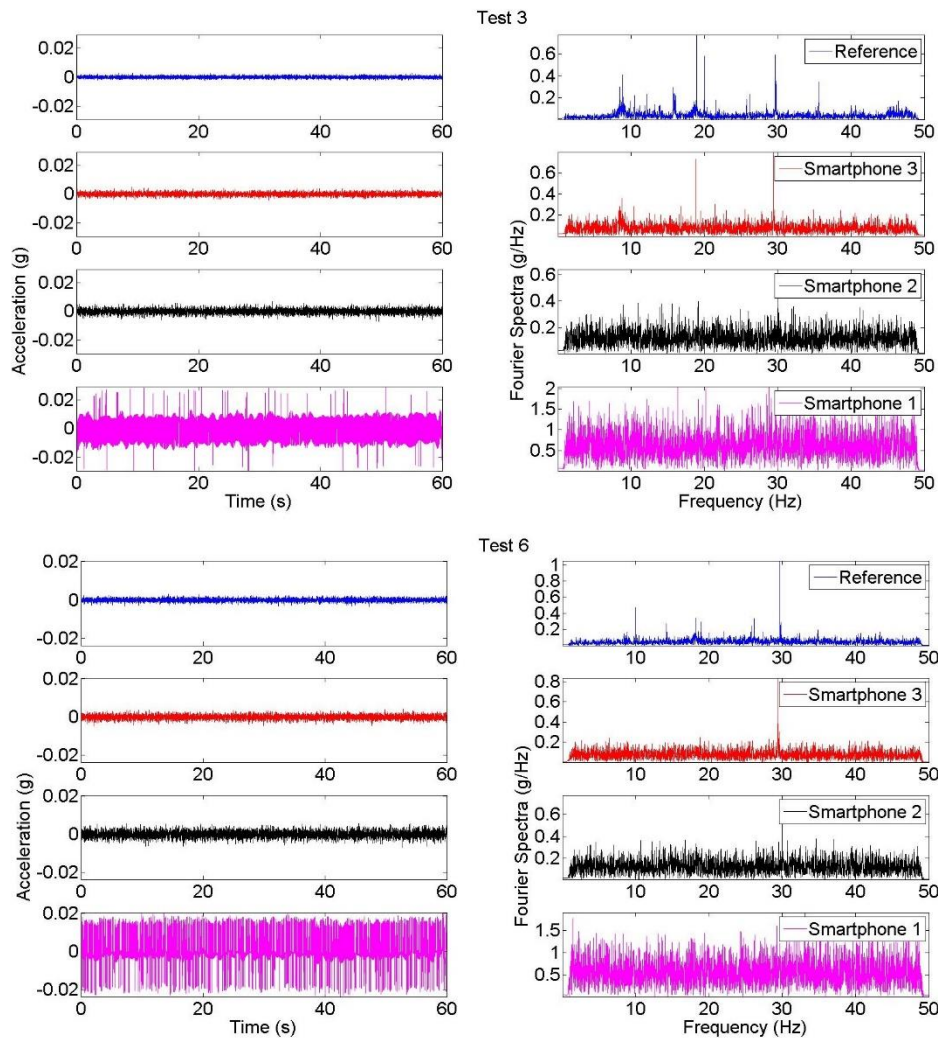


Figure 3.7: Time histories and Fourier spectra samples from Test 3 and Test 6

A long measurement duration (several minutes) is desired to measure low-amplitude ambient vibration of a real structure, in order to average out random noise. When engaging a large number of citizens to do the measurement, however, even a short measurement duration from each citizen might be sufficient, as long as the total duration of measurement is sufficiently long. This study tested this by collecting and averaging 40 individual samples as in Figure 3.7. Averaged Fourier spectra curves are obtained with no overlapping between samples. Each one-minute sample is transformed into the frequency domain with a frequency resolution equal to 0.0167 Hz. An overall dataset corresponds to 40 samples and a total duration of 40 min, because the samples are processed with no overlapping. Figure 3.8 shows the averaged spectral curves obtained from

different tests. Compared with the spectra obtained from a single sample, it is observed that noise level is significantly reduced, and peaks representing modal frequencies are much more significant.

Comparing averaged spectra of different tests, it is observed that Test 1, Test 2, Test 3, and Test 4 spectra have the same characteristics, whereas there is a significant reduction in 1st and 2nd modal frequency peaks in Test 5 and Test 6. This reveals that the proposed coupling conditions did not have a significant effect on spectral values since Test 1–4 has the same location at mid-span. The difference in Test 5 and Test 6 is due to the location difference between tests. For instance, Test 3 and Test 4 location corresponds to the location of one-third and one-sixth span unlike other tests.

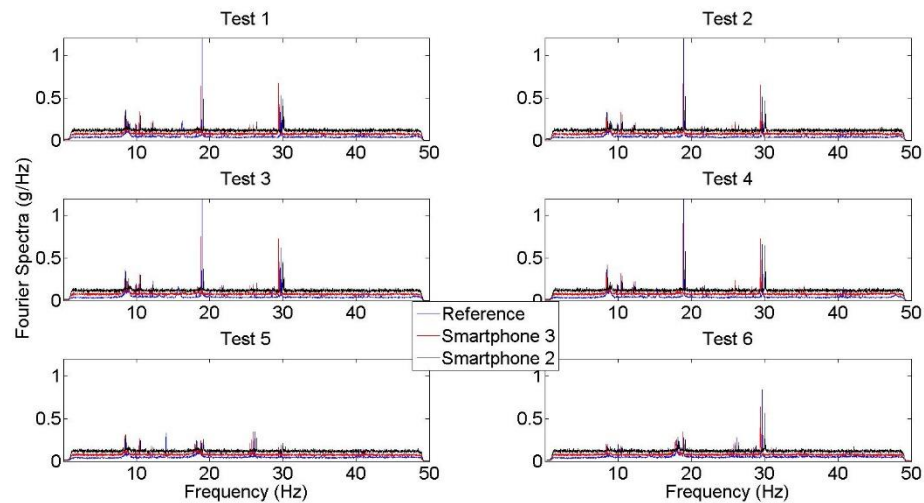


Figure 3.8: Fourier spectra from the average of 40 samples for Test 1-6

To summarize overall modal identification performance, the peak frequency values obtained from a large number of samples are plotted in Figure 3.9. It can be observed that Smartphone 2 and Smartphone 3 modal identification results match reference measurements with a significant accuracy, whereas Smartphone 1 results do not provide any modal information as they are masked by the high noise level. Moreover, the results of Test 1, Test 2, Test 3, and Test 4 show that Smartphone modal identification results are accurate even under challenging coupling conditions (i.e., free to move, with case, in bag). Likewise, modal identification results obtained from different locations still reflect structural characteristics, but the quality may change according to the modal

displacement of the measurement location. For instance, peaks obtained from Test 5 identify the second mode to a better extent, whereas third mode is more significant on Test 6 results. The reason is that second and third modal displacement is maximized at testing locations, which are Node 5 and Node 6, respectively. Finally, collecting all samples together, looking at Figure 3.9, the second and third modal frequencies are identified occasionally, whereas the first mode is identified in a small number of samples.

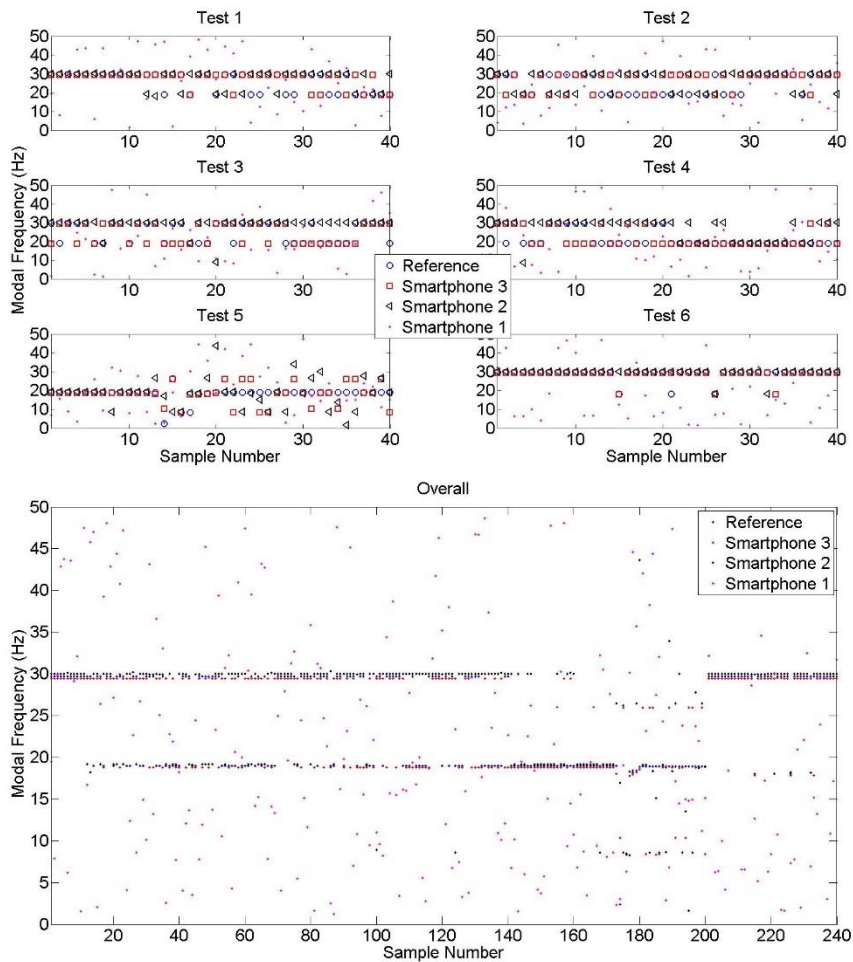


Figure 3.9: Identified frequencies obtained from different samples

In Figure 3.10, Arias intensity values are plotted to observe the energy difference between reference and smartphone sensors. The overall figure shows that there is a great difference between intensity levels obtained by Smartphone 1 and others. As explained before, the high level of noise

results in overestimation of energy in measurements, especially under low intensity ambient vibrations [1, 18]. Therefore, Smartphone 1 intensity is not demonstrated in Test 1–6 results to increase the graph resolution. According to the intensity values obtained from different tests, it is observed that the new generation Smartphone 3 performs better than Smartphone 2 due to the increased sensor sensitivity level. However, both results are considerably accurate as a means of modal identification under ambient vibration.

Table 3.3 summarizes the performance of smartphone sensors in terms of identified modal frequencies. The performance difference between different tests was insignificant and therefore not presented as individual results. The modal frequencies obtained from each averaged spectra are compared with FDD results, and error values are presented. The results show that Smartphone 1 is incapable of identifying modal frequencies. In contrast, new generation smartphones achieve highly accurate results such as 1.30%, 1.06%, and 1.05% for Smartphone 2; 0.71%, 0.79%, and 0.81% for Smartphone 3.

Table 3.4 shows mean and standard deviation values obtained from each test with 40-sample sets in terms of peak vertical acceleration (PVA) and Arias intensity. According to these results, it is seen that PVA and Arias intensity increases for older generation smartphones. For instance, the PVA value for reference sensors is close to 0.0038 g whereas Smartphone 1, Smartphone 2, and Smartphone 3 values range around 0.0045, 0.0066, and 0.0294 g, respectively.

Table 3.3: Identified modal frequencies

Sensor	$f_{1\text{averaged}}$	Error (%)	$f_{2\text{averaged}}$	Error (%)	$f_{3\text{averaged}}$	Error (%)
Reference	8.48	0.24	18.97	0.11	29.68	0.04
Smartphone 3	8.40	0.71	18.80	0.79	29.43	0.81
Smartphone 2	8.57	1.30	19.15	1.06	29.98	1.05
Smartphone 1	-	-	-	-	-	-

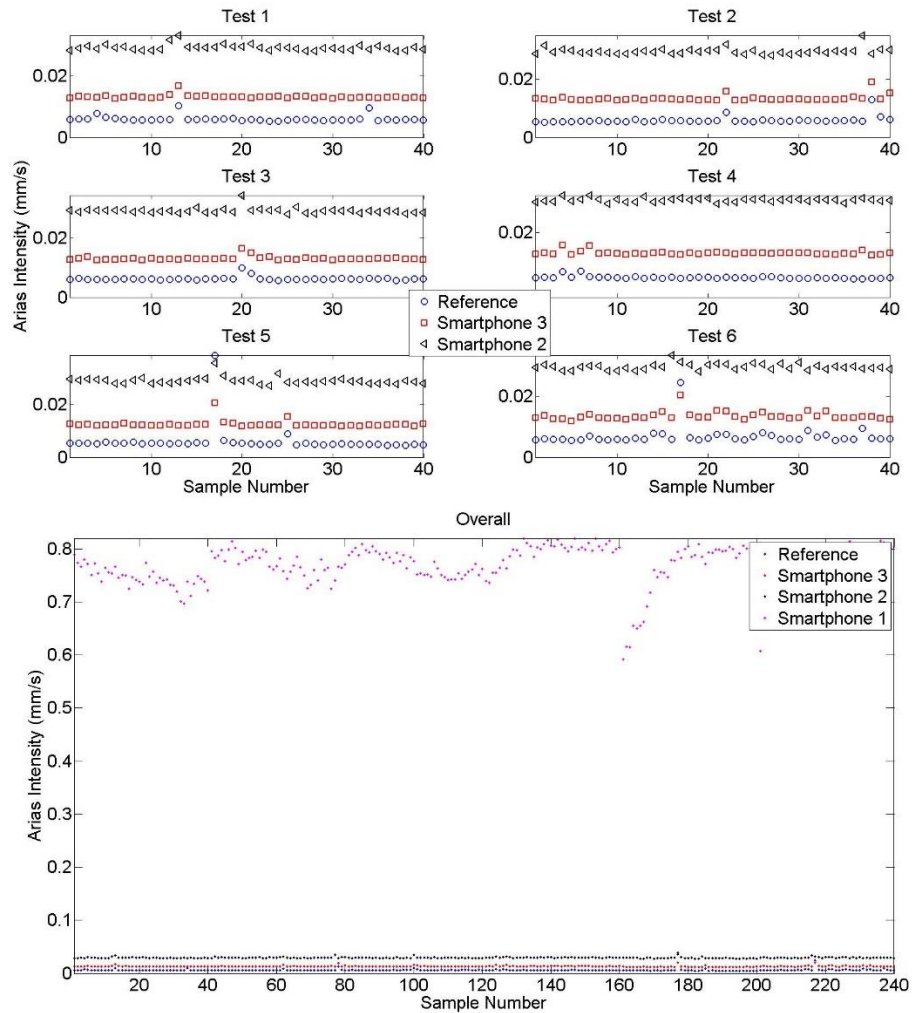


Figure 3.10: Energies obtained from different samples

Similarly, Arias intensity values are approximately 0.006, 0.013, 0.029, and 0.75 mm/s for reference, Smartphone 1, Smartphone 2, and Smartphone 3, respectively. As indicated previously, such difference is likely to stem from the sensitivity level of each sensor. For example, compared with other sensors, low quality Smartphone 1 accelerometer’s amplitudes are extremely higher in terms of PVA and Arias intensity. The PVA and Arias intensity difference between different generations show that smartphone performance, in terms of amplitude, varies significantly according to the smartphone model unlike frequency domain performance. What is more, it is observed that the intensity level is not subjected to change throughout different samples, which means, smartphone sensors’ performance is stable over time.

Finally, after investigating the citizen-induced parameters, student volunteers are assigned to test the crowdsourcing-based SHM platform. 135 samples are received, automatically processed, and the identification results are inserted into the web database. Figure 3.11 shows the distribution of crowdsourcing-based submission results compared with the results obtained from Tests 1–6. The distribution results show that there is a higher dispersion in crowdsourced identified frequencies, yet there is a similar trend with the Test 1–6 results which are conducted in a relatively controlled environment. Moreover, it can be observed that the crowdsourcing-based results tend to identify the 1st mode more often, whereas Test 1–6 results are concentrated on the 2nd and the 3rd modes.

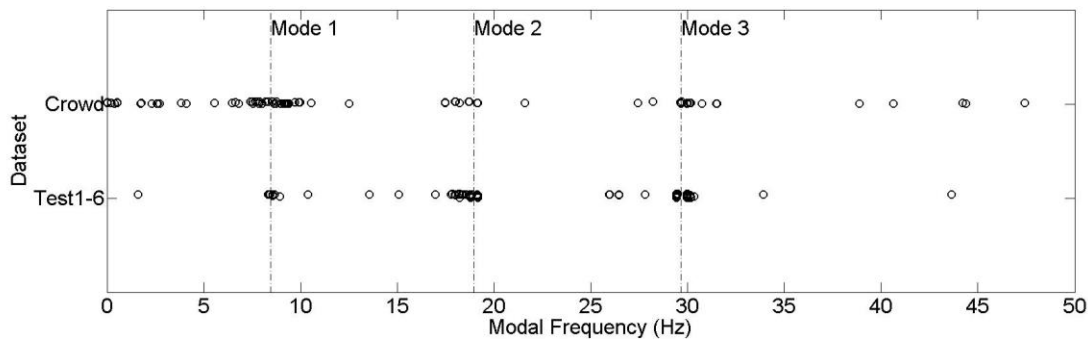


Figure 3.11: Modal identification results from Test 1-6 and crowdsourcing

In SHM practice, the dynamic load patterns might also have an effect on identification results. Test 1–6 are conducted under ambient vibration, which can be considered an output-only problem. On the contrary, operational loads such as pedestrian-induced or vehicle-induced vibrations might have dominant frequencies which will influence the identification results. For example, when a pedestrian walks on a bridge, the bridge is subjected to a harmonic vibration of approximately 1.6–2.4 Hz [84]. Therefore, pedestrian-induced vibrations tend to excite the modes which are close to 1.6–2.4 Hz. To reveal this effect, measurements are obtained under walking-induced vibration, and presented in Figure 3.12. Accordingly, it is seen that the 1st modal frequency, which is the closest frequency to pedestrian-induced frequencies, is significantly excited. This might explain why uncontrolled crowd dataset is dominated by Mode 1, whereas ambient vibration datasets frequently identify Mode 2 and Mode 3.

Table 3.4: Statistical values of peak vertical acceleration and energy

Test No	Sensor	PVA_{μ} (g)	PVA_{σ} (g)	AI_{μ} (mm/s)	AI_{σ} (mm/s)
1	Reference	0.0041	0.0030	0.0061	0.0010
	Smartphone 3	0.0044	0.0004	0.0133	0.0007
	Smartphone 2	0.0064	0.0005	0.0293	0.0010
	Smartphone 1	0.0278	0.0017	0.7455	0.0202
2	Reference	0.0036	0.0032	0.0060	0.0013
	Smartphone 3	0.0046	0.0010	0.0134	0.0011
	Smartphone 2	0.0067	0.0006	0.0297	0.0012
	Smartphone 1	0.0286	0.0022	0.7718	0.0218
3	Reference	0.0031	0.0008	0.0063	0.0007
	Smartphone 3	0.0044	0.0007	0.0131	0.0007
	Smartphone 2	0.0065	0.0006	0.0292	0.0010
	Smartphone 1	0.0289	0.0022	0.7710	0.0206
4	Reference	0.0031	0.0009	0.0061	0.0005
	Smartphone 3	0.0045	0.0006	0.0136	0.0006
	Smartphone 2	0.0068	0.0007	0.0299	0.0006
	Smartphone 1	0.0297	0.0020	0.7952	0.0210
5	Reference	0.0042	0.0048	0.0061	0.0053
	Smartphone 3	0.0044	0.0013	0.0125	0.0014
	Smartphone 2	0.0067	0.0009	0.0290	0.0014
	Smartphone 1	0.0308	0.0032	0.7560	0.0622
6	Reference	0.0049	0.0046	0.0069	0.0030
	Smartphone 3	0.0047	0.0007	0.0136	0.0014
	Smartphone 2	0.0065	0.0005	0.0296	0.0010
	Smartphone 1	0.0307	0.0023	0.7737	0.0487

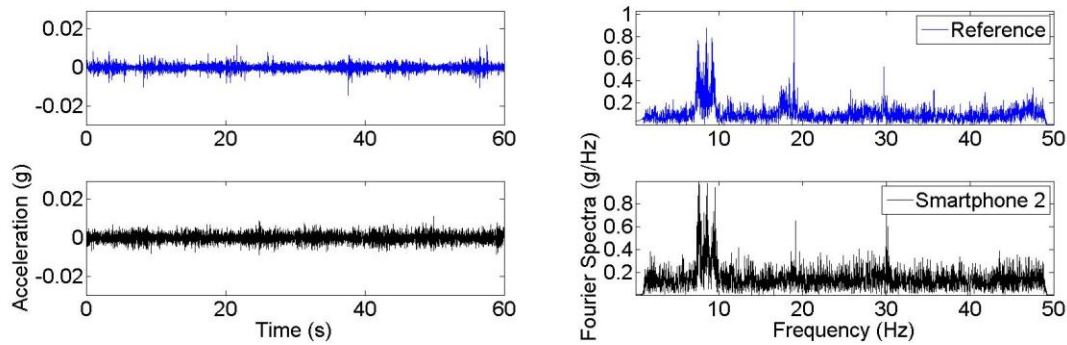


Figure 3.12: Time histories and Fourier spectra samples during pedestrian pass

To summarize, the field measurement results show that the modal identification of the bridge structure can be conducted efficiently by the developed platform integrating citizens, new generation smartphones, and web-based server capabilities. In particular, as citizens continue providing more samples, the identification results will become more reliable and will provide useful information for big data generation. Using this platform, an online, remote, automated, secure and long-term monitoring system can be established and tested on multiple structures.

3.5 Conclusions

This study develops a novel SHM platform based on citizen crowdsourcing and smartphone sensors. The platform not only provides citizens with the necessary tools to measure and submit structural vibration using their smartphones, but also automatically processes the citizen-submitted data at a server to identify structural modal parameters (such as natural frequencies) useful for long-term structural health monitoring. A mobile application called Citizen Sensors for SHM was developed for measuring structural vibration with the smartphone-embedded accelerometers and submitting the data to the server. A web-based software package was developed for receiving and processing the citizen submission data on the server. Finally, the integrated system was evaluated on a real bridge structure using different smartphone generations under varying coupling and location conditions. High-fidelity accelerometers are also used as reference sensors. Low-amplitude ambient vibration of the bridge was measured by both the reference and smartphone sensors. The structural modal properties were identified and compared. The performance of the proposed platform and the test results can be summarized as follows:

(1) The developed platform is novel in the way it utilizes ubiquitous smartphones, crowdsourcing and citizen engagement as means of vibration-based SHM. It lays a foundation for a future citizen-centered cyber-physical sensor system for monitoring the integrity and safety of spatially distributed urban infrastructure.

(2) Crowdsourcing-based SHM is a unique participatory sensing example in the way it synthesizes distinctive crowdsourcing parameters such as participatory and opportunistic involvement, multiple incentives, individual and collective data wisdom, and heterogeneous and homogeneous contribution with a hybrid human-sensor framework.

(3) Considering different generations of smartphone models, new generation smartphones provide better performance for vibration measurement. Time history data, Fourier spectra, and Arias intensity results show that as the phone generation gets younger, accuracy and sensitivity gets closer to the high quality reference measurements. In contrast, the oldest generation, Smartphone 1, is subjected to a high noise level which can mask structure's dynamic characteristics in vibration signals. Although amplitude performance changes significantly according to the smartphone generation, modal identification results obtained from new generation smartphones have extremely small errors ranging around 1%, whereas the oldest generation, Smartphone 1, is incapable of identifying modal frequencies.

(4) The results show that the presented phone-structure coupling conditions did not affect monitoring performance significantly. On the other hand, such observation is likely to change as the vibration level gets higher than ambient vibration. Therefore, coupling effects under operational or extreme environmental vibrations can be different, and should be investigated in the future.

(5) Sensor location has an important effect on identification results, since modal displacements vary according to the measurement location. For instance, data submissions from one-sixth span identify the 3rd mode frequently, whereas the 2nd mode is dominant for other submission locations.

(6) Collecting a large number of small-sized vibration data submissions and averaging their frequency spectra can generate a useful database for crowdsourcing-based modal identification and monitoring purposes. This enables the setup of a reliable large-sized database by small contributions from each citizen. In other words, retrieval of ubiquitous vibration data from

smartphones enables identification of modal frequencies accurately without excessive citizen effort.

(7) The web platform provides secure but online, automated, remote, and widely accessible media for vibration data and modal identification results. What is more, the mobile platform provides users with the opportunity to choose the preferred communication tools, which means users can submit the data either instantaneously or when preferred communication tools are available.

(8) The proposed methodology is cost-effective and sustainable since the sensor instrumentation and maintenance is provided spontaneously by smartphone users. If the crowdsourcing model is improved, and the mobile application is distributed among the community, it can become an innovative source for long-term SHM applications.

Based on the conclusions drawn from this study, a long-term monitoring study will be initialized which only relies on smartphone data rather than high-quality reference sensing platforms. The smartphone application developed herein will be distributed throughout the community and strategies for citizen encouragement will be developed. Moreover, the applicability of the proposed system will be investigated for different structures. Improvement of the multilayered platform with further tests, and validation of the system with citizen participation will be a novel contribution to the smart cities concept. Eventually, as the database size increases exponentially in the long term and the application is extended to new structures, a big data model will be introduced to effectively handle the extensive data variety, velocity and volume.

Chapter 4

Citizen-Induced Uncertainties

In this chapter, the effects of citizen-induced uncertainties on vibration measurements are highlighted, solutions to these problems using multisensory and heterogeneous data are discussed. The first (under revision in Smart Materials and Structures [85]), the second (published in the journal Smart Materials and Structures [86]), and the third (under revision in the International Journal of Distributed Sensor Networks [87]) subchapters are reproduced from the papers coauthored with Maria Q. Feng.

4.1 Orientation effects

4.1.1 Introduction

Advances in sensor technology and computational power, as well as extensive research in system identification, made structural health monitoring one of the highlighted topics in mechanical, aerospace, and civil engineering [2, 3, 88]. As a result of rapid urbanization and industrialization, the infrastructure stock tremendously increased in developed cities. Aging infrastructure, natural disasters, and manmade hazards threatened structural integrity, serviceability, and occupant safety; necessitating implementation of SHM technologies to a broader extent [89].

Shifting from nondestructive evaluation (NDE) to SHM, identification of structural characteristics gained a global, large-scale, and data-enriched perspective [90]. Gathering sensor data from multiple channels and processing data with advanced identification algorithms, structural models with uncertainties are validated, verified, or updated with monitoring data, and in this way, the actual dynamic behavior of structures is represented with a better accuracy.

Advent of the Internet, wireless communications, and cloud technology gave rise to remote

sensing, distributed sensor networks, and smart sensors in the last two decades. Due to practical and economic reasons, monitoring of civil infrastructure with temporary instrumentation became widely applicable compared with the sensor systems permanently embedded in structures. Integrating sensors with small-sized computing, data acquisition, and wireless data transfer units, smart sensor technology became a feasible choice for monitoring structural systems [91-94]. Likewise, taking advantage of the nonstationary features of the new monitoring systems, mobile sensing became one of the future directions in SHM research and industry [95-98]. In addition, the data obtained from different types of sensors is fused to integrate heterogeneous or non-homogenous data [99-102].

Smartphone industry rose tremendously in the last decade. Basically, smartphones are equipped with computing hardware such as central processor unit (CPU), randomly accessible memory (RAM), and data storage components. They are capable of sending and receiving data wirelessly with the help of Global System for Mobile Communications (GSM), Internet, and Bluetooth connection. What is more, thanks to the rapid advancements in Microelectromechanical systems (MEMS) technology, smartphones are equipped with low-cost sensors such as accelerometer, gyroscope, and magnetometer which can measure device motion in six degrees of freedom (6DOF). To summarize, smartphones can compose a large SHM sensor network which has all the features of typical smart, heterogeneous, and mobile sensing platforms.

Recent studies have shown that smartphones can be utilized for SHM purposes [1, 36, 39, 86, 103-107]. On the other hand, considering smartphone-based SHM as a participatory sensing problem, there might be a significant accuracy difference between conventional monitoring results and crowdsourced results [36, 108]. Coupling between the sensor and the measurement surface is very likely to affect the characteristics of vibration signals, as shown in mobile seismograph applications [18]. In other words, crowdsourcing-based vibration signals representing structural response can be corrupted or fully masked by the citizen-induced uncertainties. For this reason, sensor placement may play an important role in measurement results.

This study presents smartphone-based SHM solutions to citizen-induced uncertainty problems with an emphasis on the rotational distortion in the sensor position. Different smartphone sensors such as gyroscope, accelerometer, and magnetometer are used to develop a coordinate sensitive environment allowing the smart device to keep track of the orientation changes or determine sensor

position with respect to the structure of interest. Using iPhone Operating System (iOS) as an exemplary mobile operating system and developing a mobile application using Xcode, features such as attitude and heading can be extracted from Core Motion (CM) and Core Location (CL) programming frameworks.

In order to monitor the instantaneous sensor position and orientation changes, a coordinate system transformation procedure is proposed. A two-story laboratory structural model, an existing pedestrian bridge, and a large-scale suspension bridge are tested with the proposed procedure to correct sensor signals caused by improperly positioning of the sensors. The results show that the processed data matches actual vibration characteristics of structures with a significant accuracy in contrast with the distorted data. Using this procedure, location and orientation of a smartphone sensor with respect to a structure can be determined in terms of coordinate systems. Therefore, the smartphone sensor operators, namely citizens, need no prior information about the sensorial or structural coordinate systems, since the transformation between these systems can automatically be performed using smartphone sensor data. In summary, this study targets to develop a novel smart monitoring system which is capable of utilizing crowdsourced vibration data with heterogeneous and mobile sensing features despite sensors' rotational positioning uncertainties introduced by the citizens.

Chapter 4.1.2 explains an overview of smartphone sensors, including software, and hardware, with an emphasis on SHM usage. Data heterogeneity and smartness issues are discussed taking iOS environment as a mobile application platform. Chapter 4.1.3 discusses the analytical background that is used to correct distorted sensor signals with the help of coordinate system transformation procedures and multisensorial smartphone measurements. Chapter 4.1.4 presents the experimental and field applications of the proposed method on a 2DOF laboratory model and a real pedestrian bridge. Chapter 4.1.5 discusses coordinate transformation in multiple scales, using real smartphone data obtained from a large-scale civil infrastructure example, Golden Gate Bridge. Finally, Chapter 4.1.6 summarizes the overall work and presents the conclusions drawn from the test results.

4.1.2 SHM-focused smartphone features

Supported by mobile operating systems, instrumented with standalone computation and

wireless data transmission hardware such as processor, memory, and various communication technologies; smartphones have a great potential to construct an ubiquitous smart sensing and SHM network. A number of innovative SHM applications have shown that smartphones can be used for vibration monitoring of civil infrastructure. One of the unique features enabling smartphones to be used as SHM platforms is the integrated hardware and sensing environment. Smartphones are equipped with various sensors that allows users to acquire data from multiple media. What is more, thanks to the high quality CPU, RAM, and other hardware, smartphones can serve as standalone computers. These features are integrated with an advanced operating system, various developer tools and documentation enabling iOS programmers to customize their data acquisition platform. What is more, smartphones can communicate with the web, receive and transfer data via numerous tools such as cellular and Wi-Fi connection. Furthermore, with the help of embedded battery, they can operate without the need of an external power supply for a long time. All these features provide smartphones with the necessary foundation of a smart sensor, which may become a component of a distributed and wireless sensor network. In other words, with the help of smartphone hardware components; sensing, computation, communication, and programming aspects of smart monitoring procedure can all be performed on the smartphone side without the requirement of an external hardware, cable, power source, or computer. Taking iPhone 5 as an exemplary smartphone model, this chapter introduces the smartphone hardware and software components that can be utilized for vibration-based SHM.

4.1.2.1 Smartphone sensor components

Smartphones are instrumented with various sensors such as barometer, gyroscope, accelerometer, proximity sensor, camera, touch screen, microphone, ambient light sensor, magnetometer (magnetic compass), and more. This study discusses the potential of some of these sensors as smart vibration measurement devices and SHM instruments. Smartness herein is the result of multisensorial environment, as well as sensor-side acquisition, processing and storage without the need of any external computer device, storage hardware, or cables for data transfer.

First, and the most important of all, tri-axial smartphone embedded MEMS accelerometers can be used to measure acceleration in three directions. Likewise, measurement ability can be extended to 6DOF with the help of gyroscopes measuring the change in the device orientation over time.

With the help of the tri-axial gyroscope, smartphones are capable of measuring rotational rate of change as a function of time and can be used to identify the sensor position with respect to the structure, track rotational movements, and cancel out sensor distortions accordingly.

Global Positioning System (GPS) is another smartphone-embedded technology that can be used to detect the position of the structural node to be measured, or basically the sensor location. This information can be of great importance for structures where the vibration response varies according to the measurement node [36, 86]. Moreover, by monitoring the global position of a sensor attached to the structure, structural displacement time histories can be obtained. On the other hand, it has been shown that the smartphone GPS is not sufficiently sensitive to detect vibratory motion [39], although, deployment of a vast number of low cost sensors may improve the measurement accuracy [109]. Nevertheless, because that the smartphones serve as mobile sensors and they are operated by citizens in motion, smartphone location services can be essential to verify that a measurement submission is taken by the particular structure. Assuming that the structure's coordinates are stored in a central server, a match with the sensor coordinates can be the proof of a correct citizen submission. This might distinguish the location-wise proper citizen submissions with the erroneous or fake ones.

Lastly, another navigation-related smartphone sensor is magnetometer which can detect smartphone's position with respect to magnetic north by sensing the magnetic field. Using magnetic north as the reference direction and assuming that the structural coordinate system is known (via previous measurements, satellite views, etc.), the angular differences between the sensor and the structure can be compensated. Table 4.1 summarizes the properties of the fundamental smartphone sensors such as accelerometer, gyroscope, and magnetometer of iPhone 5, which are of great importance for SHM applications [110]. The previous studies have shown that the same sensor type can have different performances depending on the smartphone brand and generation [1, 36].

In addition to all of these various hardware features, another advantage of smartphones is that they are supported with an advanced operating system and Integrated Development Environment (IDE). This smart platform can take advantage of mobility of citizens, bring heterogeneous sensor data together, collect and process all the information instantaneously on the sensor side, and wirelessly communicate with a server or cloud via Internet. The following subchapter discusses

sensors from developer’s perspective, introduces iOS core frameworks, and explore the alternatives to use the operating system as means of a smart, mobile, and heterogeneous SHM instrument.

Table 4.1: Accelerometer, gyroscope, and magnetometer properties

Model	Producer	Sensor type	Sensitivity
L3G4200D [111]	STMicroelectronics	3-axis gyroscope	16684 (LSB/g)
LIS331DLH [112]	STMicroelectronics	3-axis accelerometer	4096 (LSB/g)
AK8963 [113]	Asahi Kasei Microdevices	3-axis compass	0.15 (μ T/LSB)

4.1.2.2 iOS and core frameworks

iOS IDE, namely Xcode, provides developers with numerous methods to acquire sensor data. The programming language used in iOS environment is called Objective-C, an object-oriented compilation of C. Data acquisition from smartphone sensors requires a number of frameworks such as Core Motion (CM), Core Location (CL), and more (e.g. AVFoundation). The data obtained via frameworks can have different forms such as raw or processed, and can be utilized depending on developer’s purpose. In fact, some of these forms involve signal processing procedures and heterogeneous data fusion by default. In other words, these frameworks automatically enhance the state of motion variables by fusing the data obtained from different sensors, processing the signal (filtering, conversion, algebraic operations), and returning the processed data in numerous formats.

Using CM framework, 3-axis accelerometer, gyroscope, and magnetometer data can be acquired with many different parameters such as User Acceleration, Gravity, Rotation Rate, Attitude, and Magnetic Field. User Acceleration provides acceleration time history which represents the base correction of gravity value and attempts to identify user induced accelerations rather than gravity. In other words, CM applies a high pass filter to the acceleration time history and the smartphone axis directed towards gravity replaces the mean value of -1 g with 0 g. Likewise, Gravity attempts to define sensor position with respect to the gravitational direction and

can be achieved by a low pass filter. 3-axis Gravity data are components of a resultant acceleration whose magnitude is supposed to add up to 1 g. The angle between the smartphone axes and the horizontal earth plane can be determined by the inverse tangent of Gravity values corresponding to different axes.

Accelerometer data is related to the motion in 3 directions and needs additional sensor data to extend the motion information into 6DOF. For this purpose, gyroscope measurements provide Rotation Rate in 3 directions and can be adopted to detect angle changes. Integrating gyroscope data over time, one can obtain the cumulative angle change as a function of time. Combining gyroscope data with acceleration measurements, device orientations can be represented with Attitude data which consists of Pitch, Roll, and Yaw, in x, y, and z-axes, respectively.

All CM data introduced here can be retrieved with a sampling rate of up to 100 Hz which is sufficient for civil infrastructure applications. Unlike CM framework, CL sampling ratio is very low, cannot be controlled by the developer, and the device framework automatically keeps updating the location parameters in an optimized manner. The device gathers the data obtained from different tools such as GPS, Cellular, and Wi-Fi signals and fuses these to provide with the best estimation. In order to identify the sensor location, the coordinates provided by CL framework can be used. These parameters are namely, Latitude, Longitude, and Altitude, as well as the accuracy estimation of these values such as Horizontal Accuracy and Vertical Accuracy. Similar with the other frameworks, these can be converted into parameters with higher abstraction level. In this way, the location can be monitored on the map; the address, postal code, or further information can automatically be extracted.

Another important parameter provided by CL framework is the Heading value which determines the smartphone direction with respect to either magnetic or true North Pole. Combined with Gravity obtained from CM, Heading from CL can be used to define the sensor position with respect to structural and global coordinate systems. These coordinate systems and conversion procedures are discussed in details in the following subchapter.

In order to summarize and present all the data extracted from CM and CL frameworks and show its physical meaning as well as heterogeneity, a small-scale laboratory test is carried out. Figure 4.1 shows the shaking table test setup of a smartphone inclined at three different angles. The first subfigure demonstrates the intact position of the smartphone whose x-axis is aligned

perpendicular to shake table axis. In other words, at this stage, smartphone's y-axis is aligned as parallel to the shaking direction. Then, the smartphone is rotationally distorted in z and y-axis, as shown in the second and third subfigures, respectively. Figure 4.2 shows the time histories of various CM and CL smartphone sensor data extracted from a shaking table test subjected to a 5 Hz sine wave excitation. The first column of plots show the overall vibration time history, whereas second, third, and fourth are zoomed time histories of the three states demonstrated in Figure 4.1. According to Figure 4.2, looking at the intact state, the accelerometer values read on x, and z-axes (row 1) are negligibly small due to the fact that they are perpendicular to shaking direction. In contrast, the y-axis presents the whole vibration amplitude since it is parallel to the shaking direction. When the smartphone is rotated around z-axis, the acceleration amplitude in y direction reduces whereas the one in x direction increases. In other words, the vibration is distributed into x and y-axis as vector components. Similarly, when the smartphone is rotated around y-axis, acceleration readings in z direction becomes another component of the resultant vibration.

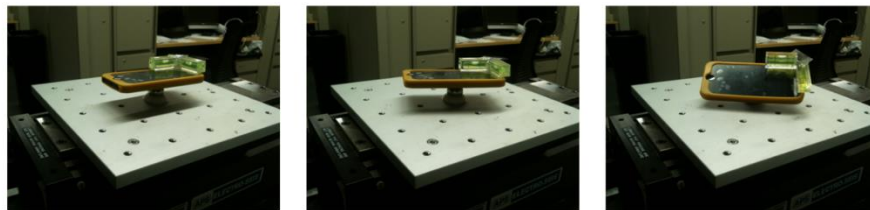


Figure 4.1: Shaking table test setup and different smartphone orientations

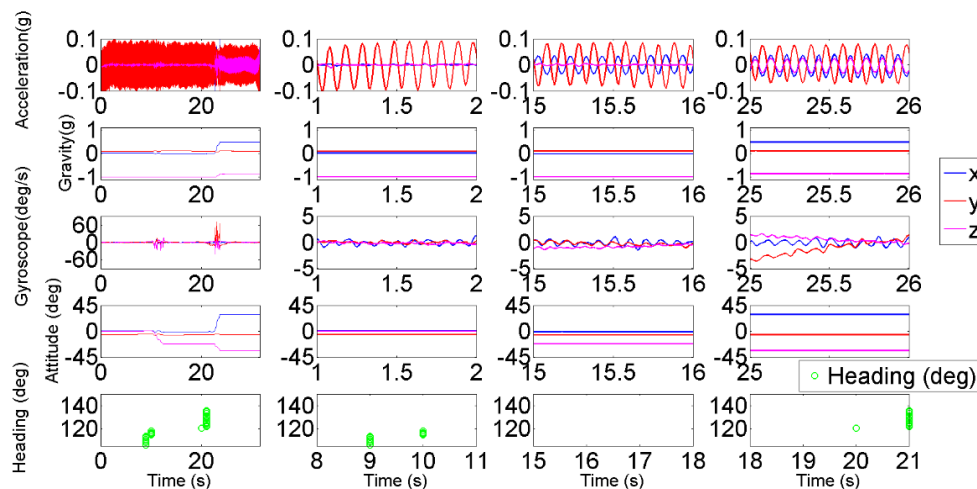


Figure 4.2: Multisensorial time histories of a distorted smartphone

Using the sensor data mentioned before, such rotary distortions of a smartphone can be tracked. Looking at the overall attitude time history plotted in Figure 4.2 (row 4, column 1), rotary changes in x, y, and z-axis can be monitored using pitch, roll, and yaw data, respectively. What is more, Figure 4.2 (row 5) shows the heading time history which is updated at the instants where the device orientation is subjected to change. Other than these, row 2 and 3 shows the gravity and rotational change rates observed on each axis. As mentioned previously, another parameter that can be extracted from smartphone sensors is the geographical position of the device. Since the major focus of this study is sensor orientation defects, global positioning parameters (e.g. latitude, longitude, and altitude) will not be discussed in details, yet its usage as a citizen submission verifier will be explained in the forthcoming subchapter. Therefore, heading will be the primary CL parameter since it is used as an orientation change indicator.

4.1.2.3 Data heterogeneity

Nonhomogeneous or heterogeneous data, is an important aspect of multisensorial monitoring systems, thus, is essential to integrate different sensor information in smartphone-based SHM systems. The multisensorial environment and data heterogeneity involve different data types, variation in the signal quality, and multi-rated clock operations. In this study, since the data extraction is bounded by the iOS core frameworks, data heterogeneity can be interpreted in terms of framework features. Figure 4.3 shows an overall look on the heterogeneous smartphone sensing platform based on CL and CM frameworks. These two frameworks have different characteristics in various aspects. First of all, the sensor difference between CM and CL is that CM framework has access to accelerometer, gyroscope, and magnetometer, whereas CL does not use accelerometer and gyroscope data but processes magnetometer data to produce heading data. Likewise, geographical information, hence, sensor position can only be obtained from CL and is not processed by CM.

What is more, CL framework is most likely to be based on complicated fusion algorithms integrating GPS, Cellular, and Wi-Fi; whereas processed CM data can be reproduced by raw sensor values. Compared with CM, CL framework has no access to the data of low abstraction. In other words, rather than obtaining the raw GPS, Cellular, and Wi-Fi signals and processing them in a customary manner, the developer can only get the processed results in terms of coordinates and

heading as the result of an estimation procedure.

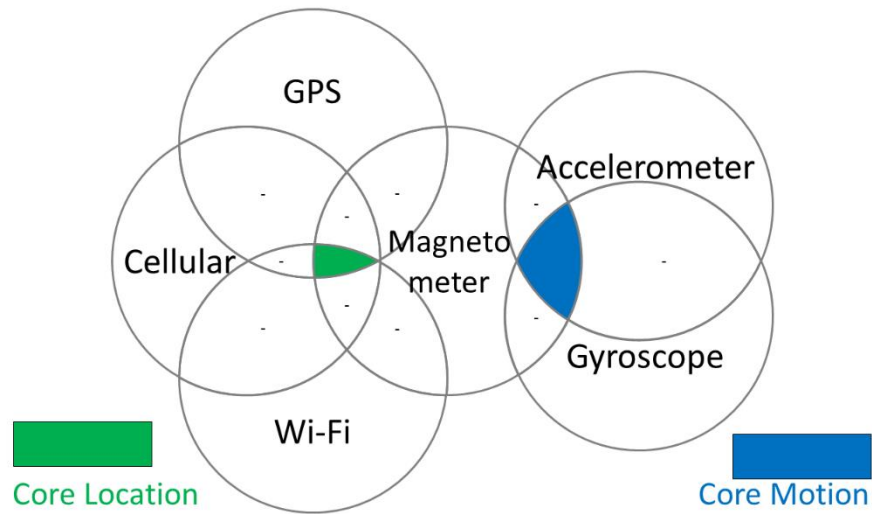


Figure 4.3: Logic diagram showing sensor data usage in iOS frameworks

Data heterogeneity also stems from the difference in framework clocks and sampling rates. CL-based sampling is very irregular and low rate compared with the CM-based sampling. Low and uncontrollable sampling rate, by nature, obstructs CL framework from producing useful frequency domain vibration data. Yet, global position coordinates obtained from CL is relatively useful for detecting sensor position rather than monitoring the structural displacement itself.

Finally, CL data quality in terms of structural vibration measurements is completely different than CM framework. Although numerous SHM studies have shown successful examples of GPS usage for displacement measurement [114-117], the geolocation sensitivity obtained from smartphones is too low for such purposes. For example, iOS IDE allows developer to modify desired accuracy in terms of distance, and the highest state-of-the-art accuracy value is 10 meters which is not sensitive enough for civil infrastructure vibrations. Yet, geolocation features can serve as a tool which verifies that the sensor position matches the structure's position. On the other hand, previous studies have shown that smartphone accelerometer, therefore CM data, is reasonably accurate for SHM purposes. Table 4.2 summarizes the heterogeneous features of smartphone sensors as structural vibration monitoring instruments in terms of usage description, active framework, measured parameter, sensor type, and sampling rate. The forthcoming subchapter discusses the mathematical background of the coordinate system transformation that can use the

heterogeneous data described herein. Further information regarding iPhone sensors, core frameworks, and iOS application development can be found in [73, 74, 76, 77].

Table 4.2: Heterogeneous smartphone sensor features

Scope	Frame-work	Primary Parameters	Technology	Sampling
Vibration Measurement	CM	User-Acceleration	Accelerometer	Regular: up to 100 Hz
Device Positioning	CL	Latitude*, Longitude*, Altitude*	GPS*, Cellular*, Wi-Fi*	Irregular: accuracy dependent
Horizontal Orientation	CL	Heading	Compass/ Magnetometer	Irregular: if distorted
Vertical Orientation	CM	Gravity	Accelerometer	Regular: up to 100 Hz
Device Distortion Transformation	CM & CL	Attitude (Yaw, Pitch, Roll)	Accelerometer, Gyroscope	Regular: up to 100 Hz
		All except*	All except *	Multi-Rate

4.1.3 Coordinate system transformation

Controlled by citizens, accelerometers embedded in smartphones constitute the core of a smartphone-based SHM platform. With the help of a proper smartphone application, vibration response of a structure can be measured by smartphone users with no engineering expertise. Moreover, mobile and smart devices bring the possibility to observe multiple structures' dynamic response with a single phone, since citizens can act as mobile SHM operators and get involved in more than one structure's SHM system. For example, depending on a pedestrian's daily route, different bridges with the same pedestrian's access can get benefit from the smartphone data

obtained from the same user. Extending this concept to multiple users or to a larger community, a mobile crowdsourcing service can become an SHM system which continuously receives periodical vibration response measurements, processes vibration signals, identifies modal parameters, and stores the analysis results [36].

The nature of smartphone-based SHM, on the other hand, cannot guarantee high quality vibration response data since the measurement configuration is dominated by the smartphone user. Especially in a crowdsourcing-based SHM scenario, the citizen incentive is the key to receive successful vibration response samples. In other words, smartphone users' state of knowledge, motivation, and comfort can play an important role in the quality of vibration measurements. For instance, there might be different posture scenarios that define citizens' mobility while taking vibration measurements from a civil infrastructure. Taking a pedestrian bridge as an example, the best but not the most comfortable case is the citizen placing the smartphone on the floor. In this case, although the smartphone is not fixed to the structure and free to move on the ground, it can obtain structural vibrations with a good accuracy [36]. Yet, previous studies ignored the fact that the devices placed on a structure by citizens can be different than the requested configuration.

The more likely scenarios can be standing citizens holding the phone arbitrarily, getting direct or indirect support from the structure (e.g. sitting on a bench or leaning on handrails). What is more, the phone may rest in a bag or pocket which lays on the ground or carried by a person. Therefore, different citizen-induced vibration measurement scenarios might vary in terms of sensor-structure coupling and interaction, and have a wide range of quality difference depending on the citizen mobility. That is to say, a pedestrian can stand still on a bridge for a certain duration, or keep walking while taking the vibration measurements, and depending on the mobility of the pedestrian, the vibration characteristics can extensively change. To summarize, mobility can introduce various uncertainties in vibration measurement and SHM procedure. Nevertheless, these can be reduced with the help of a smart monitoring system processing multiple sensor data.

In order to narrow down the definition of citizen-induced uncertainties in smartphone-based SHM, two significant sources, device position and orientation, become the focus of this study. Taking vibration measurements from a walking pedestrian or a pedestrian holding the device introduces even more uncertainties in measurement procedure. Besides, the structural vibrations can be masked by the predominant frequencies due to human body dynamics, biomechanics, or

the motion characteristics [84, 118-120]. For this reason, indirect measurements such as walking pedestrians, or citizens holding phones are excluded in this study. On the contrary, majority of the vibrations is produced by structural and environmental sources in addition to temporary device distortions that could result in positioning and orientation changes. Further aspects will be discussed thoroughly in the future.

4.1.3.1 Coordinate system transformation fundamentals

In order to utilize smartphone-based citizen-induced vibration data with rotational uncertainties, transformation between changing coordinate systems can be performed. Transformation between two coordinate systems can be interpreted in terms of Eulerian angle differences between the two systems. In flight dynamics, a particular application of Euler angles introduces yaw, pitch, and roll as the attitude values describing the rotation of a coordinate system in 3 directions [121]. For instance, rotational rigid body motion of an object shown in Figure 4.4 can be defined by the initial and final coordinate systems as well as the attitude parameters relating two systems with each other. One way to do this is to develop a transformation matrix, specifically, a cosine direction matrix which can represent the rotations in three dimensions [41]. Note that pitch and roll parameters, defining rotations around x, and y-axes, here is consistent with the iOS syntax, and can be labelled vice versa in other sources [102, 121].

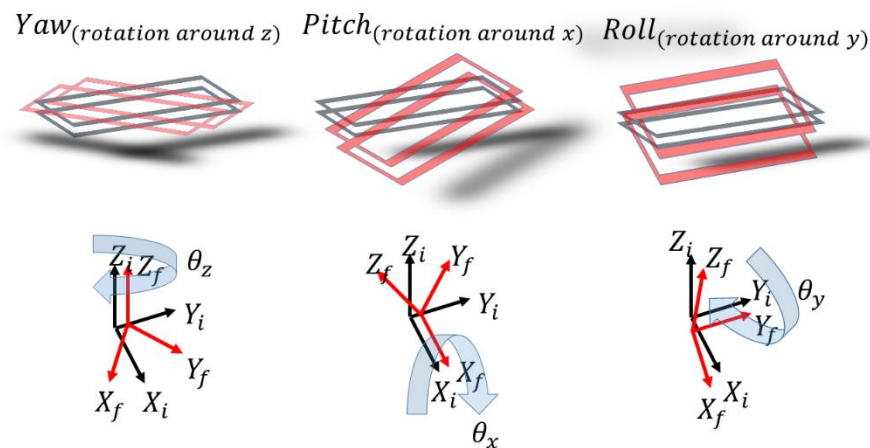


Figure 4.4: Relation between initial and final axes, attitude data, and device orientation

A cosine direction matrix can represent rotary changes of a coordinate system in terms of Euler angles and can be used to transform from the initial coordinate system to the final coordinate system,

$$A_{T^*} = \begin{bmatrix} [\cos\theta_y \cdot \cos\theta_z] & [\cos\theta_y \cdot \sin\theta_z] & [-\sin\theta_y] \\ [\sin\theta_x \cdot \sin\theta_y \cdot \cos\theta_z - \cos\theta_x \cdot \sin\theta_z] & [\sin\theta_x \cdot \sin\theta_y \cdot \sin\theta_z + \cos\theta_x \cdot \cos\theta_z] & [\sin\theta_x \cdot \cos\theta_y] \\ [\cos\theta_x \cdot \sin\theta_y \cdot \cos\theta_z + \sin\theta_x \cdot \sin\theta_z] & [\cos\theta_x \cdot \sin\theta_y \cdot \sin\theta_z - \sin\theta_x \cdot \cos\theta_z] & [\cos\theta_x \cdot \cos\theta_y] \end{bmatrix} \quad (4.1)$$

where A_{T^*} is the cosine direction matrix, $\theta_x, \theta_z, \theta_y$ are the angle of rotations around x, z, and y-axes, respectively. Given that the rotations around each axis is known, the final coordinate system can be constructed based on the initial coordinate system. Likewise, the transformation from final coordinate system to initial coordinate system can be performed by taking the inverse or, since it is orthonormal, transpose of the transformation matrix presented above. Then, the transformed components of the motion can be presented with a linear algebraic operation such as

$$T(\vec{x}) = A_T(\theta_x, \theta_y, \theta_z) \cdot \vec{x} \quad (4.2)$$

where $T(\vec{x})$ is the transformed vector from final to initial coordinate system, \vec{x} the vector corresponding to the final coordinate system and A_T is the inverse or transpose of A_{T^*} . As a result, A_T can be formulated as

$$A_T = \begin{bmatrix} [\cos\theta_y \cdot \cos\theta_z] & [\sin\theta_x \cdot \sin\theta_y \cdot \cos\theta_z - \cos\theta_x \cdot \sin\theta_z] & [\cos\theta_x \cdot \sin\theta_y \cdot \cos\theta_z + \sin\theta_x \cdot \sin\theta_z] \\ [\cos\theta_y \cdot \sin\theta_z] & [\sin\theta_x \cdot \sin\theta_y \cdot \sin\theta_z + \cos\theta_x \cdot \cos\theta_z] & [\cos\theta_x \cdot \sin\theta_y \cdot \sin\theta_z - \sin\theta_x \cdot \cos\theta_z] \\ [-\sin\theta_y] & [\sin\theta_x \cdot \cos\theta_y] & [\cos\theta_x \cdot \cos\theta_y] \end{bmatrix} \quad (4.3)$$

Using these principles, as long as the Eulerian angle differences or attitude parameters are known, any coordinate system can be projected into another coordinate system. In this way, vibrations in an arbitrary orientation can be converted into the desired coordinate system components.

The ultimate goal is to modify the sensor coordinate system such that the orthogonal vibration modes can be achieved by converting the improperly positioned or distorted sensor's coordinate system into the structural coordinate system. Yet, the proposed system does not expect citizens to arrange the sensor coordinate system or find out the Euler angle differences based on prior

structural information. Therefore, taking advantage of vectors with constant physical quantities such as gravity or earth's magnetic field, a third reference coordinate system can establish the connection between the sensorial and the structural coordinate systems. For this purpose, the following subchapter proposes three citizen-induced SHM coordinate systems, namely, sensorial, structural and global coordinate systems, and discusses the connection among each other.

4.1.3.2 Coordinate systems in smartphone-based SHM

In this study, coordinate systems in smartphone-based SHM are classified into three elements. The first element is the smartphone or sensorial coordinate system, which is controlled by the citizens or smartphone users and is subjected to change over time. Built-in iOS sensor axes system, namely, x, y, and z can be used to define the sensor coordinate system. Accelerometer, gyroscope and magnetometer data can be utilized such that smartphone position can be determined and changes can be tracked by taking magnetic north and gravitational directions as reference vectors. Combining all these sensor data together, this can be done by calling attitude angles (yaw, pitch, and roll) in CM framework and heading angle from CL framework.

The second element of coordinate systems is structural coordinate system, which is essential to interpret vibration modes in physically meaningful directions. Generally, structural coordinates describe whether the deformations are in vertical, longitudinal, or lateral directions. For example, a multistory building's coordinate system can be composed of two horizontal and one vertical directions, which is adequate to define vibration modes as well as node locations on the structure. Likewise, a bridge structure's coordinates is likely to be composed of a longitudinal, transverse, and gravitational directions.

The third and the final element is global coordinate system, which establishes the connection between two independent local coordinate system, such as the sensor and the structure. The conversion from sensorial to structural scale can be performed by using the global coordinate system as an intermediary step. In order to find a convenient global coordinate description for SHM, gravitational and magnetic north directions can be used as the first two coordinate axes. The third coordinate system axis is defined as the vector product of gravitational and magnetic north vectors, enabling the orthogonality between coordinate axes. Figure 4.5 shows the coordinate systems of different scales, and the interrelation between global and local coordinates.

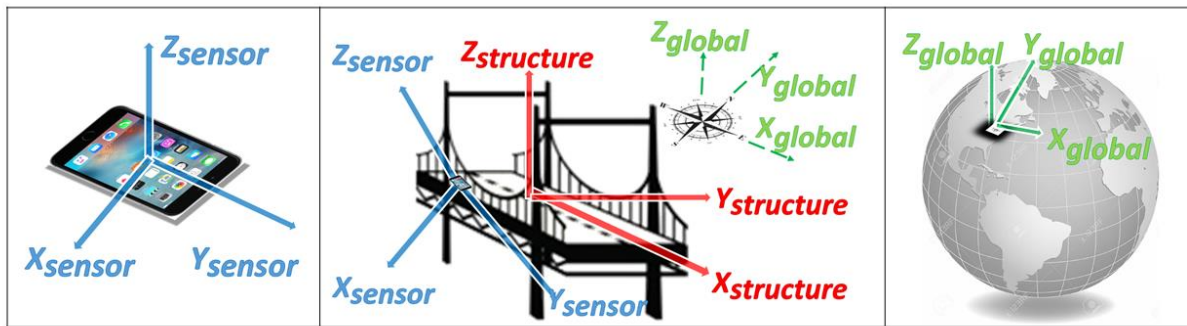


Figure 4.5: Local to global measurement coordinate system scales

The first and the second, namely, the sensor and the structural scales refer to the local coordinates whereas the third scale refers to the global scale. The distinction between local and global coordinates stems from the uniqueness of the global coordinate system (defined by gravity and magnetic north), in contrast with the infinite number of possible local coordinate systems. Since the smartphones are operated by citizens and there is no control over the sensor configuration, it is assumed that sensors can have any arbitrary orientation at any given instant, regardless of structure's coordinates. In other words, Euler angles between the sensorial and structural coordinates cannot be controlled by the receiver and may change in time. Likewise, there may be millions of different structures with different coordinate systems, but, their coordinate systems are unlikely to change unless the structure undergoes a modification (adaptive structures, retrofitting, etc.). In other words, once the structural coordinate system is determined, it can be stored in a database for future reference.

It is essential to have a sensor configuration that could identify structural modes of vibration in correct directions, because, a mismatch between the sensorial and structural coordinate systems can cause erroneous analysis results. Therefore, the relation between the sensorial and structural coordinate systems should be established with the help of a known reference coordinate system. For this reason, an intermediate coordinate system with known parameters, global coordinates, can be utilized to convert from sensor to structural coordinate system. Since global coordinate system cannot be subjected to any change, they can be maintained as a reference coordinate system for any local coordinates.

Based on these definitions, a transformation procedure is generated. First of all, the procedure

extracts Eulerian angles between the sensorial and the global coordinate systems and develops the transformation matrix in between. For a stationary sensor case, the Eulerian angles in x, y, and z-axes can be represented with the inverse tangents of gravity ratios obtained from CM framework, and magnetic heading obtained from CL framework. Therefore, transformation matrix from intact sensorial to global coordinate systems is defined as

$$A_{T(ig)} = A_T(\arctan(G_y/G_z), \arctan(-G_x/G_z), heading) \quad (4.4)$$

where G_x, G_y, G_z are the gravity values observed on x, y, and z-axes, respectively.

Similarly the transformation matrix from structural to global coordinate systems can be represented with the same angles. If, assuming that one of the structural axes is perfectly vertical like a high-rise building, in other words is parallel to the direction of gravity, coordinate system transformation can simply be defined by the angle between the structure's lateral axes and the magnetic north pole. Likewise, a bridge-like structure can be defined by the angle between its longitudinal axis and the magnetic north, assuming its vertical axis is perfectly parallel to the direction of gravity. By doing this, the transformation terms can be reduced, while the assumption holds for most of the civil infrastructure with either vertical or horizontal alignment. Afterwards, structure's magnetic heading is sufficient to produce the transformation matrix. Therefore, the transformation matrix can be reduced to

$$A_{T(sg)} = A_T(0,0, heading) = \begin{bmatrix} [\cos heading] & [-\sin heading] & [0] \\ [\sin heading] & [\cos heading] & [0] \\ [0] & [0] & [1] \end{bmatrix} \quad (4.5)$$

Because that the transformation is linear and the coordinate system axes are orthogonal to each other, the transformation matrix is invertible, and the transformation from global to structural coordinate systems can be derived by taking the adjoint matrix and dividing it by the determinant. Thanks to the orthogonality, the same derivation can simply be performed by taking the transpose which is equal to

$$A_{T(gs)} = A_{T(sg)}^{-1} = \begin{bmatrix} [\cos heading] & [\sin heading] & [0] \\ [-\sin heading] & [\cos heading] & [0] \\ [0] & [0] & [1] \end{bmatrix} \quad (4.6)$$

Considering the transformation steps discussed so far, it is possible to adjust vibration measurements of an arbitrarily placed sensor. In addition to these, any distortion in sensor coordinate system can be tracked by pitch, roll, and yaw data obtained from CM framework. With

the help of gyroscope, rotational changes can instantaneously be recorded and distorted signals can be converted into intact sensor coordinate system. These changes can be represented by change in pitch, roll, and roll values in synchronization with accelerometer data,

$$A_{T(di)} = A_T(\text{pitch}, \text{roll}, \text{yaw}) \quad (4.7)$$

where pitch, roll, and yaw are the distortion-induced orientations such as rotation in x, y, and z-axes, respectively. To summarize these coordinate system transformations as consecutive operations, the coordinate system transformation from distorted sensor to structure can be generalized as in Figure 4.6. In addition, the intermediate coordinate transformation system steps between distorted sensor and structure are intact sensor and global coordinate systems, respectively.

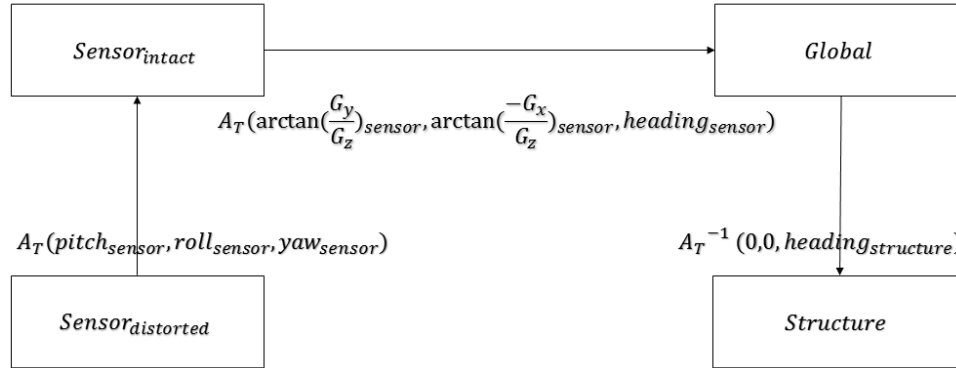


Figure 4.6: Block diagram for overall coordinate system transformation

The generalized expression can be reduced to one single term by algebraic multiplication of all these transformation matrices. In this way, a complete transformation solution from distorted sensor state to structure can be established by multiplication of all transformation matrices such as

$$T_{ds}(\vec{x}) = A_{T(sg)}^{-1} \cdot A_{T(ig)} \cdot A_{T(di)} \cdot \vec{x} = A_{T(ds)} \cdot \vec{x} \quad (4.8)$$

where di, ig, sg, and ds represents distorted to intact, intact to global, structure to global, and distorted to structure, respectively.

In summary, the proposed transformation procedure can be interpreted by the integrated steps given below:

1) Using changes in attitude data which is yaw, pitch, and roll; angular deviation errors can be eliminated by transforming back from distorted sensor position into the intact sensor position.

2) Intact position of a sensor can be identified such that the inverse tangent values of gravity ratios relate sensor layout with gravity direction, whereas heading determines the angle between sensor's y-axis and the magnetic north pole. With the help of pitch, roll, and heading, intact sensor coordinate system can be converted into global coordinate system.

3) Conducting inverse transformation from global to structural coordinate system, vibration modes observed in a sensor signal can be uncoupled, since the original signal content is distributed into its components in terms of structural coordinate system.

The integrated system described herein is advantageous for the following reasons:

1) A citizen can operate a smartphone without any prior knowledge on the sensorial or the structural coordinate systems,

2) Transformation operations can take advantage of integrated computational capacity by using both of central server and mobile user platforms.

3) Taking citizen initiative and device mobility into consideration, measurements subjected to angular distortions can be recovered.

4) The process can lead to further integration of citizens into SHM system by enhancing measurements under different pedestrian postures.

4.1.4 On campus applications

In order to test the proposed coordinate system transformation procedure with real smartphone data, two studies are presented in the following subchapters. The first study is a small scale laboratory model, and has been subjected to impact hammer tests in Burmister Laboratory, Columbia University. For this purpose, an iOS application which retrieves multisensorial CL and CM data is developed. The second study is based on ambient vibration monitoring of a pedestrian link bridge connecting two high-rise buildings, Mudd and Schapiro, on Morningside Campus, Columbia University. The developed application is used to determine orientation and location of the device, while long term acceleration response is recorded by another commercial application, iSeismometer. The reason to use a second software is that the application developed by the authors is suitable for short-term data which temporarily keeps the time history until transferred via web view, and does not need to access smartphone database. In contrast, iSeismometer stores acceleration time history in smartphone hard disk as a csv file, which allows the users to record

longer time histories.

The distorted and transformed data are compared with those obtained from a reference monitoring system. The reference system has 2 piezoelectric accelerometers in each of the x, y, and z directions. These accelerometers are of model 393B04 PCB Piezotronics, have a sensitivity of 1000 mV/g, and are used to sample with 100 Hz by the data acquisition system of National Instruments SCXI-1531.

4.1.4.1 Sampling rate and tilt corrections of a 2DOF model

A 2-story shear structural model is instrumented with 6 reference piezoelectric accelerometers and a smartphone on the second story. The steel columns with rectangular cross-sections are designed to be strong in the y-axis and weak in the x-axis. Beams with square cross-sections are made of aluminum, and have very large stiffness due to their bulky dimensions compared with the columns. Figure 4.7a shows the experimental setup, Figure 4.7b shows the design drawings of the 2DOF structure, and Figure 4.7c-g shows the plan and the elevation views of the second story with intact and distorted smartphone positions. Reference magnetic compass and leveling instruments are used to maintain the horizontality of the structure throughout the tests and keep the structure's heading within the initial values.

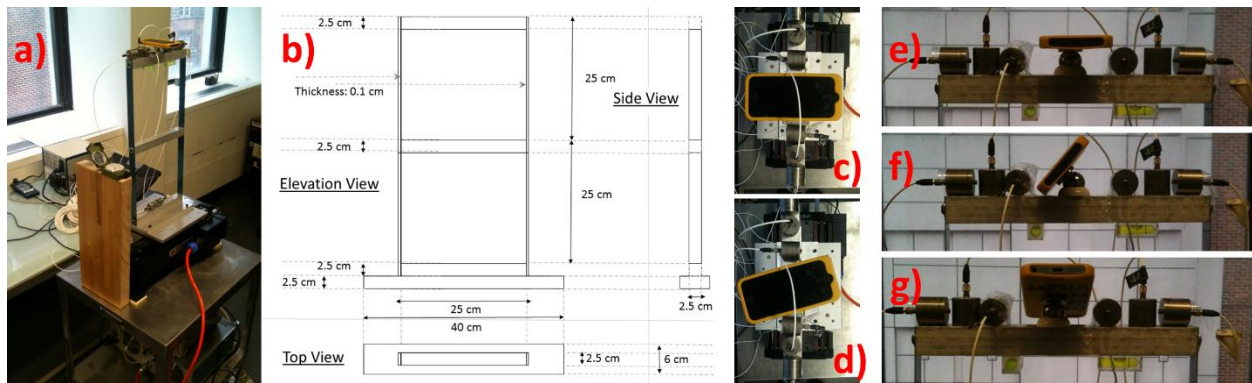


Figure 4.7: Setup, drawings, and rotationally distorted device positions

Initial position of the smartphone can be described as the screen facing the opposite of gravitational direction. In addition to this, initial sensorial x-axis is in the same direction with the structure's weak axis. Afterwards, the smartphone is subjected to distortions and the acceleration

response is recorded under deviated orientations. The distorted data is reconstructed by plugging the heterogeneous smartphone data into the proposed transformation procedure.

Figure 4.8 shows the time history and Fourier spectra comparison of distorted and transformed data. In contrast with the distorted time history, the significant match between reference and corrected signals shows that the error between reference and smartphone sensor reduced by 53% in terms of root mean square error (RMSE) as a result of coordinate system transformation. Similarly, the reference and the corrected Fourier spectra amplitudes show agreement in contrast with the distorted data whose sensor coordinate system captures coupled vibration behavior rather than representing orthogonal axes. On the other hand, modal frequencies are still observed within the same frequency values. This is due to the fact that the coordinate system differences result in changes in the signal amplitudes, whereas it does not introduce any modulation in the frequency domain.

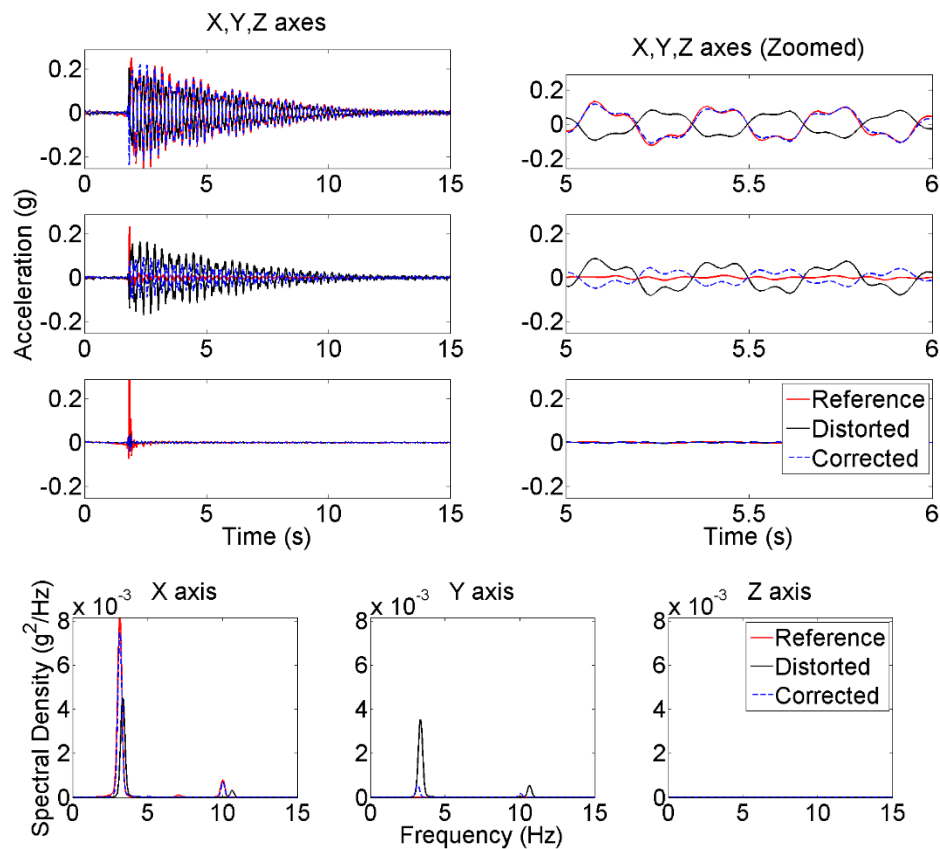


Figure 4.8: Rotationally distorted and corrected accelerometer data

In order to quantify the error reduction in the time and the frequency domain, a number of reference parameters are compared with those obtained from the distorted and the corrected sensor coordinate systems. At this stage, heterogeneity in the sampling rate is also taken into consideration. Looking at the timestamps obtained from the smartphone data, it is observed that the acquisition cannot achieve the targeted sampling rate which is set equal to 100 Hz. The observed number of samples in the time domain are approximately 6% less than the targeted value, therefore, the Fourier spectra is corrected according to the achieved sampling rate in addition to the coordinate system transformation operations. As a result, the corrected modal frequency perfectly matches the reference value, whereas sampling irregularity causes a 6% increase in the identified frequency for the raw case. What is more, reference spectral density at the peak frequency is achieved with an 8% error by the coordinate transformed case, whereas such value increases to 44% due to the distribution of weak axis motion into two horizontal axes of the distorted smartphone. Similarly, acceleration sign at a particular instant show that the distortion not only results in amplitude difference, but also phase error as a result of the direction difference between the sensorial and structural coordinate systems. The differences obtained from distorted and corrected sensor data are summarized in Table 4.3.

Table 4.3: Dominant modal parameters and accelerations in x-direction

	Reference	Distorted	Corrected
f_1 (Hz)	3.16	3.35	3.16
Error (%)	-	6.01	0.00
$PSD_{at f_1}$ (g^2/Hz)	$8.15 \cdot 10^{-3}$	$4.54 \cdot 10^{-3}$	$7.48 \cdot 10^{-3}$
Error (%)	-	44.3	8.22
$RMSE_{36 peaks}$ (g)	-	0.0325	0.0153
Phase	+	-	+

4.1.4.2 Pedestrian bridge example

To serve the influence of the proposed coordinate system transformation procedure on modal identification results of a real structure, a short span pedestrian bridge located in Columbia University Morningside campus is monitored. The structural system is a single span bridge, serving as a link between two adjacent high rise buildings. The structure is composed of steel columns, beams and an arch, where the integration among structural members is maintained by moment resistant connections.

In order to test a number of representative smartphone positions, 4 sets of different tests are conducted. These tests involve different smartphone configurations with respect to the structure, where the coordinate system transformation method could perform as a correction tool. Table 4.4 presents the geometrical descriptions for smartphone orientations corresponding to different tests.

Table 4.4: Pedestrian bridge test properties and smartphone configurations

Test No	Generalized Layout	Gravity $\langle x, y, z \rangle$	Rotation	Yaw	Pitch	Roll
1	Face up	$\langle 0, 0, -1 \rangle$	-	0°	0°	0°
2	Portrait	$\langle 0, -1, 0 \rangle$	X-axis	0°	90°	0°
3	Landscape	$\langle -1, 0, 0 \rangle$	Y-axis	0°	0°	-90°
4	Inclined	$\langle 0, -0.71, -0.71 \rangle$	X-axis	0°	45°	0°

The same reference monitoring and data acquisition system is used to compare the raw and transformed smartphone sensor data with a conventional system. The system is installed on the bridge mid-span with 6 accelerometers, where all accelerometers are attached to a planar mat with double sided adhesives. The purpose of installing the sensors on a reference plane is to avoid the effects of local irregularities on the bridge deck surface, and provide each sensor with the same coordinate system. Similar with the previous case study, each of x, y, and z directions are instrumented with two reference accelerometers, those average is to be compared with the smartphone sensor measurements. Figure 4.9 shows the 3-dimensional sketch of the structural model, the coordinate systems referring to the structure, intact (Test 1), and distorted (Test 2-4)

sensor positions. In addition, Figure 4.10 illustrates the sensor configuration installed on the planar mat located on the mid-span of the structure, and the corresponding attitude values due to distortion are printed on the smartphone application interface.

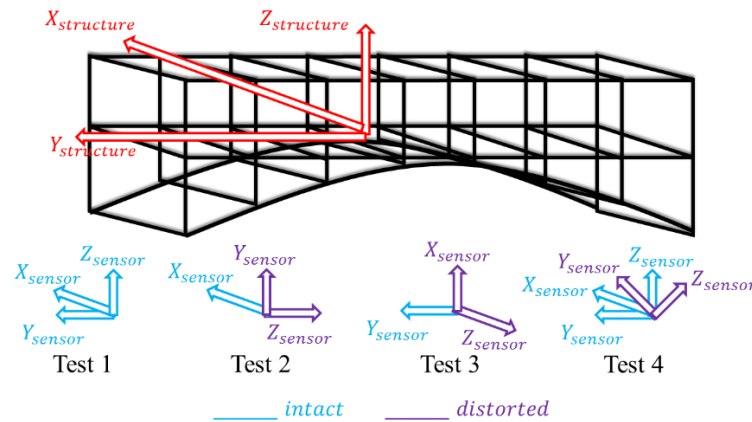


Figure 4.9: Structural and sensorial coordinate systems of Test 1-4

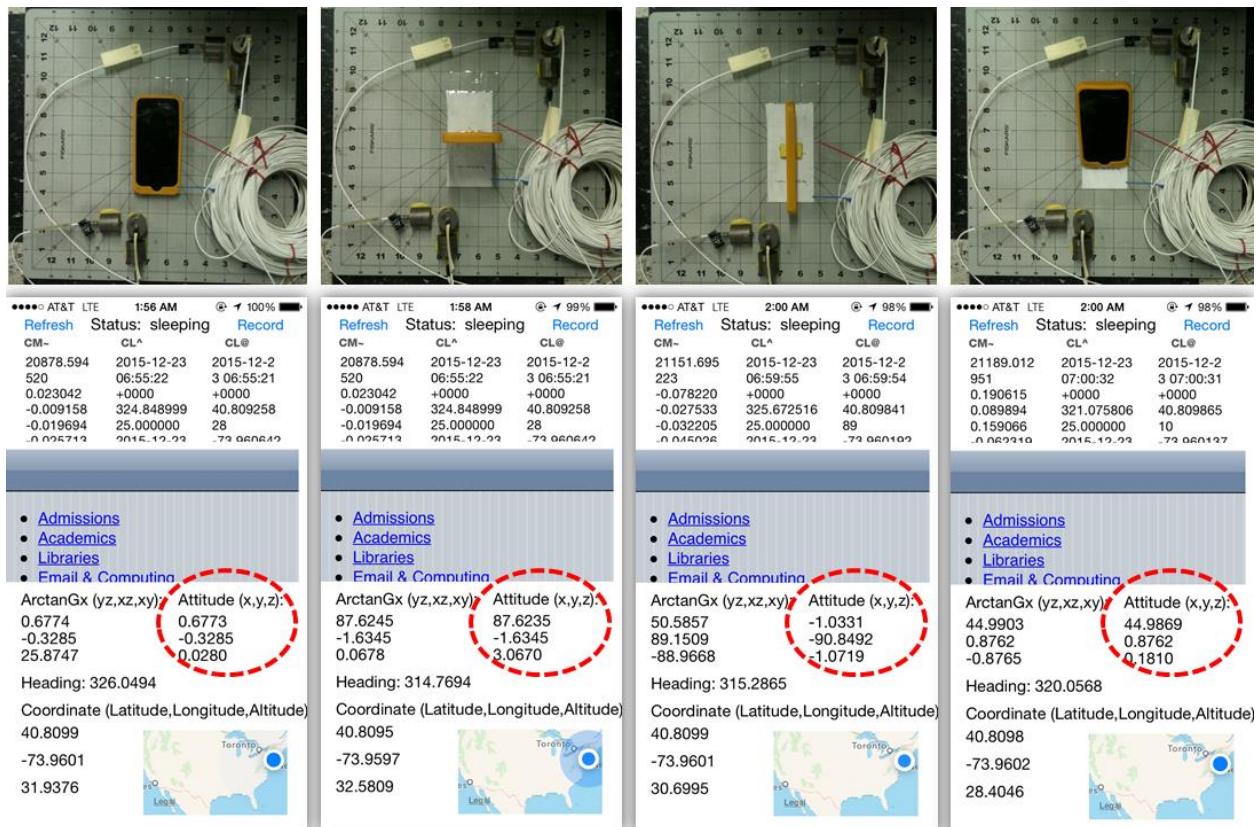


Figure 4.10: Reference and smartphone sensor configuration and application interface

As mentioned previously, another position-related smartphone sensing feature is geolocation services on CL framework. CL framework provides the device with location information with an accuracy evaluation for each estimation. This is important because, in smartphone-based SHM, it is expected that the mobile sensors operated by citizens can have positioning errors. What is more, since the citizens are engaged in multiple monitoring activity, a citizen may submit the vibration data to the wrong structure's database without an automated location verification system.

Theoretically, latitude and longitude values obtained from CL framework can detect which structural node is instrumented with the sensor, or at least verify whether the data logged by a citizen corresponds to the correct structure. In practice, the location estimations may vary in accuracy starting from 10 meters up to 3 kilometers. The proposed range is considerably high for detecting the location on a particular structure, therefore, some of these estimations might mislead the verification accuracy. Yet, CL framework allows the developers to target the desired accuracy level, and if necessary, location estimations with large errors can be disregarded by setting a threshold for the estimation accuracy. Figure 4.11 shows the Universal Transverse Mercator (UTM) coordinate estimations provided by CL framework. The yellow spots show that for a structure of short size (10-meter span), the estimation cannot clearly identify a particular node (e.g. mid-span), yet, the geolocation service can verify that the measurements are taken from the structure of interest.



Figure 4.11: Coordinate estimations by smartphone geolocation services

Figure 4.12 shows the reference and the smartphone accelerometer time histories obtained from Test 1-4. The tests are conducted under ambient vibration and it can be seen that the signal

amplitude is dominated by noise. Therefore, there is an amplitude resemblance among time histories obtained from x, y, and z-axes regardless of sensor orientation. Compared with the reference time histories, it is observed that smartphone peak to peak distance is large due to the low sensitivity. Therefore, dominated by the noise level rather than low-amplitude structural vibrations, there is a significant difference (over 100%) between the reference and smartphone data with or without coordinate system transformation. Figure 4.13 shows that such difference is reflected on the spectral density values observed on peak frequencies as well as the density increase distributed throughout the overall frequency domain.

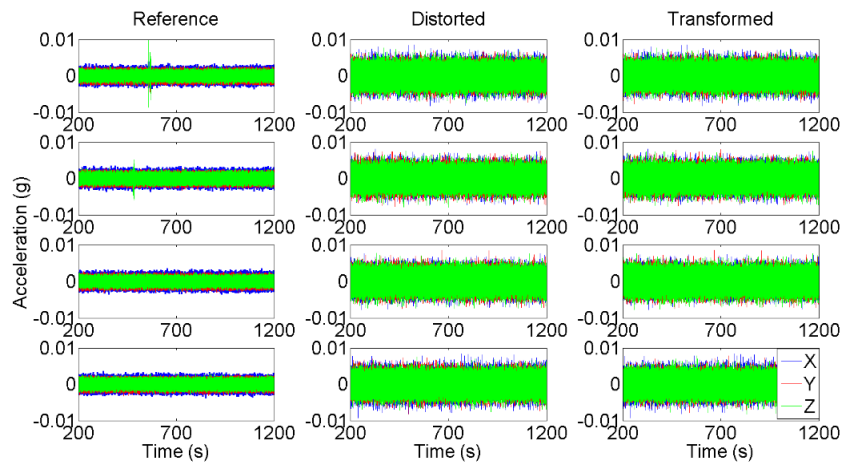


Figure 4.12: Time histories of Test 1-4

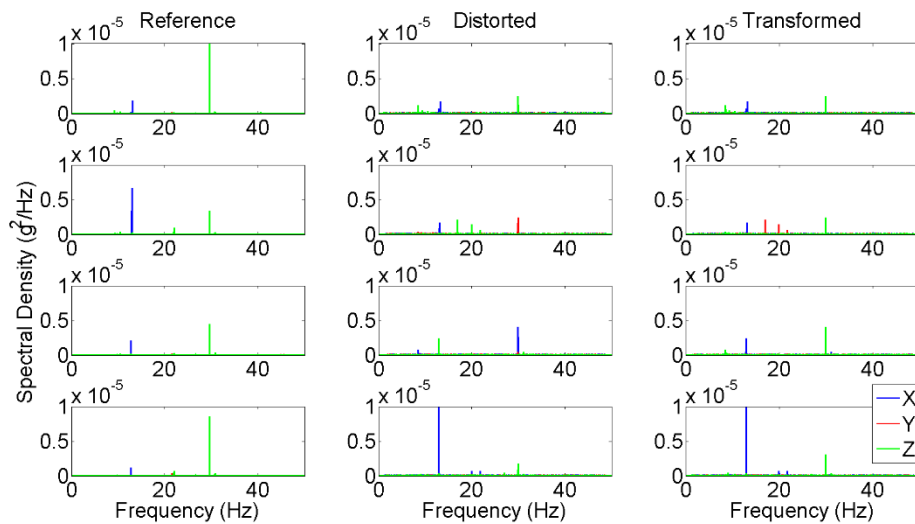


Figure 4.13: Spectral densities of Test 1-4

Table 4.5 and Table 4.6 presents the peak values in the time and the frequency domain of Test 3 and Test 4, respectively, in order to compare the difference between the reference and the smartphone time histories as well as Fourier spectra. Looking at the Test 3 peak frequencies, the error between the distorted and the reference values is very large (56%) since the mode identified by the distorted sensor corresponds to another direction in the structural coordinate system. As a result of coordinate system transformation, the smartphone sensor axes can fit the structural coordinate system, therefore, identify the modal frequency with an error below 1%. Similarly, the error between smartphone and reference sensors reduces from 45% to 9% as a result of coordinate system transformation. Yet, as observed from Figure 4.12 peak to peak values, it can be concluded that the error between peak vertical accelerations (PVA) is independent of the coordinate system, since it is masked by the low signal to noise ratio. To summarize, the effect of coordinate system transformation can be seen more clearly in the frequency domain compared with the time domain which is suppressed by noise.

Table 4.5: Test 3 dominant modal parameters and bridge accelerations in z-direction

	Reference	Distorted	Corrected
f_3 (Hz)	29.66	12.94	29.94
Error (%)	-	56.4	0.94
$PSD_{at f_3}$ (g^2/Hz)	$4.43 \cdot 10^{-6}$	$2.42 \cdot 10^{-6}$	$4.04 \cdot 10^{-6}$
Error (%)	-	45.4	8.80
PVA_{mean} (g)	~0.002	~0.005	~0.005
Error (%)	-	>100	>100

Table 4.6: Test 4 dominant modal parameters and bridge accelerations in z-direction

	Reference	Distorted	Corrected
f_3 (Hz)	29.66	29.97	29.97
Error (%)	-	1.05	1.05
$PSD_{at f_3}$ (g^2/Hz)	$8.61 \cdot 10^{-6}$	$1.79 \cdot 10^{-6}$	$3.08 \cdot 10^{-6}$
Error (%)	-	79.2	64.2
PVA_{mean} (g)	~0.002	~0.005	~0.005
Error (%)	-	>100	>100

4.1.5 Transformation procedure on landmark bridges

This subchapter presents structural vibration measurement and modal identification of a landmark suspension bridge, Golden Gate Bridge, located in San Francisco California with the application of the proposed coordinate system transformation procedure. Golden Gate Bridge is one of the most popular landmarks in the United States, and being used by 110000 vehicles every day, is an important component of California's transportation network. The structural system consists of a truss bridge deck hanging on steel bridge cables, transferring loads to the bridge towers. The main span is 1280 meters long, and has access to pedestrians, therefore can be a suitable platform for citizen-induced smartphone-based SHM.

On September 4, 2015, approximately 35 minutes of vibration data is acquired from the bridge mid-span using the smartphone application iSeismometer as an acceleration recorder. Similar with the previous cases, three-axial acceleration is obtained by an iPhone 5 which is placed free to move on the pedestrian lane deck without any additional adhesion elements. In other words, sensor and structure coupling is maintained by the friction between bridge the deck surface and the rear face of the smartphone. Smartphone measurements are taken such that the sensorial y-axis is aligned perpendicular to the bridge's longitudinal axis, or structural y-axis according to the coordinate systems prescribed in the previous subchapters. Figure 4.14 shows the sensorial, structural, and

global coordinate systems proper with the proposed multiscale coordinate system framework. Specifically, the structural y-axis coincides with the sensorial x-axis, or the angle between the structural y-axis and the sensorial y-axis is 270° . To be consistent, San Francisco-San Rafael direction defines the positive y-axis for the structural coordinate system.

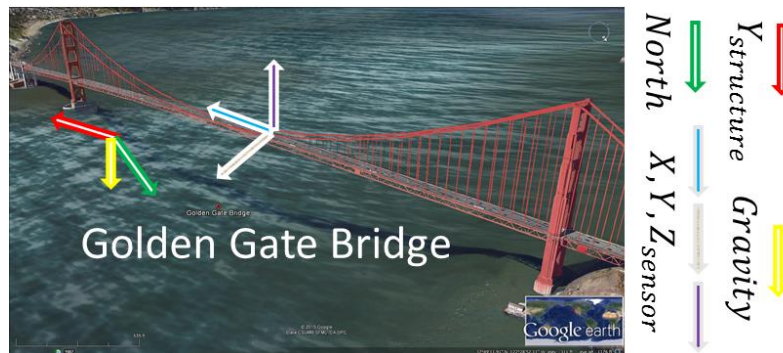


Figure 4.14: Coordinate systems and aerial views of Golden Gate Bridge

Figure 4.15 shows the time histories of the mid-span bridge vibration response obtained from the smartphone sensor after the coordinate system transformation is performed. Lateral, longitudinal, and vertical labels refer to the structural axes named x, y, and z according to the multiscale transformation procedure proposed in the previous subchapters. According to the time history plots, it is seen that the peak to peak vibration response ranges between approximately 0.06 g for the lateral and the vertical directions, and 0.04 g for the longitudinal directions. Unlike the ambient vibration study presented in the previous study, the plots show that there are significant peaks in the time histories, therefore, the vibration response exceeds ambient level. This might result from the vehicle traffic acting as operational vibrations, increasing the signal to noise ratio compared with the ambient vibration case. Figure 4.16 shows the spectra of the vibration response obtained from the Fourier transform of the 3-axial acceleration time histories. Some of the vibration modes are demonstrated on the spectral peaks ranging from 1st to 8th mode. Looking at the ratio of the peak spectral values with the baseline values, it can be observed that the vertical modes are excited more than the lateral and longitudinal modes as a result of the operational vibrations acting in the gravitational direction.

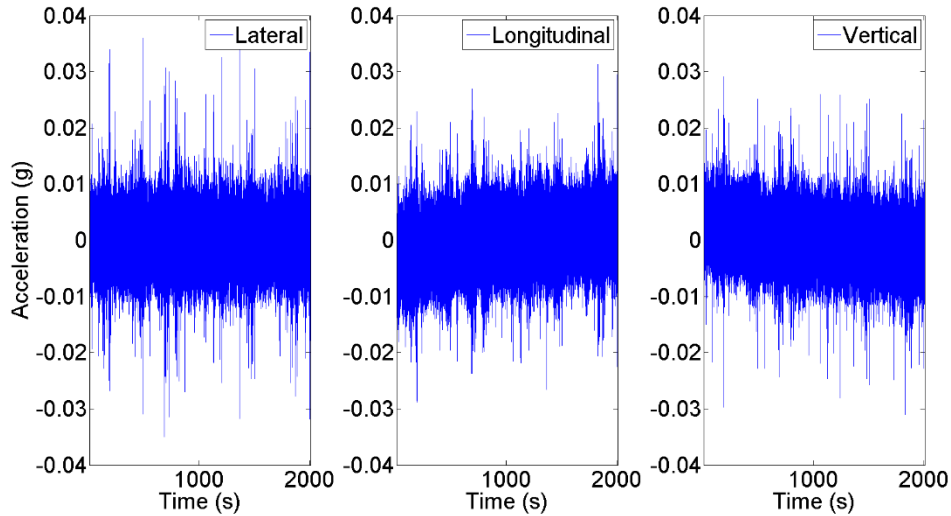


Figure 4.15: Time histories from Golden Gate Bridge

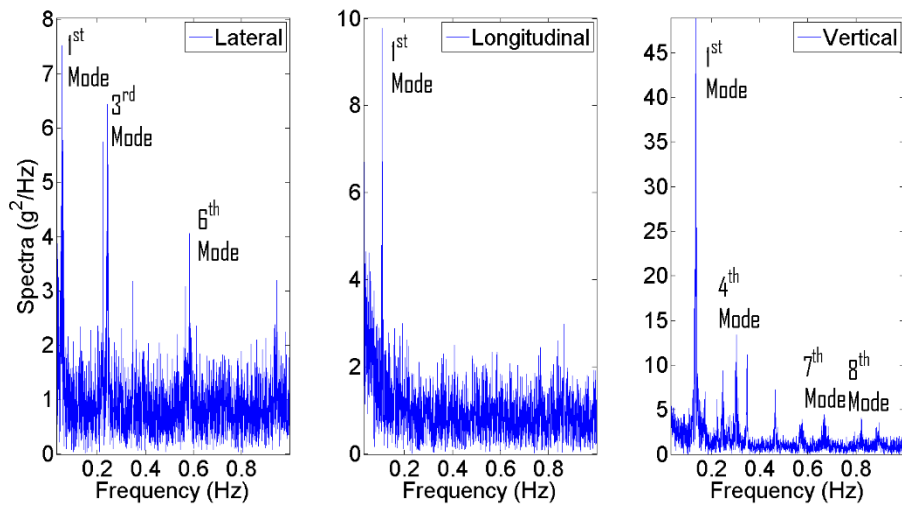


Figure 4.16: Fourier spectra from Golden Gate Bridge

Previously, vibration response analysis and modal identification studies of Golden Gate Bridge is conducted in 1985 [122]. Compared with the smartphone-based measurements, it can be seen that there are a number of identical modes, although the overall spectra looks different. In order to compare the error between the identified modal frequencies in 1985 and 2015, the spectral peaks in vertical direction are compared with each other. Table 4.7 includes the 1st to 4th modal frequencies obtained from the two comparative studies. Because that the reference study classifies vertical and torsional modes separately, vertical modes obtained from torsional behavior are

omitted in Table 4.7. In addition, only the symmetric modes are taken into consideration because that the measurement location is bridge mid-span. Accordingly, the largest error observed in Table 4.7 is the 1st mode with the error of 10%. Other than those, the modal frequencies identified in 1985 is reasonably close to the values obtained in 2015 with the error values around 5%. The difference between the reference and the smartphone identification results may stem from the quality difference between accelerometers, the variation in environmental factors and operational loads, as well as the coupling conditions resulting from the integration between sensor and the structure. Besides, previously it has been shown that smartphone accelerometer performance decreases at the very low frequencies (e.g. 1st mode at 0.12 Hz) [1]. What is more, the bridge underwent a number of retrofiting projects between two comparative datasets [123]. With a combination of long term monitoring factors such as fatigue, these structural modifications might have caused changes in modal frequencies. Nevertheless, the values are encouraging considering the large scale of the structure and the detailed identification results gathered from the reference study.

Table 4.7: Identification results of Golden Gate Bridge

Frequency	Description	Smartphone	Reference [122]	Error (%)
f_1 (Hz)	Vertical	0.1346	0.1221	10.24
f_2 (Hz)	Vertical	0.1723	0.1770	2.66
f_3 (Hz)	Vertical	0.2460	0.2625	6.29
f_4 (Hz)	Vertical	0.3028	0.2930	3.35

Further studies conducted on similar landmark structures will not only produce valuable information for condition assessment of civil infrastructure but also uniquely benefit from citizen-induced and smartphone-based crowdsourcing power for SHM purposes.

4.1.6 Conclusions

In this study, a smart, heterogeneous, and mobile SHM method is presented with the

implementation of multiple coordinate system scales and transformation between coordinate systems. The method utilizes multisensorial smartphone data such as acceleration, rotation rate, and magnetic field intensity in order to determine and track smartphone's orientation with respect to gravitational and magnetic north directions. Using the change in attitude parameters such as roll, pitch, and yaw, a smartphone's angular distortions can instantaneously be detected and corrected according to the intact sensor coordinate system. Moreover, the Eulerian angles between the sensorial and the global coordinate systems can be determined by attitude data obtained from CM and heading data obtained from CL. Similarly, a structure's orientation can be defined by the Eulerian angles between the global directions and the structure's lateral, longitudinal, and vertical axes. As a result, a citizen with no prior coordinate system information can gather vibration data with any arbitrary sensor configuration and the proposed smart monitoring system will convert it into structural coordinate system. The connection between the sensorial and the structural data can be enhanced by a third reference coordinate system, which is defined by the global vectors such as gravity and the magnetic north.

Application of smartphone-based vibration monitoring and coordinate system transformation is demonstrated on impact hammer testing of a 2DOF laboratory model, ambient vibration testing of a pedestrian bridge, and operational vibration testing of a large-scale landmark structure, Golden Gate Bridge. The results show that the heterogeneous data obtained from CM and CL frameworks can be integrated to detect angular distortions of the sensor, determine device orientation with respect to global coordinate system, and convert the vibration signals from an arbitrary sensorial coordinate system into the structural system. Vibration response time histories and spectral densities show that the angular distortions have a significant effect on signal amplitude and phase accuracy. An error in the frequency domain can occur due to the imperfect sampling rate and the identification of a vibration mode in a direction other than the desired axis or the coupling among the orthogonal axes. Imperfect sampling rate problem can be solved with the help of timestamp data provided by CM, whereas the vibration data in orthogonal modes can be extracted with the help of coordinate system transformation thanks to CM and CL frameworks.

The results show that a coordinate system transformation method can be implemented into SHM procedure with the help of heterogeneous data obtained from different sensors and mobile data sensitive to angular distortions. In addition, with the help of the computational power, IDE,

and an advanced mobile operating system; these operations can be conducted on the sensor side, representing a successful smart monitoring application. The proposed method can compensate rotational control deficit over crowdsourcing-based structural vibration measurements or citizen-induced SHM sensor configurations. The procedure is demonstrated on an iOS device with real smartphone data, yet, can be extended to other mobile platforms as well as customized smart monitoring systems.

4.2 Spatiotemporal effects

4.2.1 Introduction

Sensor technology and advanced system identification algorithms provide vibration-based SHM systems with the necessary foundation to evaluate structural integrity in a rapid, remote, quantitative, objective, and automated fashion [2, 3]. Compared with the sole analytical and numerical structural analyses for response prediction or performance assessment, monitoring data reveal the dynamic characteristics of structures to a better extent and can be used to calibrate simulation results with experiments to mimic actual structural behavior [33, 34]. Finite element model updating, damage detection, and reliability estimation are some but not all of the possibilities that can adopt SHM findings for extended accuracy [28, 29].

In spite of all improvements mentioned previously, implementation of SHM systems still requires considerable efforts in terms of expertise, labor force, instrumentation, signal processing, system communication, and data storage. These practical and financial problems lead researchers to develop innovative methods which offer more sustainable solutions in comparison with conventional monitoring systems. These innovations get benefit from sensing systems in terms of smart, mobile, and heterogeneous data [91-102]; as well as electronics and computer science tools such as networks, wireless communication, Internet, and cloud computing. Likewise, taking advantage of upcoming smart and mobile features of these novelties, wireless and distributed sensor network (DSN) systems become an important part of SHM [124-131]. Efficient adaptation of such a multidisciplinary framework can bring SHM to a more widely used and applicable level in the near future.

Combining all these features together, one of the novel and promising adaptations is

smartphone-based SHM which can utilize multisensorial mobile phones for vibration monitoring [1, 18, 36, 39, 103, 104]. Enabling community's crowdsourcing power as the driving force, smartphones can be implemented as structural vibration response measurements with no cost to monitoring administrators and decision makers [36]. On the other hand, the fundamental drawback of crowdsourcing-induced systems is that the data quality and quantity collected by citizens are purely based on the voluntary initiative and responsibility. This hinders the SHM system developer to have a control over the instrumentation configuration and operation schedule. As voluntary operators, citizens determine how frequent, how long, and where the measurements take place, in addition to coupling uncertainties due to device positioning. As a result, crowdsourcing-induced smartphone-based SHM is subjected to uncontrollable sensing system variation in time and space, which, in general, can be called as spatiotemporal uncertainties in sensor operation. With the multisensorial smartphone environment and smart features offered by mobile operating systems, some of these uncertainties such as angular distortion or orientation can be reduced to a significant extent [85].

With the advent of WSNs and DSNs, decentralized SHM system features necessitate time synchronization in system components [132-134]. Likewise, most of the up-to-date system identification algorithms assume that the multichannel vibration data is acquired with identical timestamps [135-137]. In addition to these, conventionally most of the sensor instrumentation is built upon a careful consideration of sensor location and orientation, whose performance is maximized with optimized sensor configurations [138-140]. Spatiotemporal uncertainties in smartphone usage is therefore a unique sensor network problem which requires a different perspective in the time and the space domains. For this reason, this study proposes novel solutions to temporal and spatial control lack due to citizen-led sensor instrumentation by taking advantage of mobile and smart features of smartphones.

In the forthcoming subchapters, the information processing outline is presented in a procedural framework. Chapter 4.2.2 discusses how to infer sensors' spatial information and set the geometrical relationship between the location of a smartphone and the structural nodes. Chapter 4.2.3 presents a signal-to-power conversion approach to cancel out the temporal variations in the crowdsourced vibration data. Chapter 4.2.4 demonstrates how to synthesize the acquired location and vibration data to deduce modal parameters. Chapter 4.2.5 applies the proposed procedure to

an existing pedestrian bridge, and Chapter 4.2.6 presents the results and discussions. Finally, Chapter 4.2.7 summarizes the work conducted and presents the conclusions.

4.2.2 Sensor position and node identification

As mentioned previously, sensor position has an important role on identified parameters. The spectral values obtained from different sensors reveal the modal displacement of the corresponding structural node. For example, the mid-span node of a symmetric, both end-supported structure is subjected to higher vibration amplitudes due to symmetric modes compared to antisymmetric modes. Likewise, the signal obtained from the basement of a multistory building can be utilized as an input motion representing support excitation and is free of any modal displacement unless the soil structure interaction is considered.

It is a well-known fact that sensor configuration optimization is essential to obtain accurate structural response measurement and to reveal dynamic characteristics to the best extent. Therefore, studies have developed numerous optimization methods to maximize the use of limited number of sensors and determine the most functional sensor locations covering the desired number of modes [138-140].

On the other hand, in case of smartphone-based SHM, it is foreseen that the control over sensor instrumentation cannot be achieved, yet, sensor location still has an effect on identification results. For example, like mentioned before, a sensor located at the mid-span of a bridge is less likely to identify antisymmetric modes compared with the symmetric modes. Therefore, identification of structural modes without sensor location information can be cumbersome or misleading.

For these reasons, it is important to determine the sensor location such that the identification results can be assisted with nodal information. In other words, knowing that the measurements are sent from a particular node, identification process has a prior state of knowledge regarding the vibration characteristics of the corresponding signal. One possible advantage of such process is that, missing modes can be analytically completed even though the submission locations are bounded and restricted. For example, with the help of simplified analytical models, mid-span vibration signal can be used to estimate anti-symmetric modes even though spectral peaks in the frequency domain does not contain such information. Likewise, beam models [141] or finite element models [142] can simulate buildings' structural response even though the acquired data is

from a single node. Yet, applicability of this phenomena is very limited for structures with complex geometry, therefore, is not investigated in this study.

In a crowdsourcing-based system identification scenario, data ubiquity is the last of a SHM system's problems. Millions of smartphone sensors are already spread around the world, and can be activated with a proper decentralized SHM strategy. What is more, in order to cancel out spatial uncertainties resulting from uncontrolled sensor location, multisensorial smartphone technologies can be used. In this study, utilization of two smartphone technologies, GPS and camera, is discussed from this perspective.

The first alternative to detect sensor location is the smartphone GPS which returns the sensor location with an accuracy determined by the application developer. iOS Core Location (CL) framework fuses the GPS measurements with cellular and Wi-Fi data to return the optimal location estimations [143]. The data is provided in Universal Transverse Mercator (UTM) format, which includes latitude and longitude coordinate values [144]. The problem with this technology is, for relatively small structures such as short span bridges, these estimations contain a high error level and may not be capable of detecting the actual node identity. What is more, especially for indoor spaces and extremely cloudy weather, received GPS signals may not be reliable since the signal is insulated by the surrounding environment.

Another alternative is deploying node labels on the structure's particular locations, and these labels provide the smartphone with the actual node identity. The location information or the node identity can be compressed into barcodes or matrix codes, which can automatically be read by the smartphone camera and the embedded image processing features [145]. This alternative can be useful especially for the cases where the GPS data is unavailable or unreliable. After determining structural node with one or more of the proposed technologies, the information can be processed to link the structural nodes with the sensor data in terms of the response location.

After the location of a sensor is determined, a relation between the structural node and the sensor position can be established. Taking a single span structure with a horizontal layout as an example and assuming that the sensor is located on the longitudinal axis of the structure, the sensor location can be represented with the ratio between the sensor distance to a reference point and the whole span. This normalized distance value is sufficient to describe a particular location on a horizontal structure in a generic fashion such that

$$r_{normalized} = \frac{r}{l} \quad 0 < r_{normalized} < 1 \quad (4.9)$$

where r defines the sensor distance from the structure's start point, l defines span length, or the distance between the structure's start and end points. Using this relation, mobility of a sensor position can be formulated to cancel out spatial uncertainties in the measurements.

Extending this definition to two dimensions, longitudinal axis of a structure can be defined as a line connecting the initial and the final coordinates of the structure. Likewise, the sensor location lies on the line defined by these coordinates which are

$$[x_{initial}, y_{initial}] \text{ and } [x_{final}, y_{final}] \quad (4.10)$$

and can be converted into a linear function and its slope such as

$$y = y_{initial} + m_{if}(x - x_{initial}) \quad m_{if} = \frac{y_{final} - y_{initial}}{x_{final} - x_{initial}} \quad (4.11)$$

respectively. If the sensor is located on the longitudinal axis of the structural coordinate system, this linear function needs to be satisfied by the sensor coordinates which are

$$[x_{sensor}, y_{sensor}]$$

If the sensor location deviates from the structure's longitudinal axis line, its coordinates can still be used to formulate the sensor location with respect to the structure by using the projection of sensor coordinates on the longitudinal axis. In order to find the point on the structure's axis which has the shortest distance to the sensor location, a perpendicular line can be drawn from the sensor location to the structure's axis. Then, this line has a slope which is equal to the negative reciprocal value of the structural longitudinal axis' slope, such that,

$$m_{sc} = -\frac{1}{m_{if}} \quad (4.12)$$

Combining this with the sensor location, the normal line can be formulated as

$$y = y_{sensor} + m_{sc}(x - x_{sensor}) \quad (4.13)$$

and the sensor's projection point on the structural axis is

$$[x_{cross}, y_{cross}] \quad (4.14)$$

which should satisfy both of the equations defined above, and can be found by setting the two functions equal to each other such as

$$y_{cross} = y_{initial} + m_{if}(x_{cross} - x_{initial}) = y_{sensor} + m_{sc}(x_{cross} - x_{sensor}) \quad (4.15)$$

Using this relationship, $[x_{cross}, y_{cross}]$ can be found. Once it is determined, normalized r value can be found by the proportion between the sensor's projected distance and the main span length. This value is equal to

$$\frac{r}{l} = \frac{\sqrt{(y_{cross} - y_{initial})^2 + (x_{cross} - x_{initial})^2}}{\sqrt{(y_{final} - y_{initial})^2 + (x_{final} - x_{initial})^2}} \quad (4.16)$$

Using these geometrical relationships, sensor coordinates can be converted into normalized values defining its position on the structure. In this way, if the sensorial and the structural coordinates are available, one can remove the measurement uncertainties due to spatial distribution, and interpret the measurement results with the consideration of sensor mobility. For structures with discrete nodes such as trusses, the ratio defining the sensor location can simply be shifted to the nearest structural node with the relation,

$$node_i(r) = 1 + round\left(\frac{r}{l} \cdot (node_{total} - 1)\right) \quad (4.17)$$

which can be used for conversion from continuous location data to discrete and normalized nodal coordinates.

Using this procedure, the location data obtained from a smartphone can be used to determine the sensor position with respect to the structure. In addition to spatial uncertainties, the crowdsourcing-based SHM concept states that the measurement time and the duration is uncontrolled as well. The following subchapters aims at solving these temporal variation and uncertainties by normalizing measured acceleration energy with respect to time.

4.2.3 Energy normalization

Response displacements can be decomposed into modal displacements to understand the dynamic characteristics of a structure. If the input (loading) and output (response) functions are determined in the frequency domain, the structural system function can be constructed by the transfer function between the input and the response spectra. For multi-degree of freedom (MDOF) systems and multichannel structural response measurements, such transfer function takes the

matrix form, relating the nodes' spectral correlations among each other. Then, using the spectra obtained from multichannel measurements, modal frequencies and mode shapes can be determined.

Yet, this approach relies on the fact that the multichannel response is recorded simultaneously, which provides the identification process with the phase information of each node's vibration response. In a spatiotemporally varying sensor network which is solely controlled by citizen initiatives, such information becomes unavailable. Considering the temporal variation among different sensors, the acquired signal is not only asynchronous but also sparse in time domain which hinders the system to extract the timewise relation between two channels. What is more, combination of spatial variation among sensors with unequal measurement durations disturb the relationship between two channels in terms of amplitude. If the input motion spectra is constant over time, proper with the Parseval's theorem, such difference will be directly related to the measurement duration.

For cases where the input motion is free of narrow-banded dominant frequencies and can be idealized as white noise, the system frequency spectra can be extracted directly from the output only response measurements. In this study, ambient vibration is idealized as white noise excitation, and regardless of the input information, frequency spectra obtained from measurements are used for identifying structural system's modal frequencies. This assumption is likely to be violated where operational loads such as human-induced vibrations have a certain frequency content.

To cancel out the measurement duration difference among different structural nodes, the signal energy is converted into signal power, therefore, spectral functions with different durations and energies can be normalized into the same unit time interval. Assuming that the input motion's spectra is constant over time, the signal power and the signal energy can be related to each other by normalizing the energy term with respect to the measurement duration, and obtaining the power term [146, 147]. Since the measured signals are discrete, the time can be interpreted in terms of the sampling rate and number. This information is provided either by the timestamp object in Core Motion (CM) framework or the sample number counted in response time history array. But, it should be noted that the samples obtained from CM framework cannot perfectly fit the targeted sampling rate, and there might be a slight shift between the attempted and the achieved timestamps. Therefore, the results obtained from the counted samples and the targeted sampling may be slightly different from the achieved timestamps [85].

Nevertheless, the energy definition, and the relationship between the signal energy and the average power is defined as,

$$E_{t_2-t_1}(t) = \frac{\pi}{2g} \sum_{i=n_1}^{n_2} a(i)^2 \Delta t \quad (4.18)$$

$$P_{t_2-t_1}(t) = \frac{E_{t_2-t_1}(t)}{t_2-t_1} \quad t_2 - t_1 = (n_2 - n_1) \Delta t \quad (4.19)$$

where $t, n, E, P,$ and a is time, data number, energy, power, and acceleration, respectively. Obtaining the spectral peaks which are normalized with respect to time, not the spectral phases but the absolute modal displacements can be estimated. To introduce the phase information into the absolute spectra, baseline models or measurements can be used. This is briefly explained in the next subchapter, the integration framework of multisensorial smartphone data to conduct modal identification under spatiotemporal sensor variation.

4.2.4 Multichannel data synthesis and modal parameters

This subchapter presents the integration of location, time, and vibration data obtained from spatiotemporally sparse smartphone data and determination of modal frequencies and mode shapes in spite of control lack in the operated sensor network. Without detecting the sensor location, even if the multichannel data is acquired synchronically from a centralized system, the modal parameters will be incomplete due to lack of location information. Likewise, given that the location information is available, but the measurement durations obtained from different nodes are unknown, the Fourier spectra obtained from different nodes cannot be quantitatively compared with each other since the acquired power during measurements is different for each test. In order to solve these problems, previous subchapters explained the node identification and the normalized Fourier spectra concepts with the help of the multisensory smartphone environment. Once both of these data are available, the signals obtained from different channels can be synthesized as the spatial and temporal information is processed and uncertainties due to the uncontrolled sensor configuration and operation schedule are removed.

After the normalized spectra are classified according to the node identity, the spectral values can be composed together for identification of modal parameters. First of all, in order to determine

the global structural spectra, local spectra obtained from the network nodes can be integrated to get the envelope of the overall network data. Then, assuming that each node provides information to the acquired data, the structural modal frequencies can be determined by the peaks observed on the envelope spectra. After the modal frequencies are determined, looking at the Fourier spectra of a particular node, modal displacements of the corresponding node can be represented with the spectral value at the identified modal frequency. Collecting all modal displacements from different nodes and integrating them with the spatial information, the absolute distribution of modal displacements can be obtained. The only missing component herein is the phase information which decides whether two node are in or out of phase with respect to each other. In order to provide this information, a baseline such as prior experiment results or numerical models can be used. As a result of adding the phase information to the absolute modal displacements, eventually, mode shapes can be determined. To summarize, Figure 4.17 shows the block diagram of the proposed overall flowchart and the information flow through the framework components.

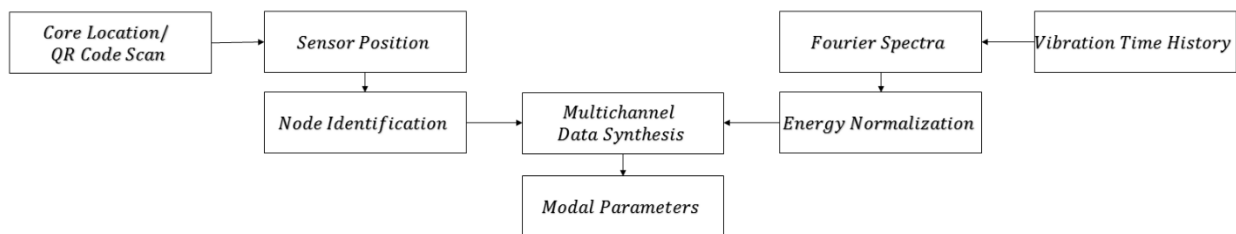


Figure 4.17: Procedural framework

4.2.5 Field tests

In order to test the procedure explained above, field tests are conducted on a single span pedestrian bridge located in Morningside Campus, Columbia University in the City of New York. The pedestrian bridge is a link bridge connecting two high-rise buildings, namely, Mudd and Schapiro. It has a moment resistant steel structure with a lower arch, and the structure spans approximately 11 meters in the longitudinal direction and 3 meters in the transverse direction. Considering the even distribution of structural members in the longitudinal direction, it can be observed that there are 7 sub-spans of equal length, and each of these spans are connected via nodes which are used to define the measurement locations on the bridge. Figure 4.18 demonstrates

the bridge views from different perspectives such that the satellite (a), outer (b), and the inner (c) views are presented.

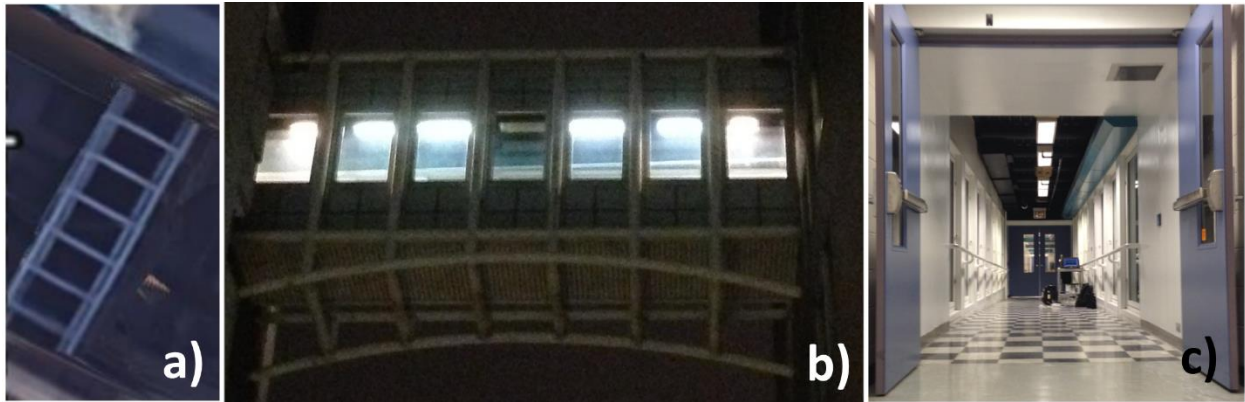


Figure 4.18: Satellite, outer, inner views of Mudd-Schapiro Bridge

Formerly, the bridge was instrumented with 6 piezoelectric accelerometers of type 393B04 PCB Piezotronics, distributed evenly along the longitudinal direction. The reference data was simultaneously sampled at 100 Hz and acquired with National Instruments SCXI-1531 system with cable connections. Using the Frequency Domain Decomposition (FDD) method, the modal frequencies and mode shapes were identified. The 1st, 2nd, and 3rd modal frequencies identified by the reference system were 8.46, 18.95, and 29.67 Hz, respectively. Figure 4.19 shows the singular values in the frequency domain and the first three mode shapes [36].

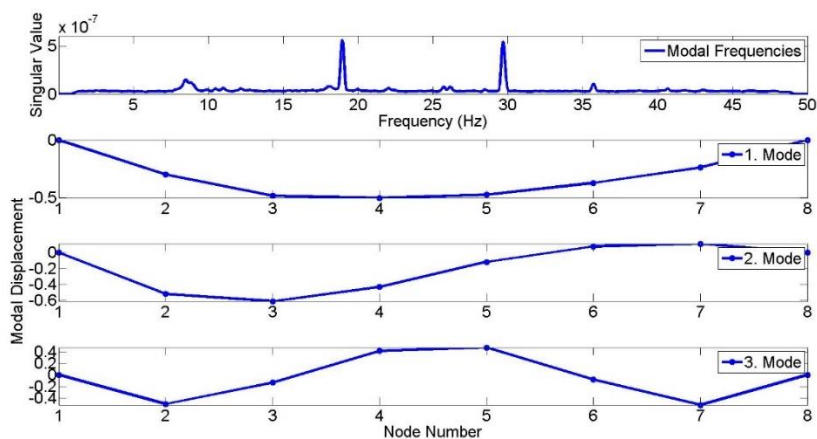


Figure 4.19: Identified modal frequencies and mode shapes from FDD

Figure 4.20 presents the node identities proposed for the bridge, and their relation to the node location and the span length. This procedure can be generalized by normalizing the node location with respect to the main span. In this way, the parameter becomes dimensionless, and can be interpreted as a generic relationship for any bridge structure. Accordingly, Table 4.8 presents the actual and the normalized node locations with respect to the corresponding node identities.

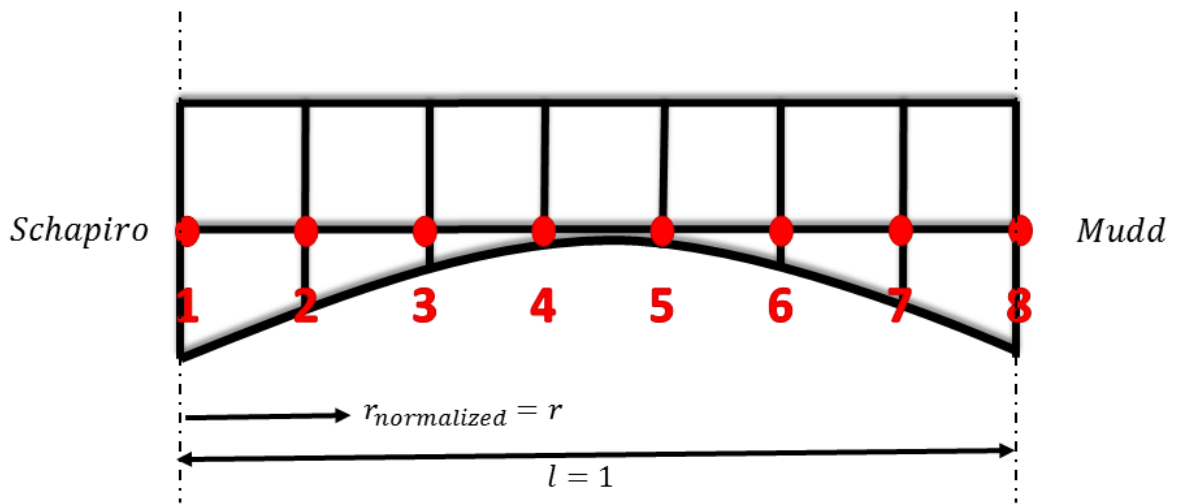


Figure 4.20: Node configuration of Mudd-Schapiro Bridge

Table 4.8: Relationship between the node identities and the node locations

node identity	1	2	3	4	5	6	7	8
r (m)	0.0000	1.5429	3.0857	4.6286	6.1714	7.7143	9.2571	10.8000
$r_{normalized}$	0.0000	0.1429	0.2857	0.4286	0.5714	0.7143	0.8571	1.0000

In order to find the node identities based on the smartphone information, 2 different methods utilizing different technologies are proposed. The first one uses geolocation data obtained from the smartphone core location services, whereas the second method is based on reading QR code images which are attached to the structure. The location, node identities, or the structural information can be compressed into QR codes and can be scanned by the smartphone camera to determine the sensing location.

Geolocation method takes advantage of CL services provided by iOS. CL framework produces geolocation data such as latitude, longitude, and altitude by fusing GPS, Wi-Fi, and Cellular signals, and eventually, returns the best estimation. What is more, the framework provides user with the horizontal accuracy and vertical accuracy, to quantitatively evaluate the latitude, longitude, and altitude estimation reliability. In vertical structures such as high-rise buildings, skyscrapers etc. altitude data can be of importance to detect sensor location. For structural layouts with horizontal alignment like bridges or large buildings with high horizontal-to-vertical aspect ratio, latitude and longitude parameters become useful to describe the sensor location. By locating the sensor position, the accelerometer data obtained from a smartphone sensor can be interpreted accordingly.

The horizontal accuracy thresholds defined by iOS comprises of 5 different levels. From the highest to lowest accuracy, these levels are nearest, ten meters, nearest hundred meters, one kilometer, and three kilometers, respectively. The reason to set different accuracy targets is to minimize the location update requests depending on the service needs. In order to determine a sensor's position with respect to the structure, since the structural response is very sensitive to the measurement location, it is essential to use the best accuracy level available. For the up-to-date smartphone models, nearest range and ten meters range are equal to each other. Therefore, the location estimations obtained from a smartphone are filtered by ten meters accuracy, eliminating the estimations with higher errors and less reliabilities. Then, assuming that the device is stationary throughout the sensing process, the filtered results are averaged to come up with an overall mean estimation.

In order to test the field performance of smartphone geolocation services, 8 structural nodes on Mudd-Schapiro Bridge are consecutively instrumented with the same smartphone (iPhone 5) in different time intervals. Similar with the configuration in [36] and double-sided adhesives, the phone is placed on the bridge deck surface where the rear face is directed towards gravity. Knowing that the main bridge span is only around 11 meters and the sub-span between two adjacent nodes is less than 2 meters, it is expected to have large errors due to the limitations of smartphone location estimation. Figure 4.21 shows the actual location identification results of Node 1-8, and it can be observed that the node identification precision can be very low for structures with small dimensions presented here. Resulting in the inadequacy of the geolocation

results, the geolocation method is not followed further.



Figure 4.21: Node identification using geolocation estimations

As a second alternative, the structural node locations are compressed into QR codes which can be scanned by the smartphone camera. Provided that a structure is instrumented with QR codes, the smartphone can automatically gather and process the location data without additional user efforts. Figure 4.22 shows the QR codes posted on the 1st to 8th nodes of Mudd-Schapiro Bridge, respectively. These codes define the nodes' location with respect to the structure. In the future, similar approaches can be extended to provide the phone with any further information such as structure's name or identity number.



Figure 4.22: QR code instrumentation from 1st to 8th node

After identifying the structural node's location or identity, the vibration time history obtained from the corresponding location can be interpreted accordingly. Herein, the uncertainties in the time and the space domains are interrelated, since the data duration from a certain location is uncontrolled and can result in different spectral values in the frequency domain. For example, previously it was seen that a 40-minute data obtained from quarter-span was approximately more

than 30 times of a 1-minute data [36]. Assuming that the structural input is white noise excitation with a constant amplitude and the power emitted by the structure is independent of time, the spectral values in the frequency domain are expected to be proportional with the measurement time. On the other hand, violation of this assumption due to temporary effects such as pedestrian passes is expected to change the power level, as well as the spectral distribution in the frequency domain as a result of walking-induced dominant frequency band [36]. Yet, as the data size increases, these temporary changes are likely to become less influential.

For these reasons, following the procedure explained before, conversion from-energy-to-power concept is followed to cancel out the measurement duration irregularities. This can be conducted by splitting a complete time series into smaller segments and averaging the spectra obtained from these segments. In order to do that, a unit sample length is set to 1 minute, and any measurement longer than this value is normalized by averaging with respect to its total duration. Using this principle, submissions with different lengths can be compared with each other in terms of spectral peaks in the frequency domain.

Using the same smartphone, iPhone 5 accelerometer (LIS331DLH- ST Microelectronics), for all tests, the structural response of each node is measured with the ascending order in terms of node numbers. Therefore, each test is conducted with no time overlap with the other tests, automatically disabling the possibility to set a timewise correlation between the vibration time histories of different nodes. Figure 4.23 shows the starting, duration, and ending timestamps followed throughout the tests. Finally, the details and findings regarding the monitored data and the identification results are presented in the following subchapter with further discussions.

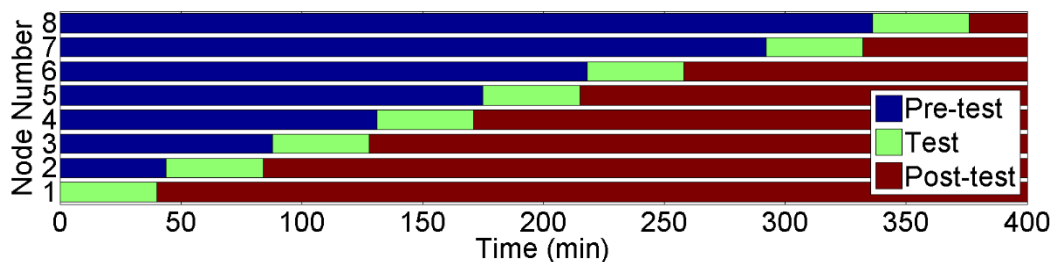


Figure 4.23: Test timeline

4.2.6 Results and discussion

Following the timeline and the sensor locations presented in the previous subchapter, acceleration measurements are recorded throughout 8 different smartphone tests. Posterior to the field tests, the overall data is separated into one-minute components and each component's time history is subjected to Fourier transform and plotted together to monitor the frequency distribution over time. In other words, Fourier spectra obtained from consecutive samples are plotted to conform a Short Time Fourier Transform (STFT) surface [148]. Figure 4.24 shows the STFTs which demonstrate the time-frequency characteristics obtained from each test. Based on the STFT results, one can distinguish that the modal characteristics remain the same with minor fluctuations over time. It can be observed that the spectral peaks are sensitive to the measurement location. For example, at Node 4 and Node 5 which are the closest points to the mid-span, the 2nd mode (antisymmetric) becomes invisible, whereas the 3rd mode (symmetric) peaks are maximized. In contrast, such behavior is reversed in case of Node 3 and Node 6, which are close to the one-third of the main span.

In order to test the energy stability over time and observe if the constancy assumption is violated, the total energy is calculated for each sample and presented in Figure 4.25. It is observed that the energy variation over different samples is insignificant except few samples observed in Test 2, Test 3, and Test 5. Based on the test records (pedestrian passes recorded with time instants), each of these fluctuations result from pedestrians inducing additional energy to the structure. Yet, from the figures, it can be observed that the deviation between samples in general is very low, and the energy level is consistent around 0.03 mm/s. Afterwards, in order to compare the spectral peaks obtained from different nodes, each test set is averaged based on the samples obtained throughout the measurements. Figure 4.26 shows the averaged spectra from each tests, showing the individual modal peaks obtained from different sensor locations.

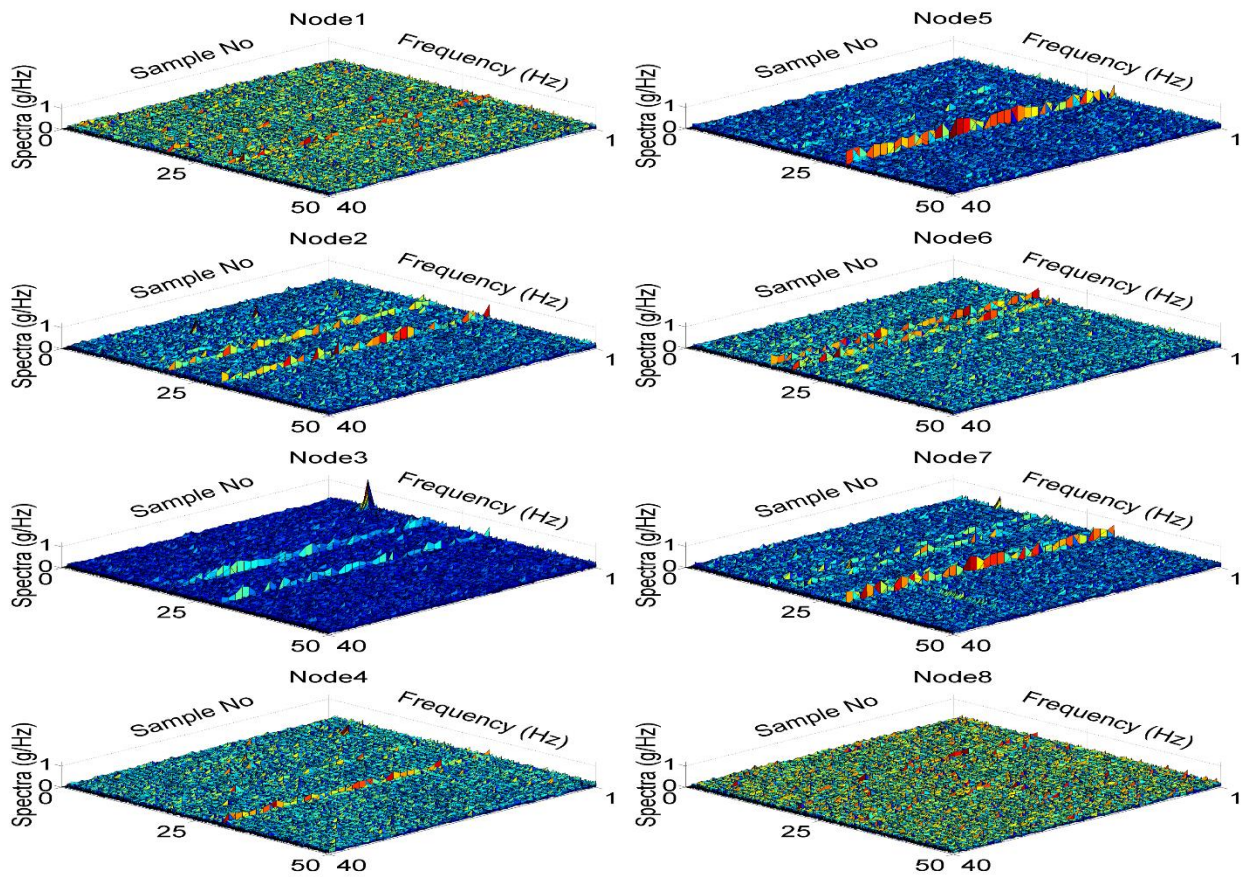


Figure 4.24: STFTs obtained from Test 1-8

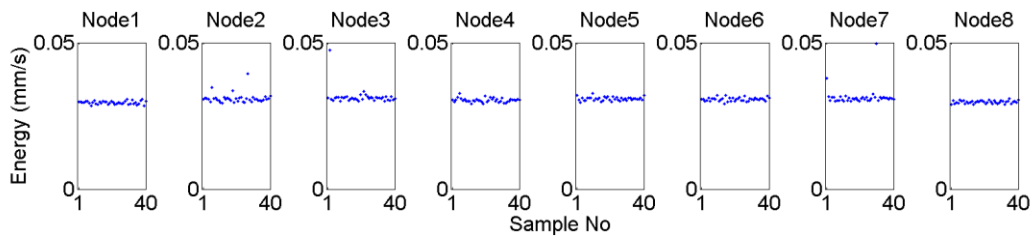


Figure 4.25: Sample energies from Test 1-8

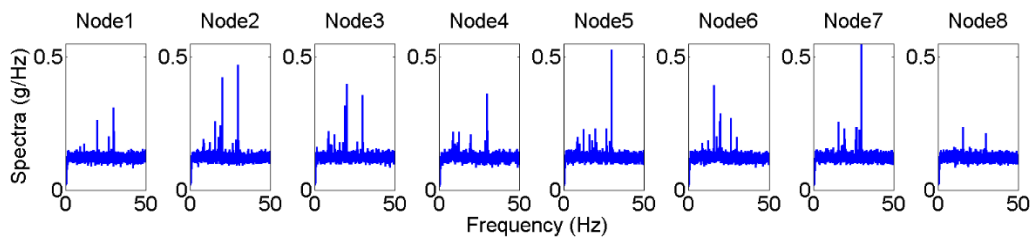


Figure 4.26: Averaged spectra from Test 1-8

Finally, in order to construct the global structural spectra based on spatiotemporally varying local measurements, the spectra obtained from 8 different channels are combined, the envelope of the resultant spectral values are taken, and the envelope spectra of the energy-normalized measurements is illustrated in Figure 4.27. According to the figure, the 1st, 2nd, and the 3rd modal frequencies obtained from the envelope spectra are 8.55, 20.0, and 29.99, respectively. That is to say, the errors between the smartphone and the reference systems are 1.8%, 6.4%, and 1.9%, for 1st, 2nd, and 3rd modes, respectively, which is reasonably accurate considering the uncertainties associated with the test timeline and locations. Looking at the spectral peaks of different tests corresponding to the modal frequencies obtained from global results, one can get the modal displacements. The only lacking parameter herein is the phase information between each nodes' responses. Using a baseline test data like reference identification results or a numerical model, such information can become available.

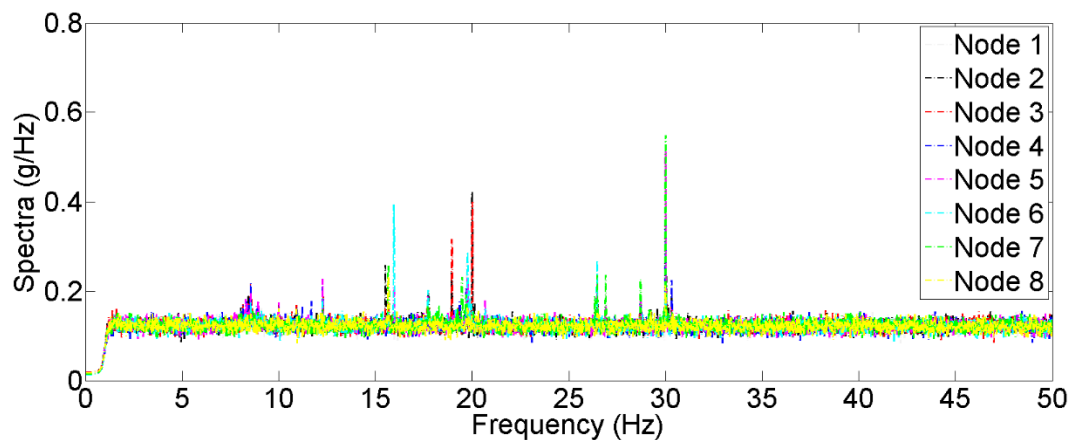


Figure 4.27: Envelope spectra from Test 1-8

Eventually, combining the phase information with the absolute modal displacements, the structural mode shapes can be determined. Figure 4.28 shows the mode shapes obtained from the analysis results. Looking at the Modal Assurance Criteria (MAC) [149] between the smartphone-based mode shapes and reference mode shapes, which are 0.98, 0.80, and 0.94 for 1st, 2nd, and 3rd modes, respectively, it can be concluded that the mode shape estimations are considerably accurate. The modal displacement values obtained from the smartphone deviate from the reference values as the value gets close to zero. In other words, for nodes which are subjected to very small

modal displacements compared with the other nodes (e.g. Node 5-7 for the 2nd mode, Node 3 for the 3rd mode), the smartphone tends to overestimate the actual value as a result of relatively low sensitivity. This observation is expected to vanish as the younger phone generations have accelerometers with higher sensitivities [1, 36].

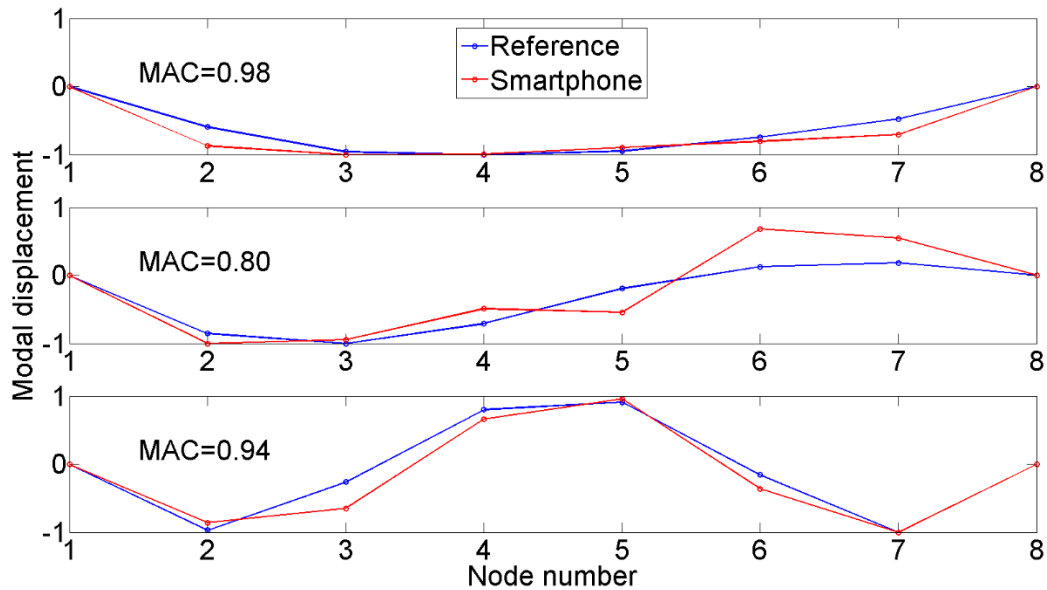


Figure 4.28: Identified mode shapes

In summary, it can be concluded that even under extreme spatiotemporal uncertainties, modal parameters can be identified with a significant accuracy. Composing a global envelope spectra from local measurement results, one can accurately identify modal frequencies. Besides, even the data obtained from different nodes vary in length and acquired at different times, they can be comparatively merged together and form mode shapes. With this approach, even though the device numbers are limited, mobile, and spatiotemporally uncontrollable, smartphones can be used to determine modal frequencies and mode shapes with a dense node array and reasonable accuracy.

4.2.7 Conclusions

In this study, smartphone-based SHM problems due to crowdsourcing-induced spatiotemporal sparsity are discussed, and solutions are formulated based on the multisensory location, time, and

vibration measurements. An unorthodox DSN and model identification problem is addressed, where, unlike conventional SHM systems, the network components cannot be controlled in the space and the time domain because of the smartphone users' initiatives. Combination of the sparse smartphone vibration data with no temporal connection is a unique SHM problem, since the existing applications, by default, carefully select sensor configuration and acquire multichannel data synchronously. Multisensory smartphone technologies are utilized to overcome these problems with an emphasis on sensor node identification, energy-to-power conversion, and synthesis of the sparse data.

First of all, sensor localization using smartphone geolocation services is discussed. The geometrical relationship between the sensor and structural node locations is established. Alternatively, QR codes are used to compress the location information, which can be scanned by the embedded camera, and might be essential for cases where the geolocation data is unavailable or unreliable. Afterwards, an energy normalization procedure is proposed to eliminate the duration differences between uncontrolled measurement submissions. Finally, the location, vibration, and the normalized spectral data collected from different submissions are synthesized to identify the modal frequencies and mode shapes.

The procedure is tested on a real pedestrian bridge with real smartphone data where each submission is independent of each other considering the sparse timeline of the test schedule. Time variation in different samples are monitored using the energy and STFT plots, and it is seen that the ambient vibration behavior is steady over time proper with the assumptions made. Despite all the spatiotemporal uncertainties discussed above, the modal frequencies are obtained with a significant accuracy around 3%. Likewise, the average MAC values gathered from the identified mode shapes are considerably high ranging around 0.91.

Based on the results obtained from the field tests, with the proposed procedure, it is observed that multichannel modal identification can be conducted even if the sensor configuration is limited, mobile, and uncontrollable in the time and the space domains, which is in correlation with the crowdsourcing-based SHM principles. The necessary data to resolve spatiotemporal uncertainties is provided by the smartphone sensors and the mobile operating system. Further advancement in this approach will construct a novel and sustainable multi-output SHM framework by utilizing the decentralized, cost and maintenance free, citizen-engaged, and ubiquitous smartphone data.

4.3 Human biomechanical effects

4.3.1 Introduction

Advances in system identification, statistical learning, and sensor technologies have boosted the influence of SHM on civil infrastructure assessment in the past three decades [2-3]. SHM has brought opportunities to support and improve conventional methods by means of structural response prediction, damage detection, performance evaluation, and reliability assessment [28, 29]. As new mobile [95-98], heterogeneous [99-102], smart [91-94], wireless, and distributed [124-129] sensing technologies emerge, SHM systems became more practical, cost-effective, and sustainable for not only laboratory and but also field applications.

With their embedded batteries, various sensors, and on-board computing capabilities, smartphones have brought a new possibility to compose novel mobile sensor networks for SHM applications [1, 36, 39, 103-107]. Engaging citizens through “Citizens for SHM” (CS4SHM) for structural vibration response measurement, as proposed by the authors, opens a new avenue of sustainable sensor systems, but faces significant technical challenges due to numerous uncertainties in the measurement process [1, 36]. Uncertainties in the time and the space domains [86] as well as in the device orientation [85] can be eliminated by multisensory data as long as the sensor is in direct contact with the structure of interest. Yet, the usability of sensor data carried or worn by human is still of question. For example, when a pedestrian’s smartphone is used to measure vibration of a bridge, the measurement data not only contains the structural vibration, but also the pedestrian’s biomechanical features. Using human biomechanical models, isolation of pedestrian features from smartphone data could reflect structure’s actual vibration characteristics in contrast with the raw data masked by biomechanical vibrations.

Biomechanical Models are widely used in automotive and aircraft industry as well as medical studies to understand vibratory effects on human bodies. Standing [150-157], seated [158-163], or both [164-165] human body vibrations were studied with the consideration of posture effects. Yet, these models were prone to variation stemming from numerous sources of uncertainties including individual subject characteristics [166]. Numerous multi degree of freedom (MDOF) and single degree of freedom (SDOF) biomechanical models are introduced to represent human bodies, but the variation among different individuals makes it difficult to adopt deterministic models for

particular cases. Besides, modeling human body and activities plays an important role on defining pedestrian and crowd loads on civil infrastructure, where the human-induced motion and structural response is not independent of each other, and should be examined together to involve human-structure interaction [84, 167-174].

For these reasons, it might be beneficial to avoid generalized models and instead collect customized sensor data in order to build pedestrian's biomechanical features. For example, studies have shown the possibility of using sensor data to identify posture and activity [175-177]. Likewise, similar vibration data collected from a pedestrian can be used to develop data-driven transfer functions and later on, filter human content out of onsite measurements. An advantage of smartphones is that they can be used to identify biomechanical properties in a mobile and individual-oriented framework. As mentioned previously, considering crowdsourcing as a data source for structural vibrations; citizen initiative and control in the measurement process produce numerous challenges in sensor positioning, orientation, and mobility [1, 36, 85, 86]. Pedestrians as crowd participants may be in various postures and be engaged in different activities; and depending on the action type, mobile data can be utilized in different ways. For example, the vibration data measured by walking pedestrians' smartphones or other wearable devices (e.g. smart watches, activity trackers) can be used to identify the human-induced forces on a structure, which would be helpful to determine the demand on the structure. The vibration data by the pedestrians' phones can also be used to estimate the bridge vibration and identify these modal properties, if the human body effects can be eliminated. Modal parameters such as natural frequencies reflect a structural system's properties that are linked to the health conditions or the capacity of the structural system. Pedestrian participation using smartphone sensors represents an innovative approach to SHM considering its cost-effectiveness, citizen engagement, and sustainability.

This study aims at understanding of the bridge structural vibration behavior and pedestrian forces imposed on the bridge through analysis of the vibration data measured by the pedestrians' smartphones. Firstly, accelerometer time history of a walking pedestrian is used to estimate forces imposed to the bridge. Secondly, smartphone accelerometer data measured by a user standing on a rigid platform are employed to develop transfer functions representing pedestrian's biomechanical system, which are used to extract the bridge structural vibration out of the data. Chapter 4.3.2 introduces the methodology and framework involving the biomechanical models,

transfer functions, and walk-induced forces, and describes field tests on a pedestrian bridge. Chapter 4.3.3 applies the proposed methodology to analyze the bridge test results. Finally, Chapter 4.3.4 summarizes the findings and draws conclusions from this study.

4.3.2 Methodology and framework

A fundamental difference between CS4SHM and a conventional monitoring system is that structural vibrations are indirectly measured through smartphone users rather than sensors fixed on the structure. In other words, smartphone users appear as an intermediary medium between the sensors and the structure.

Smartphone users may play different roles during a structural vibration measurement process depending on structural type and service needs. For example, for buildings, smartphone users are building occupants, who likely maintain a stationary position for a long time interval. In contrast, for bridges, smartphone users are moving pedestrians whose presence is transitional and whose position spatiotemporally varies. Monitoring of building structures can utilize smartphone sensors as stationary devices, since phone position and fixity can be predetermined and maintained throughout long measurement durations. The building occupants may leave their phones at the prescribed locations to directly collect vibration data. In contrast with the building occupants, bridge pedestrians are unlikely to leave their smartphones on the bridge unattended for a long time for the purpose of bridge SHM. For this reason, it is more feasible to collect sensor data from smartphones held in hands or carried in bags by the pedestrians. As a result, the sensor data contains not only bridge vibration but also the pedestrian's biomechanical features.

The human body of a pedestrian on a bridge can be considered as an intermediary mechanical system, in which (1) the vibration data measured by his/her smartphone is the output, (2) the bridge structural vibration is the input, and (3) the human body is the system. And this mechanical system can be represented with transfer functions or signal filters. These transfer functions or filters can represent pedestrians' mechanical system properties. If the system (i.e. the transfer function) is known and the output can be measured, eventually, the system input (i.e. the bridge vibration) can be obtained.

In this study, stationary human-induced effects are considered as the effects of a biomechanical system, which can be modeled as transfer functions. Likewise, motion record of a pedestrian

moving on a bridge can serve as a dynamic force measurement. To make a distinction between these two major cases, two pedestrian mobility scenarios are taken into consideration, which are (1) standing and (2) walking. The following subchapters introduce exemplary biomechanical models existing in the literature, then use these models to define characteristics of the pedestrian vibrations. In addition, a citizen-centric biomechanical model development procedure is proposed, with the help of the mobile data obtained from smartphones to characterize their individual users. Then, a pedestrian bridge is implemented as a testbed to discuss the presented methodology's validity through experimental verification.

4.3.2.1 Biomechanical models

As discussed previously, pedestrians, in other words human body and their accessories, can act as mechanical systems modifying the structural vibrations into vibrations indirectly measured by the smartphone user. To add, a smartphone in a backpack, pocket, bag or luggage might have a different transformation procedure as well as pedestrian's posture such as sitting, standing or walking. Figure 4.29 illustrates certain citizen statuses which might have different biomechanical effects and accordingly transform structural vibrations into a modified signal. Depending on the pedestrian posture, activity, and the coupling between the smartphone and the user, the vibration signals can be converted into a different character. Considering all of these effects as the pedestrian system, if the mechanical properties are well-defined, the final output or the pedestrian-measured data can be converted back into the structural data as the input source. In order to do that, human body biomechanical models are investigated as follows.



Figure 4.29: Exemplary citizen postures and activities

In literature, human body vibratory effects are commonly represented with biomechanical systems which are extensively studied in numerous ranges from mechanical engineering to biomedical sciences. A variety of biomechanical human models are proposed by researchers

considering stationary postures such as seated, and standing, or systems in action such as jumping or running. Likewise, there is a significant variation in modeling details, for example, the same posture, i.e. seated pedestrian, is represented with models of multiple or single DOFs [178-181]. Figure 4.30 illustrates exemplary human biomechanical models varying extensively in the modeling abstraction, showing that the model complexity might change depending on the developer’s choice and modeling purpose.

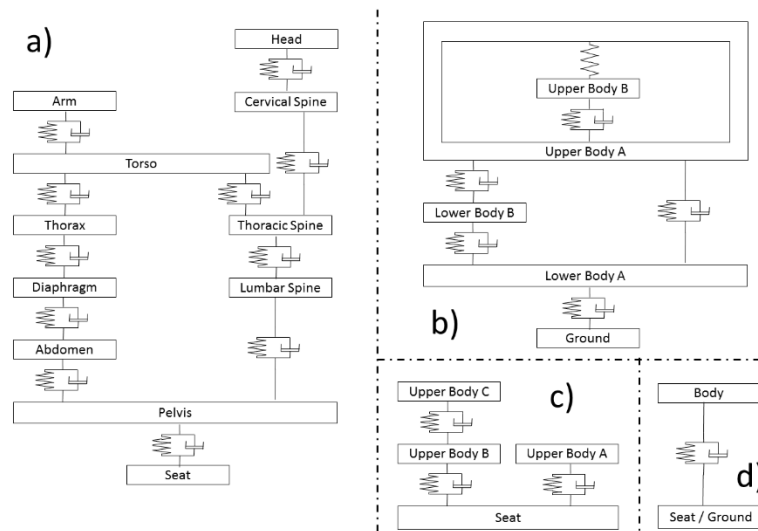


Figure 4.30: Human biomechanical models of different detailing

Spatiotemporal variation or changes in the device orientation are previously discussed scenarios in a citizen-centric mobile SHM framework [85-86]. Likewise, in smartphone-based SHM systems, it is expected that the monitoring results are significantly affected by the uncontrollable sensing environment due to crowdsourcing initiatives. These initiatives can result from pedestrian identity (height, weight, age, gender, etc.), mobility (stationary, walking, running, etc.) as well as wearables and accessories (bag, backpack, pocket etc.). In addition, these uncertainties are likely to interact with each other and therefore, representation of such complex behavior might be cumbersome. This problem is decisive in the identification process, detailed and predefined theoretical models may not be sufficient to investigate indirect and highly uncertain structural vibration signal characteristics obtained from pedestrians. Likewise, the parameters defining a pedestrian’s model may have unique features which are not captured by the benchmark

approaches in the literature. For this reason, it might be beneficial to define biomechanical characteristics of a pedestrian in an individual-oriented scope.

To paraphrase, rather than relying on generic definitions existing in the literature, smartphone data is utilized to identify the pedestrian's biomechanical system and targets to extract useful information for SHM purposes. In addition, for multiple scenarios such as different postures and activities, customized biomechanical models can be developed with the help of vibration data obtained from smartphone sensors. In other words, according to the proposed method, smartphones are firstly used to describe biomechanical features of individual pedestrian for various posture and activity cases, then are used to diminish these features from the smartphone data when the pedestrian conducts vibration measurements on civil infrastructure. With this data-driven approach, neither detailed nor simplified generic analytical models do not need to be pursued; yet, individual and unique pedestrian features can be distinguished. Next subchapters investigate existing pedestrian force models as well as transfer functions representing human biomechanical features.

4.3.2.2 Walk-induced vibrations

This subchapter addresses the first pedestrian mobility scenario which is related to the walk-induced forces on a bridge structure. Early modeling principles in pedestrian loads assumed that the motion imposed to the structure by the human body is independent of structure's characteristics and a variety of pedestrian-induced force models exist in literature. One of the most widely used model is a deterministic expression representing pedestrian forces with Fourier series [182].

$$F_p(t) = G + \sum_{i=1}^n G \cdot \alpha_i \cdot \sin(2\pi i f_p t - \varphi_i) \quad (4.20)$$

where G is the person's weight, α_i is the Fourier coefficient of the i^{th} harmonic, f_p is the activity rate, and φ_i is the phase shift of the i^{th} harmonic. Some exemplary values used to define walk-induced vibrations in the literature are Model 1 (Vertical: $\alpha_1 = 0.257$); Model 2 (Vertical: $\alpha_1 = 0.400, \alpha_2 = 0.100, \alpha_3 = 0.100$); Model 3 (Vertical: $\alpha_1 = 0.37, \alpha_2 = 0.10, \alpha_3 = 0.12, \alpha_4 = 0.04, \alpha_5 = 0.08$); and Model 4 (Longitudinal: $\alpha_1 = 0.204, \alpha_2 = 0.083, \alpha_{\frac{1}{2}} = 0.100, \alpha_{\frac{3}{2}} = 0.026, \alpha_{\frac{5}{2}} = 0.024$) [168].

Figure 4.31 shows the deterministic model time histories with different coefficients presented

above as Model 1-4 for $G=700$ N and $f_p = 2.0$ Hz. According to the figure, similar with the biomechanical model abstraction variety, some methods simplify the pedestrian-induced vibration as a single sine function, whereas others include harmonics with decreasing amplitudes, and some considering longitudinal and transverse directions as well. As previously mentioned, these models constitute a reliable base for pedestrian modeling, yet, may not be perfectly representative of individual pedestrians in real life. Therefore, extraction of human body acceleration time history from smartphone sensors while walking may be a novel and promising approach to estimate pedestrian forces directly related to that particular smartphone user.

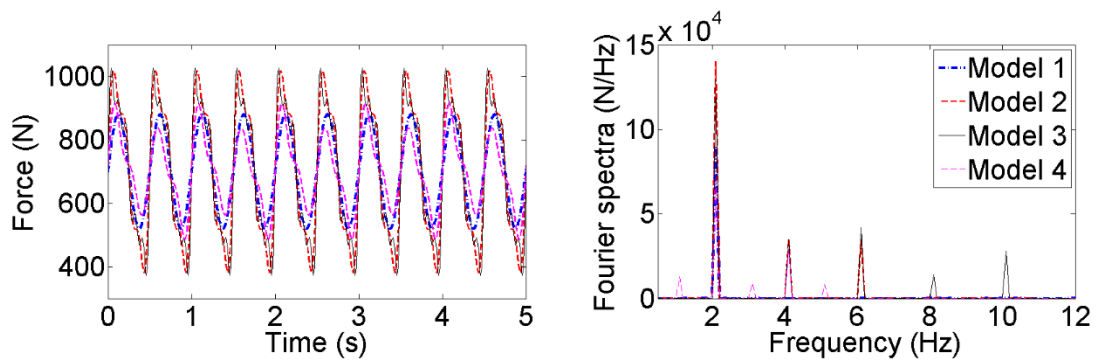


Figure 4.31: Walk-induced pedestrian force models

The walk-induced force modeling approaches discussed so far exclude the effects of pedestrians and structures on each other. After numerous studies, it is found out that the interaction between the pedestrian's and the structure's mechanical systems recursively affect each other. In other words, similar with the transition from rigid support models to soil-structure interaction, or from simplified moving vehicle loads to vehicle-structure interaction, conventional pedestrian load models evolved into comprehensive approaches introducing human-structure interaction. In this study, the interaction between the structure and the pedestrian is not explicitly considered, yet few remarks will be presented in Chapter 4.3.3 as the field test results are discussed.

4.3.2.3 Transfer functions

The previous subchapter discussed widely used pedestrian load models related to walk-induced vibrations. This subchapter introduces how human biomechanical features are interpreted using

transfer functions, and how standing pedestrian data can be used for modal identification. In order to understand the vibration transmission from structural to pedestrian mechanical systems, a multiphase signal processing procedure can be pursued. According to the proposed scheme, determination of structural vibration is the key goal to identify structure's dynamic characteristics. On the other hand, such vibration cannot be directly measured in case of a wearable or smartphone sensor scenario. Instead, the measured pedestrian vibration response is a combination of structural vibration response with human body's biomechanical features. For this reason, in order to obtain structural vibrations from indirect pedestrian data, pedestrian's dynamic system properties should be determined. If the system properties are accurately selected, pedestrian vibration response can be converted back into structural response by transfer functions as transformation media in the frequency domain. In this way, although the pedestrian data is indirect and masked with human biomechanical features, transfer functions can be used to convert pedestrian measurements into structural vibration response data by isolating biomechanical effects from smartphone data. The generalized formulation for transfer functions, representing MDOF human biomechanical systems as single-input single-output processes, is given as [149],

$$H_{system}(w) = \sum_{r=1}^N \frac{A_r}{(w_r^2 - w^2 + 2 \cdot i \cdot w \cdot w_r \cdot \xi_r)} \quad (4.21)$$

where r is the mode number, w_r is the modal frequency, ξ_r is the damping ratio, i is the complex number, w is the frequency variable, and A_r is the complex modal constant. For a SDOF system, this form can be interpreted in terms of the mechanical system parameters such as [183],

$$H_{system}(w) = \frac{1}{\sqrt{(k - w^2 \cdot m)^2 + (w \cdot c)^2}} \quad (4.22)$$

where m , c , and k are the mass, damping, and stiffness constants of the SDOF system.

Researchers have adopted various different biomechanical models for different actions and postures. Besides, it is widely discussed that the biomechanical properties extensively vary among different test subjects. For instance, 8 subjects are represented with SDOF models of the same stiffness and damping such as $k(\text{N/m})=116000$, and $c(\text{Ns/m})=2310$, but different masses such as $m(\text{kg})=\{90,84,99,70,82,91,94,72\}$ [181].

Using these parameters, Figure 4.32 presents exemplary transfer functions of subjects ranging between 50 kg and 95 kg. Similar with the force models existing in the literature, transfer functions

of different subjects may not accurately represent others' behavior, e.g. resonant frequency of a 95 kg (5.5 Hz) subject can be significantly different from a 50 kg (7.6 Hz) subject. In other words, generic models may be incapable of representing different pedestrians as well as different postures and activities of the same pedestrian. For example, dominant frequency of a standing pedestrian can range between 5-10 Hz depending on the pedestrian's biomechanical properties. Therefore, this study proposes a data-driven and customized approach to construct transfer functions representing pedestrian behavior individually. For this purpose, the smartphone data obtained from each pedestrian is converted from the time domain into the frequency domain through Discrete Fourier Transform (DFT) for a particular individual and posture scenario. The definition of posture or action, and the user identity can be entered by the smartphone user, and be associated with the corresponding transfer function. In this way, transfer functions do not necessarily have to be the same for different pedestrians, postures, and activities.

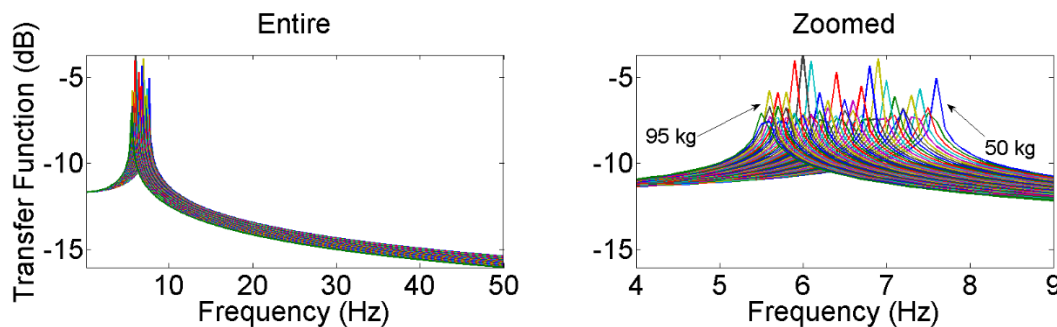


Figure 4.32: Transfer functions based on biomechanical models of different subjects

Figure 4.33 shows a conceptual signal transformation path from structural vibration source to sensor data through a multilayered mechanical system chain. Initially, the vibration source is dependent on surrounding media such as operational, environmental, or ambient nature. Then, the source vibration signal is processed through the structural system and transferred to the pedestrian body as an input motion. In other words, structural response vibrations, which is the eventual target parameter, act as the input to the pedestrian's mechanical system. Then, the vibration continues to evolve through the pedestrian's body and the additional mechanical components (e.g. accessories such as bag, pocket, or phone case), and ultimately is sensed by the smartphone sensor.

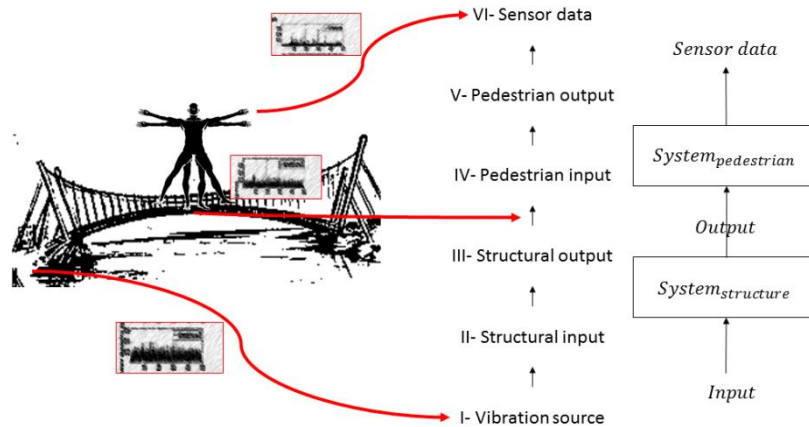


Figure 4.33: Signal flowchart through the vibration source and the sensor data

In summary, the evolution of a vibration signal through a citizen-centered smartphone-based SHM system is composed of two distinct mechanical systems which are the structure and the pedestrian, respectively, and shall be distinguished from each other through an inverse process. In order to consider structural and pedestrian mechanical systems as separate components, pedestrian biomechanical properties need to be determined. In order to set the framework for this separation, transfer functions can be utilized. That is to say, the transition from structural response to pedestrian's sensor measurement is a function of the pedestrian biomechanical system, therefore can be interpreted in terms of this biomechanical system's transfer function. Likewise, knowing the biomechanical system properties enables to switch from pedestrian sensor data to the structural response by isolating the biomechanical features with the help of the transfer function.

Linear signals and systems principles suggest that, response vibration time histories can be considered as the convolution of the input and the structural motion time histories, and convolution of two vibration time histories refers to the multiplication of two frequency spectra [79]. In other words, processing vibration signals through systems in series can be interpreted in terms of spectral changes in the frequency domain. In this way, procession of a vibration signal can be formulated with three components such as

$$F_{output}(w) = H_{system}(w) \cdot F_{input}(w) \quad (4.23)$$

where F_{input} is the input, H_{system} is the system, and F_{output} is the output values in the frequency domain. In other words, these parameters represent the forcing function, the transfer

function, and the response function of a mechanical system, respectively.

Adding multiple mechanical systems on top of each other in series can be represented with convolution operands in the time domain or multiplication operands in the frequency domain [184]. Following this approach, two in-contact mechanical systems such as a structure and a pedestrian body can be represented with individual systems connected to each other where the structural output is imposed as the pedestrian input. Accordingly, the multilayered mechanical system can be formulated with two transfer functions such as

$$F_{intermediary}(w) = H_{structure}(w) \cdot F_{source}(w) \quad (4.24)$$

and

$$F_{sensor}(w) = H_{pedestrian}(w) \cdot F_{intermediary}(w) \quad (4.25)$$

where $F_{intermediary}$ is structural response, $H_{structure}$ is structure's transfer function, F_{source} is structural input, $H_{pedestrian}$ is human biomechanical transfer function, whereas F_{sensor} is the output obtained from the smartphone sensor signal. Eventually, provided that the source function, and the biomechanical system is known, these two equations can be merged with the help of intermediary element, and the structural system can be identified from indirect pedestrian data such that,

$$H_{structure}(w) = \frac{F_{sensor}(w)}{H_{pedestrian}(w) \cdot F_{source}(w)} \quad (4.26)$$

If the source vibration is idealized as white noise, the equation can be reduced to

$$H_{structure}(w) = \frac{F_{sensor}(w)}{H_{pedestrian}(w)} \quad (4.27)$$

According to this framework, smartphone sensor signals are combinations of the structural and the pedestrian features. And eliminating pedestrian features from sensor data will result in structural features. The sensor data collected from a pedestrian standing on a bridge represents the nominator spectra, whereas, denominator spectra is constructed by collecting pedestrian data standing on a rigid zone, e.g. basements, streets without extreme vehicle traffic, or building ground levels if the substructure is negligible. Dividing sensor spectra by pedestrian spectra will return structural system spectra, which can eventually be used as a measure of modal identification. In order to present the proposed approaches with a real example, the next subchapter introduces field

tests conducted on a single span existing bridge and real pedestrian data.

4.3.2.4 Field tests

In the previous subchapters, biomechanical models, walk-induced vibrations, and transfer functions are discussed. In order to connect these concepts with mobile sensors carried by smartphone users, the methodology is demonstrated on an actual bridge example with real pedestrian data. Mudd-Schapiro Bridge, shown in Figure 4.34, is a 10 meter single span pedestrian link bridge connecting two high-rise buildings on Columbia University Morningside Campus, New York. The structural system consists of steel members with rigid connections, transferring the bridge loads to the adjacent buildings through a lower arch. Using an iPhone 5 with the accelerometer model LIS331DLH (ST Microelectronics), structural vibration measurements are indirectly measured through pedestrians, as shown in Figure 4.34.

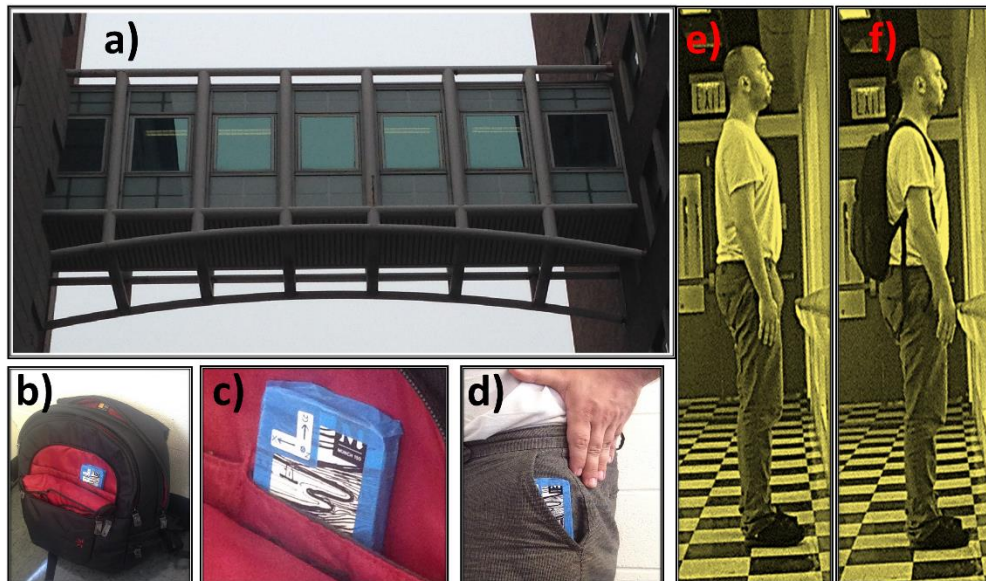


Figure 4.34: Bridge and pedestrian instrumentation

Previous studies discussed that device model, orientation, position with respect to the structure, and measurement duration plays an important role in the vibration measurements as well as the type of loading and sensor-structure coupling. Potential pedestrian postures and activities on a civil infrastructure are unlimited, therefore, only few common scenarios are tested in this study which

include: smartphone (1) directly attached to the bridge deck surface, (2) resting in a bag on the deck, (3) in a pedestrian’s pocket, and (4) in a backpack carried by a pedestrian.

Table 4.9 summarizes the variation sources in structural vibration data extracted from pedestrians, sources of uncertainties, positive and negative extremes in sensing conditions. Vibration measurements can be more representative of structural characteristics, if they are conducted under ideal conditions. For example, broad band vibrations are capable of exciting multiple modes without signal corruption due to any nonstructural frequency content. Setting a stationary position for the device, maintaining coupling conditions, and proper alignment of phone axes are other citizen-induced problems that might have influence on vibration signal quality.

Table 4.9: Sources of uncertainties in pedestrian-extracted structural vibration data

Source	Optimistic Case	Pessimistic Case	Affected Process
Vibration	Ambient (Broad Band)	Operational (Narrow Band)	Loading
Activity	Stationary	Moving	Sensing/Loading
Attachment	Direct (glued)	Indirect (e.g. pocket)	Sensing
Orientation	Face Up or Down/Portrait/Landscape	Combined	Sensing

Considering all these uncertainties together with pedestrian posture and activity, it is cumbersome to make a strict classification or adopt generalized modeling criteria. In order to simplify pedestrian posture, activity, and their effects on structural vibration measurements, the tests presented in this study are based on certain layout assumptions. For example, the phone, located in a bag or in a pocket, is adjusted to portrait position. In real life, phone layout can be different than these scenarios, yet it is possible to detect the layout with accelerometer and magnetic compass data, and even to convert the vibration axis from local layout coordinates to structural coordinates [85]. Similarly, the stationary or standing pedestrian tests are conducted at the bridge mid-span, which may not be the case as discussed in [86]. Yet, as these factors are discussed in previous works, the posture and activity tests in this study present exemplary but

fundamental cases rather than covering all possible combinations.

Table 4.10 presents the test descriptions followed throughout the field tests. A case is composed of 4 tests and each test includes 30-minute vibration data. There are 8 cases presented in this study, which, in total, is based on 16 hours of real pedestrian data. Test 1-4 (Case 1) and Test 9-12 (Case 3) sets are used to represent walk-induced forces, Test 17-24 (Case 5-6) sets are conducted under no human body involvement, Test 13-16 (Case 4) and Test 29-32 (Case 8) sets are used to develop standing pedestrian transfer function on a rigid location. And finally, Test 13-16 and 29-32 sets are used to eliminate human-induced effects from Test 5-8 (Case 2) or Test 25-28 (Case 7) sets, respectively, which are products of structure's mechanical system as well as human biomechanics.

Table 4.10: Test descriptions

Case	Test	Location	Vibration	Device	Attachment	Orientation	Coupling	Measure
1	1-4	Bridge	Operational	Moving	Backpack & Pedestrian	Portrait	Indirect	Output
2	5-8	Bridge	Ambient	Stationary	Backpack & Pedestrian	Portrait	Indirect	Output
3	9-12	Street	Operational	Moving	Backpack & Pedestrian	Portrait	Indirect	System
4	13-16	Street	Ambient	Stationary	Backpack & Pedestrian	Portrait	Indirect	System
5	17-20	Bridge	Ambient	Stationary	Backpack on Ground	Portrait	Semi- Direct	Output
6	21-24	Bridge	Ambient	Stationary	Phone on Ground	Portrait	Direct	Output
7	25-28	Bridge	Ambient	Stationary	Pocket & Pedestrian	Portrait	Indirect	Output
8	29-32	Street	Ambient	Stationary	Pocket & Pedestrian	Portrait	Indirect	System

4.3.3 Results and discussion

In the previous subchapter, the theoretical framework for biomechanical models, walk-induced forces, and transfer functions are presented to utilize mobile pedestrian data for SHM purposes. Moreover, a series of pedestrian tests, each addressing a particular mobility scenario, are conducted while smartphone accelerometers recorded pedestrian's vibrations under variety of scenarios. In this subchapter, the test measurements are presented, the proposed force and modal identification methods are implemented, and the analysis results are discussed.

In total, 8 cases and 32 tests are conducted by recruiting a smartphone user as a pedestrian subject for 16 hours of vibration measurement. Each 4 repetitive tests refer to a case representing particular measurement location, vibration source, and mobility. Basically, Case 1 and Case 3 data is processed to comprehend forces imposed by a walking pedestrian on a rigid platform, and on the bridge, respectively. Relying on the insignificant difference between these two cases, the pedestrian-structure interaction during these tests are ignored. In Case 2-7 and Case 4-8, the pedestrian is standing on the bridge (structure) and on the ground level (rigid platform), respectively. Dividing Case 2 (or Case 7) spectra by Case 4 (or Case 8) spectra over the frequency domain, the resultant spectra is expected to present sole structural modal parameters. Finally, Case 5 and Case 6 presents smartphone data which is free of human-induced vibrations, such that the device is placed on the bridge deck either in direct contact or in a bag. Figure 4.35 shows the time histories and the Fourier spectra from Test 1, 5, 9, 13, 17, 21, 25, and 29, respectively. In this study, two main pedestrian mobility phenomena are taken into consideration which are walking (Case 1 and 3), and standing (Case 2, 4, 7, and 8). Other than these, Case 5 and 6 are considered as output-only identification cases and references which are not influenced by pedestrian's biomechanical features.

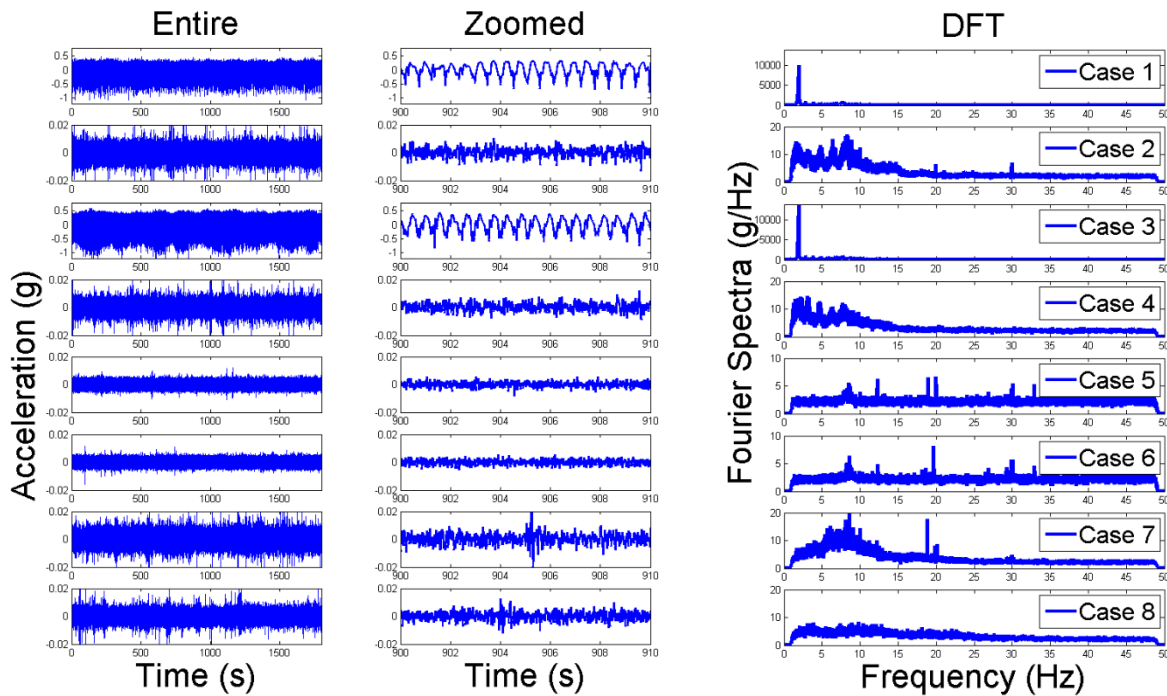


Figure 4.35: Time histories and Fourier spectra for Case 1-8

4.3.3.1 Estimating pedestrian forces

In Case 1 and Case 3, assuming that the entire pedestrian mass contributes to the walk-induced force, the accelerometer data is used to scale the pedestrian mass (e.g. 71 kg) in time series. Using the vertical component (smartphone y-axis) which coincides with the gravitational direction, walk-induced time history can be converted from acceleration to force. Figure 4.36 shows the exemplary time histories and corresponding Fourier spectra obtained from Case 1 and Case 3. It is cumbersome to compare Figure 4.36 with the theoretical model illustrated in Figure 4.31, yet the qualitative similarity is still significant both in the time and the frequency domains. Looking at the force time history estimated by the smartphone, unlike the theoretical model, it can be observed that the peaks in the positive and the negative directions are not of same pattern. It is observed that the positive peaks are smooth in contrast with the sharp negative peaks. Such difference is due to smartphone's position in pedestrian's bag, shown in Figure 4.34. As the pedestrian walks, smartphone accelerometer in y-axis records vertical pedestrian motion indirectly through the bag. Smartphone's bottom surface rests on the bag, and is not perfectly attached to the bag's pocket.

While the pedestrian and the bag move towards the gravitational direction, there is no external inertia to drag the smartphone downwards except phone's mass. In contrast, when the movement is upwards, the phone is pushed against gravity via bag's pocket. For this reason, change in the positive direction is more gradual while negative peaks are abrupt. Nevertheless, both the theory and the smartphone estimations are periodical time series, ranging around a peak-to-peak amplitude of 600 N. Another observation is that the Fourier Spectra obtained from smartphone measurement not only includes the vertical motion harmonics, but also the harmonics related to the lateral and the longitudinal motion. For example, as expected, the dominant walk-induced frequency range around 1.9 Hz, and smaller peaks such as 2.8, 3.8, 5.6, 7.3, and 9 Hz are observed as multiples of the dominant frequency. This can be due to the deviation of smartphone axis while traveling which would introduce additional components in the axes other than vertical.

Comparing the walk-induced pedestrian motions on rigid surface (Test 4) with the bridge (Test 12), the difference is insignificant both in the time and the frequency domains. According to these results, there is no clear indicator of the change in measurement environment and structural features. One possible reason for such indifference is the dominance of walk-induced vibration with respect to the structural vibrations, sensitivity and resolution of the smartphone sensor, and motion damped out by the human biomechanical system. In the future studies, if the bridge data can be distinguished from the street data, walking pedestrian data can be used for structural system identification as well as standing pedestrian data. Moreover, this would bring new frontiers in pedestrian-structure interaction research, but is not addressed in this study. At this stage, it is difficult to draw a concise conclusion based on a single structure, and collecting data from a large number of structures might provide more information.

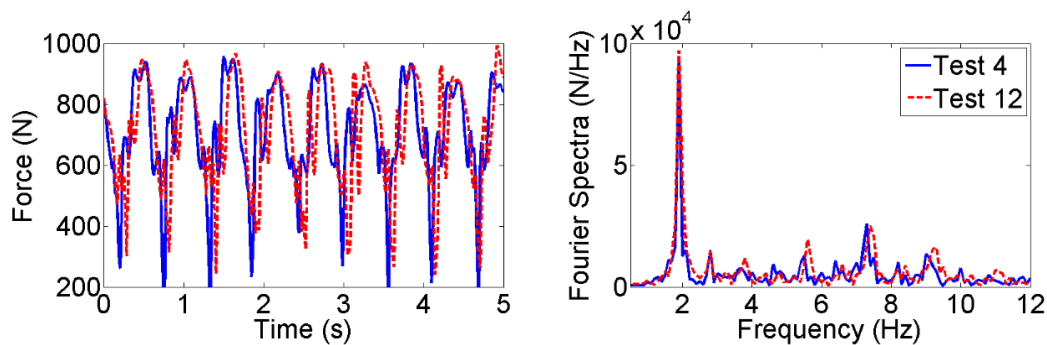


Figure 4.36: Walk-induced forces identified by pedestrian's smartphone

4.3.3.2 Isolating biomechanical effects and modal identification

In this subchapter, the main goal is to identify modal parameters of the bridge structure through standing pedestrian data sensed by smartphones. Case 2, 4, 7, and 8 refer to the standing pedestrian tests, which are used to isolate human body and accessory effects from the smartphone data. These cases aim at comparing the vibration differences between two different media such as the bridge (deformable) and the street (rigid). In addition, to understand how pedestrian state, posture, and smartphone configuration effect the vibration features, two different attachment cases are presented. The first attachment case refers to the pedestrian carrying the smartphone in a backpack whereas the latter case describes phone positioned in pedestrian's pocket. There might be a variety of other posture and accessory combinations, and these two cases only present a basic understanding of the phenomenon. The goal of demonstrating two different attachment cases such as pedestrian's bag and pedestrian's pocket is to show how the biomechanical features of the same pedestrian impact the indirect structural response data sensed by the smartphone.

In both of the attachment cases, the same transfer function procedure is utilized, but the baseline transfer function differs depending on the attachment type. As previously discussed, the sensor output, measured by pedestrian standing on a bridge, is a function of the structural and biomechanical features. Therefore, Fourier transform of the pedestrian standing on a bridge includes frequency content from the pedestrian as well as the structure. And eliminating biomechanical features from this modulated signal leads to the sole structural signal which can eventually reflect bridge's current state. For this reason, pedestrian's biomechanical system features should be removed from the output data. In order to determine system spectra of a pedestrian, vibration data of a pedestrian standing on a rigid surface can be utilized, since it is only a function of the pedestrian's biomechanical features. If pedestrian system features are determined, biomechanical contribution can be removed from the mixed smartphone sensor signal by dividing the output spectra with the pedestrian's system spectra. Finally, the spectra due to structural vibrations can be inferred as the input to the pedestrian's biomechanical system, which at the same time, is structural output. Afterwards, pedestrian input, or in other words structural output, can be used to identify structural modal properties without any biomechanical intervention. To summarize, output spectra obtained from a pedestrian standing on a bridge contains mixed characteristics from the pedestrian biomechanical system and the structural system. System spectra is constructed by

measuring pedestrian’s vibration response standing on a rigid platform (e.g. street level). Finally, input spectra, which is the division of output by system spectra, reflects pure structural characteristics isolated from biomechanical features and can be used for modal identification. Figure 4.37 summarizes how the transfer functions are used to remove biomechanical effects for modal identification in Mudd-Schapiro Bridge example.

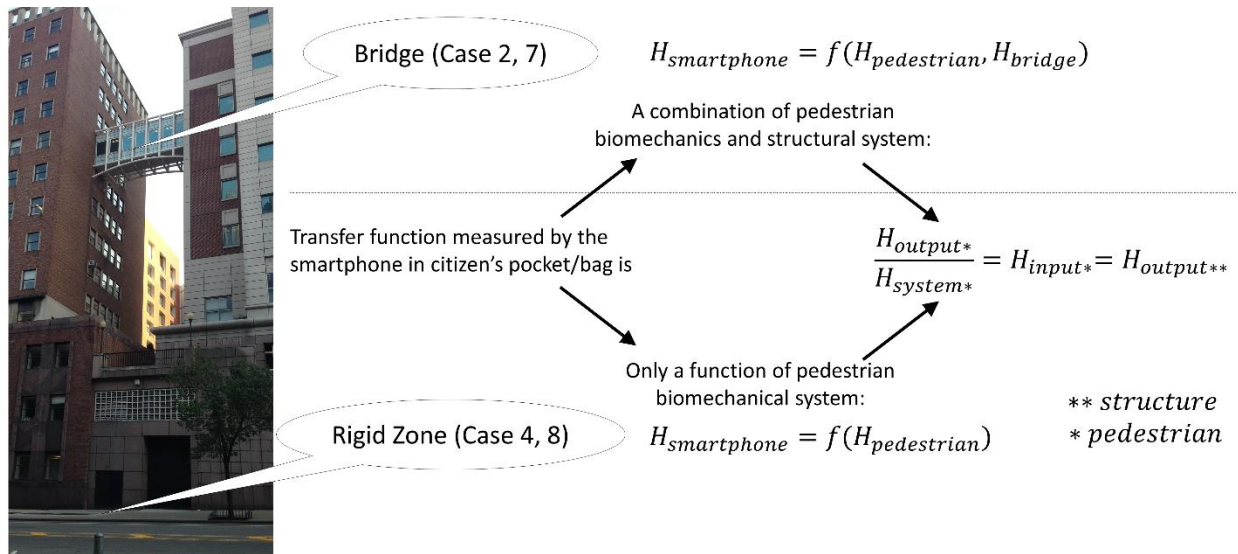


Figure 4.37: Scheme for isolation of biomechanical features through transfer functions

Figure 4.38 and Figure 4.39 shows the output, system, and input spectra for two different attachment cases, which are phone placed in pedestrian bag and pocket. Looking at the system spectra of these two attachment cases, it can be observed that the mechanical features are subjected to change as the attachment media changes, implying that bag and pocket transfer functions are not exactly the same. On the other hand, for both cases, it can be seen that the system spectra has a direct impact on the output spectra, which significantly masks the input spectra, and accordingly, structural vibrations. Finally, using the transfer function procedure proposed previously, input spectra can be reconstructed from the output (pedestrian on the bridge) and the system (pedestrian on the street or rigid surface) spectra. Looking at the input spectra which is a representative of the structural vibrations, structural peaks can be observed much more clearly than the indirect pedestrian signals (output spectra). For example, in both attachment cases, the 2nd and the 3rd modal frequencies around 20 Hz and 30 Hz are the same as the ones obtained from output-only

cases studied in Case 5-6. The 1st mode peak, 8.5 Hz, is somewhat less significant since the biomechanical system frequencies are dominant between 5-10 Hz frequency bands. Such difference can be seen looking at the Case 5-6 examples showing the spectra obtained from phone directly attached to the bridge deck surface without any biomechanical intervention. Figure 4.40 shows the Fourier spectra obtained from output-only cases, Case 5-6.

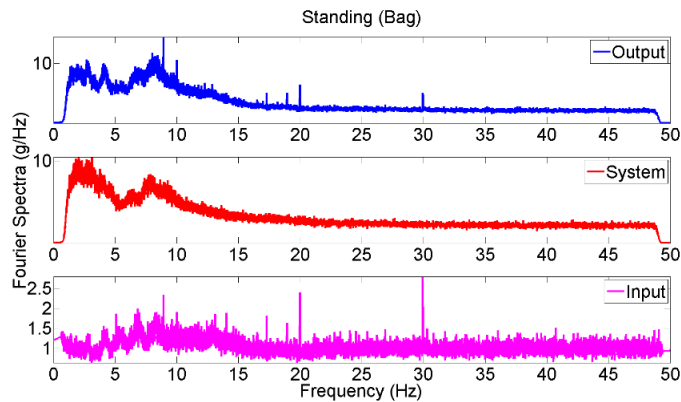


Figure 4.38: Biomechanical effect isolation process for phone in pedestrian's bag

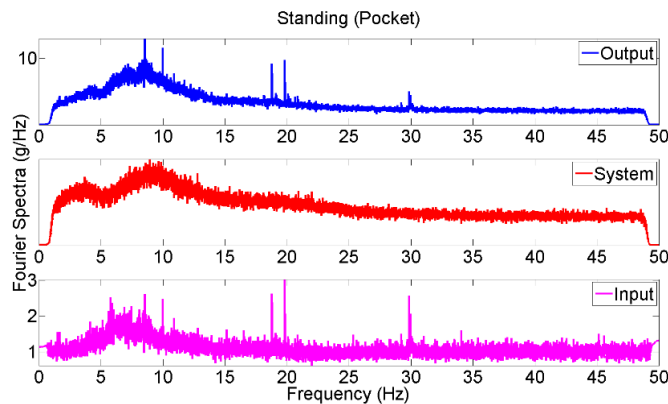


Figure 4.39: Biomechanical effect isolation process for phone in pedestrian's pocket

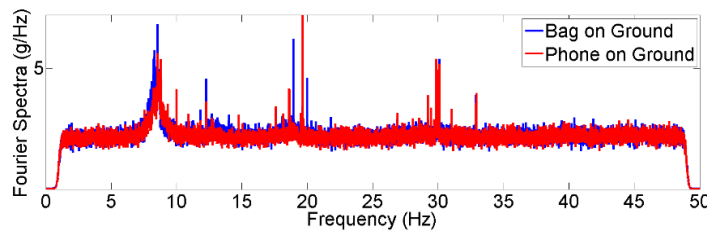


Figure 4.40: Fourier spectra for output-only cases (no pedestrian interference)

4.3.4 Conclusions

In this study, focusing on smartphone sensors, mobile pedestrian data, and participatory sensing, an unconventional modal identification and accordingly SHM problem is discussed. Pedestrians as smartphone users provide the infrastructure monitoring systems with a crowdsourcing potential, on the other hand, the data acquired by them is subjected to extensive deterioration due to citizen-induced effects. In particular, this study aims at elimination of biomechanical effects from crowdsourced data and extract structural vibrations from smartphone sensors carried by pedestrians.

This study explores the potential of using vibration data measured by mobile pedestrians' smartphones for identifying the bridge structure's modal parameters, which can be used for the bridge SHM. Pedestrians as smartphone users serve as mobile sensors with a crowdsourcing potential. However, the vibration data measured by the pedestrians' smartphones are affected by their human body biomechanics. This study addresses the technical challenge by removing the biomechanical effects from crowdsourced smartphone data to extract the bridge structural vibrations and subsequently the structural parameters.

Two major realistic pedestrian mobility scenarios are taken into consideration such as walking and standing. For the walking case, sensor carried by the pedestrian is used for rough estimation of walk-induced forces on the structure. After a thorough theoretical review, some of these models are taken as references and the smartphone-based force identification results are qualitatively compared to demonstrate the potential of crowdsourced pedestrian data. In contrast with the theoretical pedestrian force models, smartphone time histories are not perfectly sinusoidal but still periodical and is of similar peak-to-peak order in the time domain. In the frequency domain, it is seen that the smartphone measurements resembles a resultant force of lateral, longitudinal, and vertical pedestrian forces rather than vertical component alone. This is expected since smartphone axes are subject to change throughout pedestrian motion, although it is aimed to align smartphone y-axis towards gravitational direction. Nevertheless, the data acquired from walking pedestrians can be of great importance to identify dynamic loads due to pedestrians.

For the latter scenario, i.e. standing pedestrians, first of all, pedestrian biomechanical features are determined in terms of Fourier spectra. This spectra is a measure of an intermediary mechanical system between the sensor and the structure, and is constructed from smartphone sensors carried

by a pedestrian while the pedestrian stands on a rigid surface. Observing two different configurations such as smartphone in a bag and smartphone in a pocket, it is illustrated that the system spectra can change depending on the smartphone's attachment on pedestrian body.

In order to cancel out biomechanical effects due to human body, following a transfer function development and conversion procedure, the system spectra can be used to eliminate citizen-induced vibration content and produce pure structural vibration spectra from pedestrians standing on a bridge. On the other hand, it is seen that pedestrian biomechanical features extensively effect 5-10 Hz frequency bands, and this reduces the identification quality of modes within this range. For higher modes, identification results are as accurate as output-only cases by direct sensor-structure contact and no pedestrian influence.

The test results presented in this study are collected from a single pedestrian subject under controlled conditions (pedestrian standing still, walking with the same pace), and in real life the pedestrian behavior can be more uncertain, complex, and time dependent. Besides, development of a pedestrian's system transfer function autonomously can be very cumbersome, and requires deeper understanding of human motion as well as effects of accessories. Existing activity and fitness monitoring devices, their working principles and algorithms might be beneficial to solve some these problems, yet, accuracy of these motion and activity recognition technologies is not discussed from an SHM perspective. In this particular case, detecting whether a pedestrian is walking or standing may be a good start, but might need extensive improvements to understand further details about a particular pedestrian, posture, and activity. Gathering data from a large number of smartphone users systematically would help researchers to gain more insight regarding indirect structural vibration sensing and isolating nonstructural pedestrian effects. In addition, extension of this mobile sensing approach to other wearable sensors such as smart watches or activity wrists might possess similar and practical potential.

Nevertheless, the two cases demonstrated throughout this study are keystones of a novel methodology shifting from conventional SHM systems to citizen-engaged, crowdsourced, and smartphone-based SHM systems. Pedestrians can operate smartphones as mobile SHM devices, and provide the monitoring system with valuable data. As shown in this study, estimated forces and modal identification results can help to experimentally assess the structural demand and the bridge system properties, respectively. Further advancements in this field is prospective in terms

of how they combine mobile and smart technologies with pedestrian contribution, and eventually help evaluating structural features in a sustainable and self-governing way.

Chapter 5

Integration with SHM and Reliability

Using the crowdsourced modal identification results, this chapter presents a cyber-physical information processing scheme and demonstrates the integration of smartphone-based SHM with reliability estimation to assess infrastructure performance. This chapter is reproduced from the paper coauthored with Maria Q. Feng, under revision in the journal Structural Safety [185].

5.1 Introduction

Deriving economical, sustainable, and practical solutions without a compromise in infrastructure safety and integrity is a broad challenge in civil and structural engineering disciplines. Unpredictable nature of hazardous events combined with limited resources lead the current practice to inherit performance-based criteria in structural design and evaluation. Therefore, controlling the extent of structural damage rather than exclusively avoiding it, is the trending principle in up-to-date engineering codes and regulations [186, 187].

Observing the changes in vibration characteristics of structures with the state-of-the-art sensing and processing tools, SHM technologies attract significant attention in research and industry in the last three decades [2, 3, 188, 189]. On the other hand; instrumentation, cabling, operation, and maintenance of SHM systems require labor work, knowhow, and financing; declining the growth rate of SHM use in practice. Especially in the past decade, these drawbacks lead researchers to focus on innovative methods such as noncontact vibration measurement techniques [190-192], WSN and distributed sensor network (DSN) systems [124-131], as well as smart [91-94], mobile [95-98], and multisensory [99-102] sensing platforms. Eventually, smartphones are adopted into SHM such that their built-in sensors, operating systems, computation, and wireless communication capabilities can perform as structural vibration measurement devices

[1, 36, 39, 85, 86, 103, 107].

The authors' previous works present the first vibration-based SHM system (CS4SHM) using crowdsourcing power [36], and offer multisensory solutions to citizen-induced errors by considering spatiotemporal [86] and directional [85] uncertainties. Without any prior engineering education and background, citizens as uncontrolled SHM device operators can provide a central server system with ubiquitous vibration data. The acquired data is autonomously processed for modal identification which is an important indicator of structural vibration characteristics. Unlike conventional SHM systems, CS4SHM points out unorthodox monitoring issues which are concurrently discussed in the upcoming technological boom "Industry 4.0", the latter phase of digital revolution [193, 194]. Collecting the distributed crowdsensed information through a central server and conducting modal identification autonomously, civil infrastructures as physical objects are connected with server-side computing in a massive scale forming a CPS [195-199], or in some cases, an Internet of Things system [200-203]. This highlights a significant potential to evolve from pure theoretical structural response simulation (FEM) to experiment-aided and calibrated models (model updating) in massive scales. In other words, with the help of autonomous, connected, scalable cyber networks; citizen-engaged sensing; digital (FEM predictions) and physical (field measurements) civil infrastructure representations; monitoring systems can be adopted to the upcoming technological innovations. These hybrid models can be used for large-volume analysis to retrieve quick evaluation of structural status. This can be performed by utilizing the modal identification results, calibrating mathematical models, and obtaining the probabilistic failure distribution under a wide range of strong ground motions. Eventually, using identification results as model calibration tools, civil infrastructures' seismic response and structural reliability can be estimated [28, 29] to provide the decision makers with the necessary information.

This study extends the outcomes of a crowdsourcing-based modal identification platform by modifying FEMs constructed with limited information. FEMs as cyber representatives of building behavior are updated to minimize the error between the simulated models and the identification results obtained from the "physical objects". Then, the updated models, which represent the actual vibration characteristics to a better extent, are used to simulate structural response under different earthquake motion scenarios. Finally, collecting the simulation results obtained from numerous time history analyses, the demand distribution is evaluated according to the exemplary code and

regulation criteria. To summarize, the developed platform presents an innovative mobile CPS by converting the very initial physical vibrations into highly abstracted decision making information (i.e. service close, retrofitting, and reconstruction) through a digital and multiphase mathematical information processing framework.

Chapter 5.2 discusses the experimental and theoretical phases of the methodology followed throughout the study. These phases include information about the testbed bridge structure, the CPS adaptation, model updating, and reliability estimation methodologies. Chapter 5.3 presents the application to the testbed and presents the monitoring results including objective function minimization and determination of structural reliability. Finally, Chapter 5.4 reviews the overall work, introduces the future goals, and highlights the concluding remarks.

5.2 Materials and methods

The methodology presented in this study connects the experimental data obtained from civil infrastructures with the advanced mathematical modeling and analysis procedures. The following subchapters introduce the testbed structure, modal identification, FEM updating, and reliability estimation processes as a CPS framework. From sensing to decision making, Figure 5.1 represents an idealized cyber-physical information processing scheme, with a comparison of the current CS4SHM system. The up-to-date platform is capable of receiving vibration measurements from citizens and conduct modal identification on the server-side. Then, the identification results are collected to set the reference modal analysis values for FEM updating and reliability estimation procedures. These phases are currently conducted through a scripted Matlab and OpenSees [204] loop, and the ultimate goal is to handle these cyber procedures through cloud computing. Nevertheless, in both cases, the decision makers can be provided with the quantitative information regarding structural status. Depending on the changes made to the structural system, the effects will be reflected on the future vibration characteristics which completes the cyclic information processing scheme.

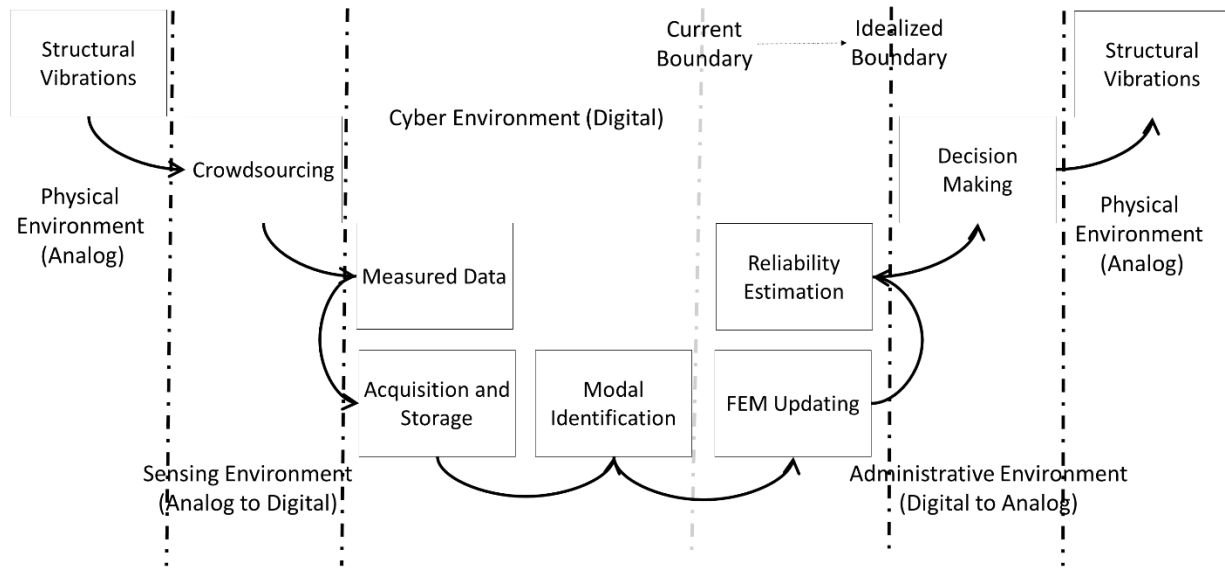


Figure 5.1: Cyber-physical processes of CS4SHM system

5.2.1 Testbed structure

In order to select a testbed structure with crowdsourcing potential, a link bridge with pedestrian access is implemented. The bridge is a steel frame structure connecting two adjacent buildings in Columbia University Morningside Campus, namely, Mudd and Schapiro Buildings. Mudd-Schapiro Link Bridge, shown in Figure 5.2, is an arch structure with rigid connections spanning approximately 10.5 meters. Using the known dimensions of a window and a vision-based scaling procedure, the structural dimensions are approximated without any supplementary documents and design drawings. These dimensions constitute the baseline for the mathematical model, which later on, will be updated with the information from crowdsourced vibration data.



Figure 5.2: Mudd-Schapiro Link Bridge

5.2.2 Cyber-physical systems

As a new emerging technology, CPSs attract significant attention from numerous research and industry field in the last decade. Link and coordination between physical objects and computational resources set the fundamental system goal, which in return, brings different disciplines such as computer, control, electronic, and mechanical systems together [205]. Combining multilayered computer architectures [206] with embedded systems, sensors and control [207], or expanding WSNs to take action in the physical world [208], CPSs present a diverse interpretation of the up-to-date existing technologies.

The overall motivation of the CPS platform presented in this study is to connect the physical, cyber, and sensor system objects through a multilayered information processing SHM framework. The physical object formulated in this scheme is the bridge structure which represents the outer layer of the developed CPS system, as shown in Figure 5.3. The physical parameter of interest is the bridge vibrations, which can be gathered by smartphone accelerometers with the help of pedestrian volunteers. Moreover, sensing process is enhanced by the hybrid foundation of pedestrians and sensors, composing the citizen sensor layer. Eventually, the bridge vibrations sensed by smartphone accelerometers are submitted to the server where the signal processing and data analytics take place. With the help of the cloud-based acceleration record manager system, which is the innermost layer, the vibration data can be stored, viewed, reprocessed, and their results can directly be extracted by the system administrators. Interconnecting these components successively form the two core elements (sensor networks and application platforms) with transactions (sensing and knowledge) of a typical CPS and produce the actuation information with intelligent decision systems to complete the cyber-physical loop [197]. To summarize, citizen sensors provide the binding components of the smartphone-based SHM network by integrating the civil infrastructure with the cloud services, and the numerical representations of the bridge (FEMs) can be fed with the actual bridge response through the cyber-physical SHM system phases.

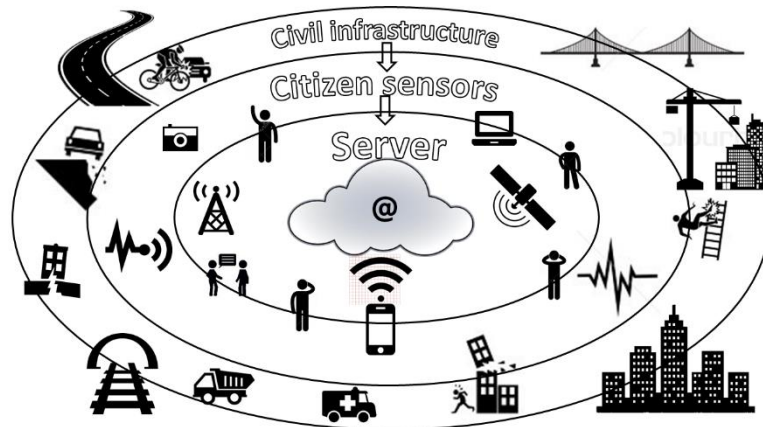


Figure 5.3: Conceptual CPS scheme for smartphone-based SHM

Formerly, the bridge is registered to the CS4SHM online server system and database to store, process, and monitor its structural vibrations [78]. An iOS application is developed as a data acquisition interface to enable smartphone users gather vibration data from the bridge and submit it to the server [75]. Pedestrians with bridge access are assigned as the test group, and submitted 135 vibration measurements in total. The data is processed through the online server system, and modal identification results are recorded. These identification results can be used to calibrate the mathematical model of the bridge by following the FEM updating procedure. Figure 5.4 shows an exemplary citizen sample in the time and the frequency domains. Based on the whole set of submission records, 1st, 2nd, and 3rd modal frequencies are identified in [36] as 8.5, 19, and 30 Hz, respectively.

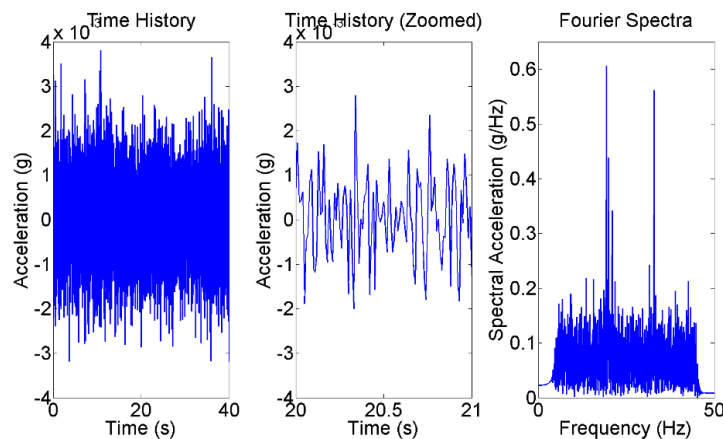


Figure 5.4: Exemplary crowdsourced time histories and Fourier spectra

5.2.3 Finite element model updating

In order to predict the structural response accurately, the available information should be effectively used such that FEM parameters can be determined to the best extent. In this modeling example, the design drawings and material properties are unavailable, therefore, the initial FEM is based on site observations and estimations. The observations include the length and the outer diameter of structural members by scaling the pixel values with respect to the known dimensions (i.e. window size). Although the outer diameter can be determined using bridge photographs, the cross-sectional thickness or the inner diameter is unknown. Likewise, support restraints are set as uncertain parameters with possible realizations such as fixed, pinned, or roller. Other than these, contribution of the nonstructural components is difficult to estimate, therefore, mass sources are assigned based on crude assumptions. Figure 5.5 shows the modeling uncertainties taking place without the necessary documentation. To summarize, tubular structural member sectional dimensions, distributed mass due to non-structural components, and support restraints all contribute to the modeling uncertainties and will be determined throughout the FEM updating process.

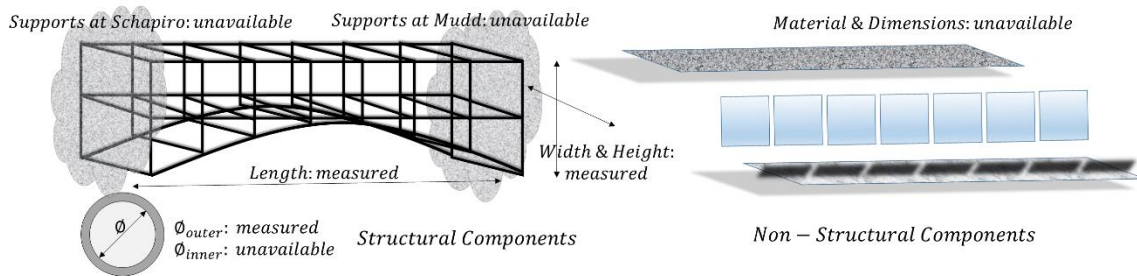


Figure 5.5: Finite element modeling uncertainties

The proposed FEM updating method consists of generating a large number of models changing in uncertain parameters, comparing the modal analysis results of each FEM with the experimental data, and selecting the model which minimizes the error between the simulation (model) and the reality (identification). In order to establish an autonomous parameter study and FEM updating procedure, an OpenSees-Matlab integration loop is performed. Specifically, OpenSees scripts are simultaneously generated, run, and evaluated by a controller Matlab code.

As mentioned previously, three different parameters are selected to create different FEM batches. These are the boundary conditions, element stiffness values, and nodal masses, respectively. For each boundary condition combination changing in fixity definitions, a set of models with varying stiffness and mass values are generated. Each of the model batches are evaluated according to the difference between the 1st, 2nd, and the 3rd FEM and identification results. This is conducted by developing an objective function quantifying the error between a model and the reference modal parameter values. In the past studies, the authors adopted Least Square Method (LSM) to formulate the objective function [28, 29]. Considering the accuracy comparisons between LSM and Maximum Likelihood Method (MLM) presented in [209, 210], in this study, the objective function is structured in terms of maximum likelihood error between the simulation and the experimental results. To specify, the objective function, which is a function of the support restraints, stiffness and mass distributions, is formulated as

$$Obj(BC, K, M) = \prod_{mode=1}^3 (sqrt((f_{mode FEM} - f_{mode EXP})^2) / f_{mode EXP}) \quad (5.1)$$

where BC, K, M represent changing FEM parameters such as boundary condition (BC), member stiffness, and mass values, respectively. Each combination corresponds to a different set of 1st, 2nd, and 3rd modal frequencies represented with $f_{mode FEM}$ term, and the model accuracy is determined based on the deviation from experimental values represented with $f_{mode EXP}$. At the end of the loop analyses, the optimal model which minimizes the error between the simulated and identified values becomes the updated model. Afterwards, this model can be used as a baseline for seismic response simulations and reliability estimation.

5.2.4 Structural reliability estimation

In the authors' previous studies, SHM-integrated reliability estimation is performed by generating fragility curves of different performance levels taking peak ground acceleration (PGA) as the random variable [28, 29]. This method can result in high computational cost as the number of available seismic ground motions increases. Compatible with the smartphone-based identification procedure presented in this study, it is expected that ground motion demands under a seismic event can be determined by a dense seismic network composed of smartphone seismometers [18]. Besides, as the number of input ground motions increases like in a mobile CPS

scenario, accuracy of the fragility curve parameters may be affected due to truncation and round-off errors. In this study, the probabilistic structural response is directly obtained from log-normal distribution of the time history analysis results. For each ground motion taken from 1994 Northridge Earthquake, a time history analysis is conducted and the simulated response is obtained. Because that the bridge considered in this study is a high frequency structure compared to the low frequency character of Northridge Earthquake records, it is assumed that the structure undergoes linear behavior and its response can be simulated with linear time history analysis. In this case, secondary performance indicators such as maximum drift or displacement become important as they are decisive in the linearity assumption. Therefore, the response from each seismic event is collected in terms of maximum deflection and finally, the distribution demand under the given set of earthquakes is obtained. Looking at the distribution demand as well as the reference code and regulation criteria, it can be predicted whether the structural response will exceed the performance thresholds. In conclusion, with the proposed reliability estimation framework, the high computational cost of fragility curve development can be replaced with a simpler approximation, provided that the ground motion response distribution matches well with log-normal type distribution features.

5.3 Results and discussion

Following the outline presented in the methodology, the testbed bridge data is used for modal identification, FEM updating, and reliability estimation with the updated model. The results obtained throughout the analysis are presented with two subchapters discussing objective function minimization (FEM Updating) and simulation of seismic response (Reliability Estimation), respectively.

5.3.1 Objective function minimization

In order to predict the structural performance under hazardous events accurately, a well-tuned baseline model is essential. With limited modeling information due to lack of design drawings and reports, an approximate model may deviate from the actual behavior of the structure. Based on the field observations, mass estimations, and fixed BCs, modal analysis results of the initial non-updated model are 8.98, 14.41, and 22.05 Hz for 1st, 2nd, and 3rd modes, respectively. Comparing

these results with the actual dynamic response obtained from the identification results, one can see there is a significant mismatch in 2nd and 3rd modes. Therefore, such modeling discrepancy should be diminished to improve the accuracy of the baseline model.

For this purpose, the FEM updating procedure explained in the previous subchapter is adopted. The updating procedure is composed of three loops each manipulating one modeling variable to generate multiple FEM instances. These three parameters are related to the support restraints, member thicknesses, and distributed mass over the entire span. Looking at the support restraints of the bridge, there are two different types of BCs. The first type is anchored to the adjacent buildings, and the second type is bolted connections. The support details observed through visual inspection show that the bolted connections are only used for the arch restraints, and the rest of the connections are anchored to the structure. To decrease the number of parameter updates, considering that anchored connections form rigid supports, the bolted connection type is considered as an updating parameter which leads to 3 different combinations such as fixed-fixed, fixed-pinned, and fixed-roller. For each BC case, 900 FEM instances are created ranging in stiffness (K), and mass (M) parameters. The objective function error between the FEMs and the modal identification results are computed to find the optimal parameter combination. Figure 5.6 shows the error surfaces of the fixed-fixed, fixed-pinned, and fixed-roller cases.

According to Figure 5.6, the uppermost three figures of each BC case shows the error due to each individual modal frequency, whereas the 3-dimensional figures show the combination of these individual components as the objective function product. The magenta spots on each subfigure points out the optimal combination of updating parameters. The overall behavior shows that the model accuracy is very sensitive to the BCs. In other words, combinatory results as well as individual modal frequency errors heavily rely on the modeling of the support restraints.

Table 5.1 presents the modal frequency errors obtained from different BC cases and Figure 5.7 presents the modal parameters of optimal combination cases for each BC case.

Table 5.1 implies that for fixed-fixed and fixed-pinned cases, the optimal solutions from each mode varies significantly, and the objective function is either dominated by one of the modes or an irregular combination of them. Fixed-roller case, on the other hand, is contradictory with the first two BC cases. Optimal combinations obtained from 1st, 2nd, and 3rd modes are very similar with each other (ranging around 21th model number), as well as the optimal objective function

solution.

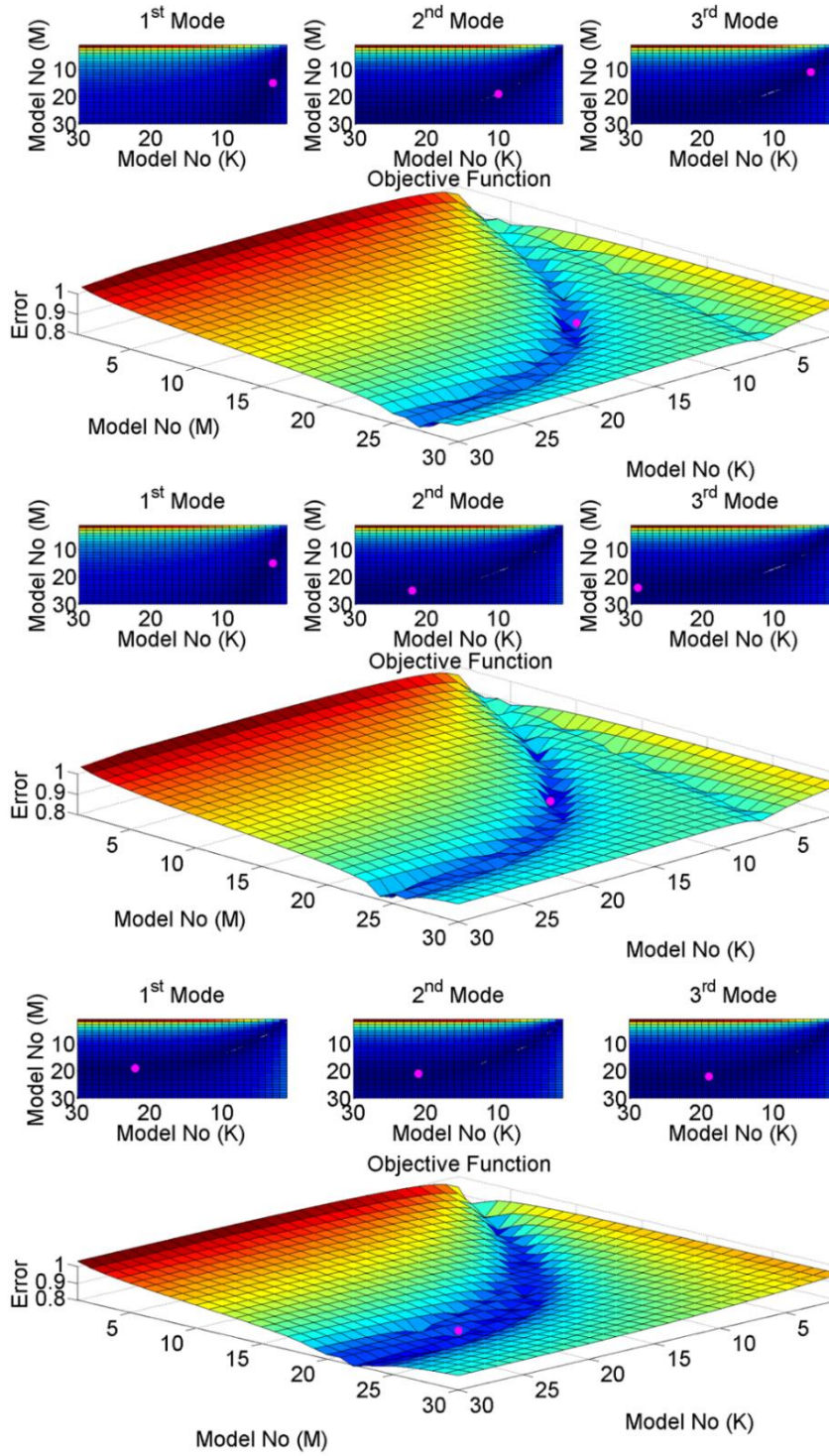


Figure 5.6: Frequency error surfaces for fixed-fixed, fixed-pinned, fixed-roller BCs

Table 5.1: Optimal models for different BCs

Boundary Conditions	Optimal	Parameter	Combinations	<K, M >
	Mode 1	Mode 2	Mode 3	Objective
Fixed-Fixed	<3, 15>	<10, 19>	<5, 11>	<10, 19>
Fixed-Pinned	<3, 15>	<22, 25>	<29, 24>	<11, 18>
Fixed-Roller	<22, 19>	<21, 21>	<19, 22>	<21, 21>

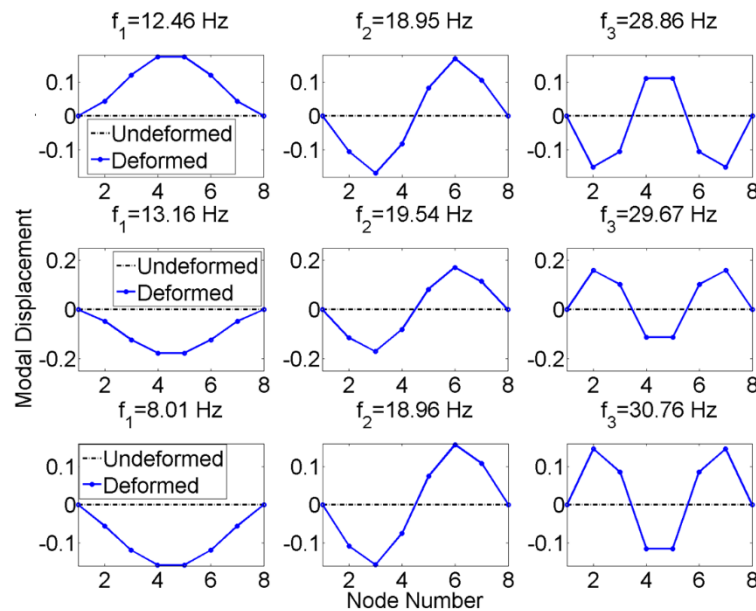


Figure 5.7: Updated modal parameters for fixed-fixed, fixed-pinned, fixed-roller BCs

To understand the difference between the fixed-roller case and the other cases, the modal frequencies obtained from each case are investigated. Looking at the 1st modal frequency of the updated models, it can be observed that the fixed-fixed and fixed-pinned cases have very high errors (47%, 55%), although the 2nd (0.3%, 2.8%) and the 3rd (0.5%, 1.1%) modal frequencies are represented well. In contrast, fixed-roller case represents all three modes with a good and even accuracy such as 5.8%, 0.2%, and 2.5%. These results show that the arch support fixities are decisive to set the proportion between the 1st modal frequency and the others, and the fixed-roller

case performs significantly better than the other BC cases.

According to Figure 5.7, compared with the ratio between the modal frequencies, it is seen that the BCs do not have a significant effect on the updated mode shapes. On the other hand, without the correct proportion between modal frequencies, even if one or two mode is accurately identified, the remaining mode will have a very high error value. This phenomena can be proven with a sensitivity study, yet it is the beyond of the scope, and therefore is not addressed further in this chapter. Specifically, releasing the arch support fixities in the longitudinal direction can tremendously increase the accuracy of the FEM modal frequencies. Conclusively, an accurate FEM is developed with the presented model updating procedure, and such model can be used to simulate the seismic performance of the structure.

5.3.2 Simulating probabilistic seismic response

After the optimal modeling parameters are determined and the FEM with limited information is updated, the resultant model can be used as a baseline to predict structural performance under hazardous events. Specifically, in this study, seismic response is scoped, yet similar analysis procedure can be extended to other damaging events. The PEER Strong Motion Database have an extensive set of real earthquake records, therefore, one of these largest sets, 1994 Northridge Earthquake is taken as an exemplary structural demand due to a seismic event [211].

151 earthquake ground motion records are taken from the Northridge Earthquake dataset and used as structural input for time history analyses. With the time history analysis of the baseline model under different earthquake ground motions, the structural response is simulated. Figure 5.8 shows an example of these analyses illustrating the time and the frequency content of the structural input and outputs.

According to Figure 5.8, it can be observed that the frequency content of the input ground motion is dominated in low frequencies (below 5 Hz), whereas the structural response peaks around 8-9 Hz. The mode with the lowest frequency, the 1st mode, is excited more than the 2nd and 3rd modes, and therefore, the response peaks are observed around the 1st frequency range (8.5 Hz). This is due to the fact that the higher structural frequencies (e.g. 19, 29 Hz) are very far away from relatively low frequency seismic activity.

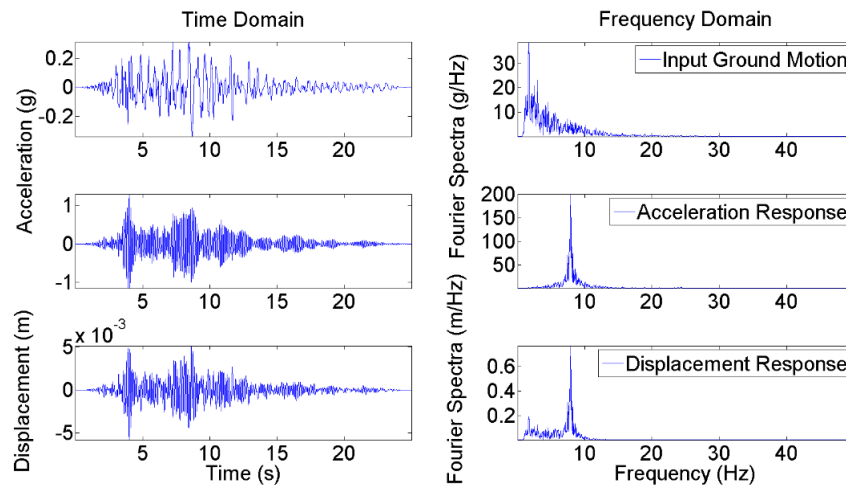


Figure 5.8: Exemplary input ground motion and simulated structural response

For these reasons, the seismic response is expected to have less structural damage compared with the low frequency civil infrastructure. As a result, the structure behaves in the linear range, yet, it should still be checked whether the bridge maximum deformations exceed certain regulations. One reason is, the nonstructural earthquake damage losses still compose a significant percentage of overall losses [212]. Likewise, even slight damages following a seismic event might result in functionality losses [213]. Besides, it is seen that the low-frequency sensitive displacement response still includes the effects of seismic input, whereas these effects vanish in case of the acceleration response. To summarize the overall dataset results, Figure 5.9 shows the maximum acceleration and displacement response values indexed according to the strong motion parameters amplitude, frequency, and duration [214], respectively.

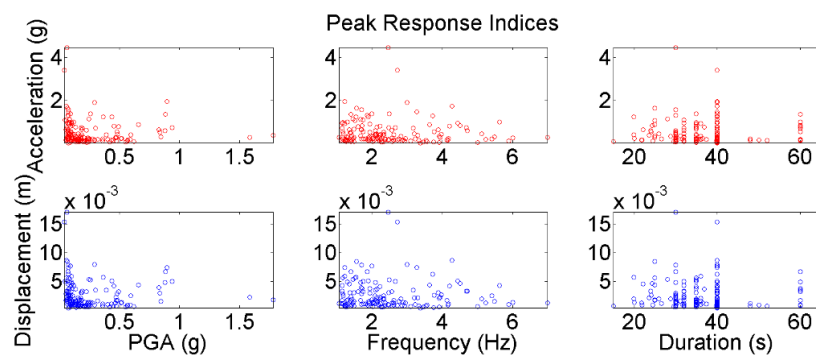


Figure 5.9: Peak responses indexed according to the strong motion parameters

Time history analysis results are recorded and the maximum response values from each analysis are collected to form a distribution demand. Figure 5.10 shows the individual and the cumulative maximum displacement distributions obtained from 151 analysis results. Assuming that the distribution type is log-normal, if the probability density function (PDF) and cumulative distribution function (CDF) are plotted, one can see that the current dataset is a good representative of such type. Log-normal distribution assumption is widely used to develop seismic fragility curves and formulate failure probability in terms of PGA, yet these methods involve a computationally expensive curve fitting procedure which can be problematic for CPS systems as the dataset volume increases. Therefore, the distribution obtained from the 151 analysis results is directly used as log-normal distribution with the specified mean and standard deviation values, rather than following a fragility curve fitting procedure described in [28, 29]. Nevertheless, the red plots show that the log-normal distribution assumption is a good representative of the data distribution. Looking at these CDF values of a particular displacement demand, one can determine the structural reliability under that particular threshold.

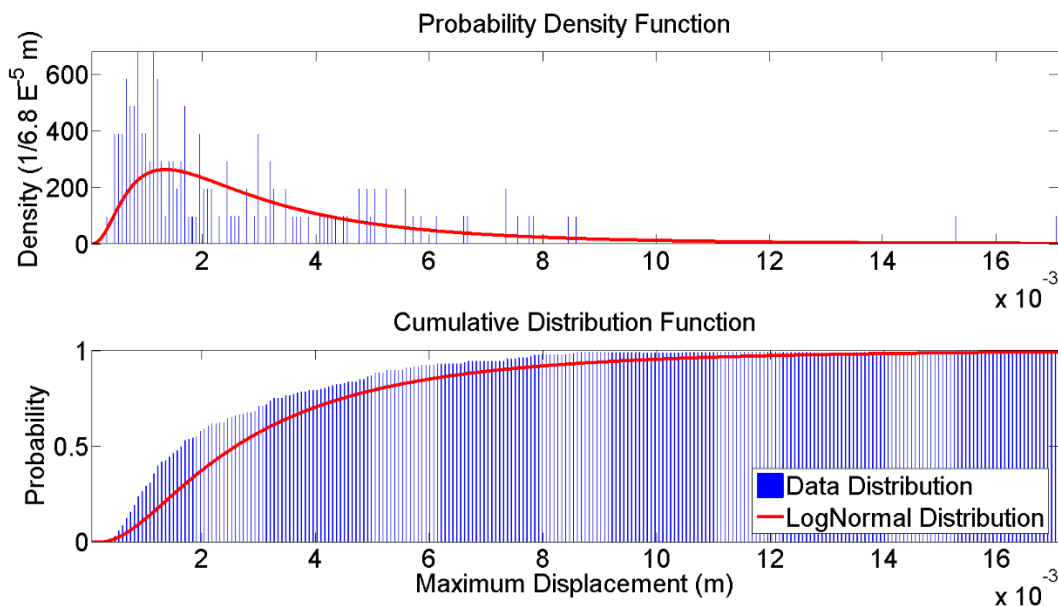


Figure 5.10: Maximum displacement demands based on Northridge Earthquake records

After the CDF is determined, the bridge performance can be evaluated according to the reference criteria. For example, the US pedestrian steel bridges under live loads are limited by a

maximum deflection value of $L/1000$ [215]. Allowable live load deflection limit for the bridges in Japan ranges between $L/2000$ (L shorter than 10 meters) and $L/500$ (L longer than 40 meters) depending on the main span length [216]. Considering Mudd-Schapiro Bridge dimensions, $L/1000$ and $L/2000$ values correspond to approximately 0.01 and 0.005 meters. Static deflection limits for the Ontario highway bridges with pedestrian sidewalks are formulated as a function of the first flexural frequency, and the allowable threshold for 10 Hz is equal to 0.002 meters [217].

Finally, the exceedance probabilities of these reference criteria are investigated according to the CDF values. Considering 0.01, 0.005, and 0.002 meters as the performance thresholds, structural reliability values of the data distribution are 0.987, 0.868, and 0.576, respectively. Likewise, log-normal distribution reliability values of the same performance thresholds are more conservative such as 0.951, 0.790, and 0.373, respectively. Based on these reliability values under Northridge Earthquake example, the authorities can take action for pre-event preparation. These can include claiming the structure's safety, service shutdown, initiating a retrofitting process, or destruction if the performance thresholds are unachievable. Yet, it should be noted that for a different set of earthquake records with different frequency character, the structural performance is likely to be different. In the future, this issue can be further investigated with ground motion simulation using site-specific spectra. Nevertheless, in summary, with the multilayered and detailed analysis procedure presented in this chapter, response distributions to different datasets can autonomously be performed by a well-structured cyber-physical SHM system.

5.4 Conclusions

In this study, present and possible future implementations of a crowdsourcing-based mobile cyber-physical SHM system are presented. Civil infrastructure as physical objects are connected to a cyber structural model and response simulation scheme, and the real vibration data obtained from smartphone users are used to calibrate these model parameters. This procedure includes a number of information processing phases such as mobile, server, and administrative components. Mobile platform digitizes structural vibrations via accelerometers, and submits it to the server. The server conducts modal identification, returns, and stores the analysis results. The identification results obtained from smartphone sensors are used to update the FEM and increase its accuracy, which is formerly created with limited information and modeling uncertainties.

Using the updated model as a baseline, structural responses subjected to 151 Northridge Earthquake records are simulated by time history analyses. The displacement demand distribution obtained from the time history analysis results is evaluated according to the exemplary maximum allowed deflection criteria. Finally, for an earthquake scenario with a wide set of records, one can determine the structural reliability according to the desired seismic performance levels. This information can provide the decision makers with a good foundation for seismic risk assessment, preparedness, and mitigation. Based on the evaluation results of this cyber-physical information flow, the bridge service can be interrupted, structural members can be retrofitted, or the existing structure can be demolished if there is no feasible maintenance scenario. As the volume of invisible operations in computational zone increases, the cyber loops will become more remote and automated.

The framework is tested on an actual pedestrian bridge structure, and the results are presented. The results show that even with limited information, accurate FEMs can be developed with the help of a model updating procedure. Besides, the necessary information is provided by smartphone sensor data and crowdsourcing which solely relies on participatory sensing and pure citizen contribution. Once the physical information is extracted from the sensors, the corresponding data can be combined with a deep mathematical process without any human intervention. Automation, connectivity, scalability, and mobility of the presented platform has a great potential for future mobile cyber-physical SHM systems. Especially, as the seismic monitoring arrays become dense and abundant (e.g. smartphone seismometers), seismic performance of a structure can be probabilistically evaluated with ubiquitous data according to the code regulations and standards.

Chapter 6

Conclusions and Future Work

In this chapter, the overall work is summarized, the conclusions drawn from this study are presented, and the future research directions are discussed.

Thanks to the multisensory features combined with built-in computational and communicational capabilities, in this dissertation, it is shown that smartphones propose a great potential for civil infrastructure monitoring and health assessment in a rapid, remote, automated, and quantified framework. Besides, it is explored that engaging citizens for participatory sensing brings a new and vital source to the vibration-based SHM which relies on a 21th century problem solution technique, crowdsourcing. The studies presented here basically imply that smartphones can serve as sensor nodes of a ubiquitous wireless network, they can get connected to a central server collecting the entire SHM information on a single and unified database, and be the core component of mobile cyber-physical SHM systems in the long run. Yet, in order to activate an SHM system operated by smartphone users, where there is no control over the instrumentation, a citizen-centric perspective should be followed and citizen-induced errors should be resolved. Retrieving all these challenges and opportunities, this dissertation presents novel vibration-based SHM solutions which utilize smartphone sensors, hardware, and community power for the first time in the literature. The following subchapters are provided to summarize the overall work, draw conclusions with an emphasis on main contributions, and suggest future research directions.

6.1 Summary

In this dissertation, an innovative and unique vibration-based SHM approach is introduced and

novel software tools are developed to utilize smartphone sensors as structural vibration measurement instruments. Throughout numerous laboratory and field examples are presented to show the feasibility of smartphone-based SHM. These applications are explained as follows.

First of all, in Chapter 2, accelerometer performance of various smartphone generations, the most important criteria in the proposed framework, is investigated to see if they are capable of capturing structural vibration characteristics. Different loading conditions are applied to observe how the identification results are sensitive to the signal parameters in the time and in the frequency domains.

In Chapter 3, a multilayered software platform, basically consisting of user and server sides, is developed to incentivize citizens for smartphone-based SHM. The user-side is an iOS mobile application software which enables citizens to gather vibration data from their smartphones and send it to the server. The server-side, or alternatively the cloud layer, receives, processes, displays, and stores the vibration data as well as modal identification results. Finally, analysis results from the initial crowdsourcing measurements of a pedestrian bridge are presented.

In Chapter 4, three major citizen-induced uncertainties are taken into consideration, while multisensory, mobile, and smart solutions are proposed to mitigate these uncertainties. The first subchapter proposes a smart monitoring framework which can correct citizen-induced errors due to changes in sensor orientation. The second subchapter reconstructs smartphone sensor data obtained on a spatiotemporally sparse domain, and conducts modal identification without any need for a synchronous and multi-output sensing system. The third subchapter encapsulates different pedestrian mobility scenarios and produces valuable SHM information, even though the smartphone is carried by the citizen during the sensing process.

Finally, Chapter 5 takes advantage of the web connectivity, and extracts the crowdsourcing-based modal identification results from the server to update the mathematical model of a structure. Furthermore, the updated model is used to evaluate the performance of the structure under a seismic event which is based on a complex numerical analysis procedure. In other words, the physical response of the structure obtained at the very beginning is fused with progressive analytical and computational procedures to compose an exemplary mobile cyber-physical SHM system.

6.2 Main contributions and concluding remarks

Naturally, the instrumentation, operation, and maintenance of a smartphone-based SHM system is radically different from the conventional systems. Citizen participation in these procedures constitute the core of a sustainable, cost-free, and ubiquitous data environment unlike the monitoring systems particularly tailored for a single structure. Conventionally, instrumentation of a structure with high fidelity sensing and acquisition equipment is a careful and long process, requiring tremendous efforts and costs to get identification results in an optimal fashion. Because of that, field implementations of SHM in real structures are very limited. In contrast, with crowdsourcing power and smartphones, the instrumentation and labor force is unlimited, and the self-governing SHM system can automatically work as an organism without any intervention from the authorities. On the other hand, citizen engagement brings numerous errors and uncertainties since there is no spatiotemporal control over the sensing platform. In addition to the low sensor quality, these factors crucially affect a crowdsourcing-induced smartphone-based SHM system. In this dissertation, these issues are progressively discussed and the results are presented within each chapter. The most important findings and remarks can be rearranged as follows.

The initial question in smartphone-based SHM is whether the sensors are of adequate quality to sense the structural vibrations. Chapter 2 takes a glance at the smartphone accelerometer performance through numerous laboratory and field tests. Besides, the variation of amplitude and frequency effects are investigated by changing the vibration source features. The results show that, in general, the smartphones are capable of measuring vibrations up to 50 Hz frequency which is a sufficient upper threshold for civil infrastructure systems. The lower limit may be bounded by embedded high-pass filters, yet, successful identification of very long span bridges indicate that even very low frequencies close to 0.1 Hz can be captured if the measurement duration is long enough. Amplitude performance is a lot more subjected to variation especially as the vibration level gets lower. As the structural vibrations get smaller and smaller, the signal to noise ratio decreases, therefore at some point, the structural properties are masked due to extensive noise level. The observations made throughout the accelerometer tests show that the bridge vibrations, even

when ambient, can be used to identify the modal characteristics of a structure. In contrast, for buildings, smartphone accelerometers are likely to be insensitive to ambient structural vibrations. Still, as the smartphone generations get younger, the signal to noise ratio increases more and more, and accordingly, the structural features become more prominent. And maybe in the future, similar identification procedures presented in this dissertation can be adopted for high-rise buildings, especially for the ones with extreme vibration problems due to wind, earthquake, subway, construction zone, etc. Nevertheless, the examples with relatively high vibration amplitudes presented in this dissertation show that the current smartphone technology is capable of SHM in a wide range.

Chapter 3 presents the technical details of the mobile and the web-based software development phases. Firstly, the smartphones provide the developers with an advantageous environment since they have advanced programmable interfaces. On account of this, the citizens have no need to understand the details of a vibration measurement and system identification procedure, instead they can easily operate their smartphone sensors through simplified and highly abstract tasks. Secondly, the web connection enables them to directly connect to the central server and easily submit data, and the entire signal processing procedure takes place in a remote and automated fashion. Yet, citizen initiatives as well as device properties have a strong impact on identification accuracy and should be properly taken into consideration. These initiatives are related to the sensor positioning, mobility, coupling conditions, and measurement duration which are then addressed in Chapter 4.

Chapter 4 discusses citizen-induced uncertainties under three main subjects providing smart and multisensory solutions to orientation, spatiotemporal, and biomechanical effects, respectively. First of all, smartphone deviating from the desired orientation can yield misleading results, yet, such deviation can be tracked and corrected through a coordinate system transformation process with the help of accelerometer, gyroscope, and magnetometer data. Moreover, knowing the structure of interest's alignment with respect to the global coordinate axes, vibrations measured under any random sensor orientation can be converted to the structural coordinates automatically.

Secondly, according to Chapter 4, the measured response characteristics is dependent on sensor position with respect to the structure, for example, a particular measurement location might have

different sensitivities to different modes of vibration. Besides, such response in the frequency domain is a function of the measurement duration. Location information can be gathered via smartphone geolocation services or predefined identities compressed into QR code images. The duration effects can be normalized through an energy to power conversion process. Synthesizing the location information with normalized energy can set the relationship among structural nodes, and convert spatiotemporally sparse single-outputs into a unified multi-output modal identification framework.

Third, and finally, by filtering out biomechanical effects from pedestrian data through a transfer function procedure, Chapter 4 proposes a modal identification method capable of extracting structural vibrations from smartphone sensors carried by standing pedestrians. However, biomechanical features of a pedestrian have dominant frequencies within 5 to 10 Hz range, and identification results between these values are subjected to distortion. Besides, different engagement cases, e.g. phone carried in a pocket or bag, might have different frequency characteristics, and therefore, it is beneficial to represent each case with an individual transfer function. In addition to these, moving pedestrian data can also be utilized for monitoring purposes. More specifically, smartphone accelerometer on a pedestrian body can reasonably estimate walk-induced forces on a structure.

Eventually, making use of the crowdsourced modal identification results, Chapter 5 conducts finite element model updating and probabilistic response assessment of a bridge structure under various seismic events to demonstrate an application of smartphone-based SHM method developed in this research. Connecting sensors through web and cloud computing services poses a great opportunity to construct mobile cyber-physical systems for SHM practice. As the system gets more integrated and post-processing phases are minimized or at least automated, the proposed platform will approach to an ideal state in terms of its cyber-physicality. Hereafter, the utmost integration of the physical and digital representations of the bridge through crowdsourcing is a novel and aspiring technology for smart, sustainable, and resilient cities and infrastructures.

6.3 Future research directions

Using smartphones for structural vibration measurements and health monitoring is a relatively

new idea, needs exploration of numerous different advancements in sensor technologies, and requires an integrative approach that can handle multidisciplinary perspectives as proposed in this dissertation. As expected, such an innovative and combinatory framework necessitates close contact with the advances in computer science, electrical engineering, communications, and information technology as well as their echoes in social and educational aspects due to citizens' role. Although this dissertation addresses most of the fundamental issues in smartphone-based SHM and provides straight to the point solutions to the most of the problems, possible extension ranges are unlimited. From the technical details of software development process to the front-end usage, so many improvements can be made to improve the quality of a citizen-engaged SHM platform. Besides, enhancing diversity in smartphone-based SHM research and strong connection with other fields would lead to numerous broader impacts. With an emphasis on the topics which are not explicitly covered in this dissertation, some of the further research directions may be listed within the subcategories such as computer vision, synchronization, data analytics, human-computer interaction, and educational impacts.

In this dissertation, computer vision techniques are not fully benefited, thus, adaptation of vision-based sensing techniques for smartphone camera can be a useful displacement monitoring methodology. Considering laboratory scale structures, the embedded camera and lens may be sufficiently accurate for this purpose, but implementation for field studies may require external lens usage to make low amplitude structural vibrations visible.

Another important aspect that requires further exploration is synchronous use of multiple devices during monitoring process. This dissertation uses the web connection as a gateway between the central system and a single device, but excludes different sensor network models that rely on alternative communication technologies such as Bluetooth. Besides, for cases where multiple devices are available for measurement at the same time, multi-output sampling with clock synchronization may reveal more information regarding dynamic characteristics such as mode shapes. On the other hand, for the time being, the imperfect sampling phenomenon stands as the fundamental challenge, which means, even though the machine to machine synchronization is somehow enabled, the data samples in the long run will deviate from the targeted timestamps. These effects might be artificially minimized by interpolating the missing samples, yet the effects of the remaining time error on the identification results is still of question.

One more important aspect that needs to be addressed in the future is how ubiquity of smartphone sensor data becomes more beneficial when it is collected at a unified data center. Monitoring case studies existing in the literature usually focus on a particular structure, and attempt to investigate their relationship with certain parameters of interest. Alternatively, environmental effects on dynamic characteristics can be observed through long-term monitoring of civil infrastructure. For example, modal frequencies can have cyclic changes in the day and the season scales as a result of temperature change or operational condition changes with respect to the daily or seasonal traffic routine. The most important point is that, there would be a significant difference between observing the time dependent changes of a single structure vs structures in a city-scale. Using information from external resources such as application programming interfaces of weather forecasting sites etc., and fusing heterogeneous data including time, geographical position, temperature, and more; correlations among different structures' identification results can explain further relationships between the environmental effects and individual dynamic characteristics. This might require a new approach to the data management procedure, where relational databases may be insufficient and big data analytics may be essential.

As a new concept introduced into the SHM process, crowdsourcing brings numerous new challenges for the sake of vibration response measurement and accordingly identification accuracy. A well-structured but vaguely presented SHM system can be barely understood by the citizens, and thus, the accuracy of the results might extensively reduce because of malfunctioning during the instrumentation and operation procedures. Inheriting advances in human-computer interaction research might be crucial to optimize citizens' role and responsibility in sensing process.

The fundamental difference between the conventional and the smartphone-based SHM systems is that millions of smartphones are already available for use without any additional investment. Moreover, these sensors are accessible by any individual as long as the proper application software is provided. Not only researchers, but also students and instructors can reach out to these SHM platforms. That is to say, promoting smartphone technology use in science and engineering education could bring new frontiers to existing curricula and learning practice.

To conclude, use of smartphone technologies for SHM applications is a promising but demanding goal and it requires contribution from different research fields as well as communities. Bringing crowdsourcing into the equation adds one more dimension to the data discrepancy which

needs to be resolved before, during, and/or after the measurement process. Finally, it is indispensable to keep track of the latest technological advancements in smartphone industry, which are comparatively much faster than the developments in conventional SHM practice. Robust implementations in smartphone-based SHM can radically influence the future advancements in smart, sustainable, and resilient infrastructures and cities.

Bibliography

1. Feng, M., Fukuda, Y., Mizuta, M., & Ozer, E. (2015). Citizen sensors for SHM: Use of accelerometer data from smartphones. *Sensors*, 15(2), 2980-2998.
2. Doebling, S. W., Farrar, C. R., & Prime, M. B. (1998). A summary review of vibration-based damage identification methods. *Shock and vibration digest*, 30(2), 91-105.
3. Carden, E. P., & Fanning, P. (2004). Vibration based condition monitoring: a review. *Structural Health Monitoring*, 3(4), 355-377.
4. Kim, D. H., & Feng, M. Q. (2007). Real-time structural health monitoring using a novel fiber-optic accelerometer system. *Sensors Journal, IEEE*, 7(4), 536-543.
5. Fukuda, Y., Feng, M. Q., Narita, Y., Kaneko, S. I., & Tanaka, T. (2013). Vision-based displacement sensor for monitoring dynamic response using robust object search algorithm. *IEEE Sensors Journal*, 13(12), 4725-4732.
6. Smith, D. L. (1999). Did You Feel It? *Engineering and Science*, 62(4), 34-38.
7. Atkinson, G. M., & Wald, D. J. (2007). "Did You Feel It?" intensity data: A surprisingly good measure of earthquake ground motion. *Seismological Research Letters*, 78(3), 362-368.
8. Wald, D. J., Quitoriano, V., Worden, C. B., Hopper, M., & Dewey, J. W. (2012). USGS "Did you feel it?" internet-based macroseismic intensity maps. *Annals of Geophysics*, 54(6).
9. Cochran, E. S., Lawrence, J. F., Christensen, C., & Jakka, R. S. (2009). The quake-catcher network: Citizen science expanding seismic horizons. *Seismological Research Letters*, 80(1), 26-30.
10. Cochran, E., Lawrence, J., Christensen, C., & Chung, A. (2009). A novel strong-motion seismic network for community participation in earthquake monitoring. *Instrumentation & Measurement Magazine, IEEE*, 12(6), 8-15.
11. Chung, A. I., Neighbors, C., Belmonte, A., Miller, M., Sepulveda, H. H., Christensen, C., & Lawrence, J. F. (2011). The Quake-catcher network rapid aftershock mobilization program following the 2010 m 8.8 Maule, Chile earthquake. *Seismological Research Letters*, 82(4), 526-532.
12. Cochran, E. S., Lawrence, J. F., Kaiser, A., Fry, B., Chung, A., & Christensen, C. (2012). Comparison between low-cost and traditional MEMS accelerometers: a case study from the M7.1 Darfield, New Zealand, aftershock deployment. *Annals of Geophysics*, 54(6).

13. Obenshain, D., Chandy, K. M., Chandy, R., Clayton, R., Krause, A., Olson, M., Rosenberg, D., & Tang, A. (2010). Community Seismic Network: Catching Earthquakes Quickly and Cheaply Through Volunteer-based Sensor Networks. *Caltech Undergraduate Research Journal*, 11(1), 31-37.
14. Clayton, R. W., Heaton, T., Chandy, M., Krause, A., Kohler, M., Bunn, J., & Aivazis, M. (2012). Community seismic network. *Annals of Geophysics*, 54(6).
15. Faulkner, M., Olson, M., Chandy, R., Krause, J., Chandy, K. M., & Krause, A. (2011, April). The next big one: Detecting earthquakes and other rare events from community-based sensors. In *Proceedings of the 10th ACM/IEEE International Conference on Information Processing in Sensor Networks (IPSN)*, Chicago, IL, US (pp. 13-24).
16. Dashti, S., Reilly, J., Bray, J. D., Bayen, A., Glaser, S., Mari, E., & Bray, P. J. D. (2011). iShake: Using Personal Devices to Deliver Rapid Semi-Qualitative Earthquake Shaking Information. *GeoEngineering Report*. Available online: <http://bayen.eecs.berkeley.edu/sites/default/files/techreps/grdcee11.pdf> (accessed on 28 May 2014).
17. Reilly, J., Dashti, S., Ervasti, M., Bray, J. D., Glaser, S. D., & Bayen, A. M. (2013). Mobile phones as seismologic sensors: Automating data extraction for the iShake system. *IEEE Transactions on Automation Science and Engineering*, 10(2), 242-251.
18. Dashti, S., Bray, J. D., Reilly, J., Glaser, S., Bayen, A., & Mari, E. (2013). Evaluating the Reliability of Phones as Seismic Monitoring Instruments. *Earthquake Spectra*, 30(2), 721-742.
19. Kohler, M. D., Heaton, T. H., & Cheng, M. H. (2013, April). The Community Seismic Network and Quake-Catcher Network: enabling structural health monitoring through instrumentation by community participants. In *SPIE Smart Structures and Materials+ Nondestructive Evaluation and Health Monitoring*, San Diego, CA, US (pp. 86923X-86923X).
20. Eriksson, J., Girod, L., Hull, B., Newton, R., Madden, S., & Balakrishnan, H. (2008, June). The pothole patrol: using a mobile sensor network for road surface monitoring. In *Proceedings of the 6th international conference on Mobile systems, applications, and services*, Breckenridge, CO, US (pp. 29-39).
21. Comparison of Smartphones. Available online: http://en.wikipedia.org/wiki/Comparison_of_smartphones (accessed on 28 May 2014).
22. ST Microelectronics. Available online: http://www.st.com/web/catalog/sense_power/FM89/SC444/PF218132 (accessed on 28 May 2014).
23. ST Microelectronics. Available online: http://www.st.com/web/catalog/sense_power/FM89/FM89/SC444/PF191236 (accessed on 28 May 2014).
24. PCB Piezotronics. Available online: <http://www.pcb.com/Products.aspx?m=393B04#.UxC-KvldV8F> (accessed on 28 May 2014).
25. Bosch Sensortech. Available online: https://www.olimex.com/Products/Modules/Sensors/MOD-SMB380/resources/SMB380_Preliminary_Datasheet_Rev13_20070918.pdf (accessed on 28 May 2014).
26. Evarts, H. All shook up. Available online: <http://engineering.columbia.edu/all-shook> (Accessed on 23 December 2014).

27. Ruane, M. E. 'Earthquake' rattles a cathedral pinnacle, but this time in the laboratory. Available online: http://www.washingtonpost.com/local/earthquake-again-rattles-cathedral-pinnacle-but-this-time-in-the-laboratory/2014/02/19/c6e42c86-959a-11e3-9616-d367fa6ea99b_story.html (Accessed on 23 December 2014).
28. Özer, E., & Soyöz, S. (2015). Vibration-based damage detection and seismic performance assessment of bridges. *Earthquake Spectra*, 31(1), 137-157.
29. Ozer, E., Feng, M. Q., & Soyoz, S. (2015). SHM-integrated bridge reliability estimation using multivariate stochastic processes. *Earthquake Engineering & Structural Dynamics*, 44(4), 601-618.
30. Saiidi MS. NEES Project Warehouse, Large-scale experimental seismic studies of a two-span reinforced concrete bridge system. Available online: <http://nees.org/warehouse/project/32> (Accessed on 5 January 2014).
31. Johnson, N. (2006) Large-scale experimental and analytical seismic studies of a two-span reinforced concrete bridge system. No. 32–10946 UMI. University of Nevada, Reno, NV, US.
32. Johnson, N., Ranf, R. T., Saiidi, M. S., Sanders, D., & Eberhard, M. (2008). Seismic testing of a two-span reinforced concrete bridge. *Journal of Bridge Engineering*, 13(2), 173-182.
33. Skolnik, D., Lei, Y., Yu, E., & Wallace, J. W. (2006). Identification, model updating, and response prediction of an instrumented 15-story steel-frame building. *Earthquake Spectra*, 22(3), 781-802.
34. Moaveni, B., He, X., Conte, J. P., & Restrepo, J. I. (2010). Damage identification study of a seven-story full-scale building slice tested on the UCSD-NEES shake table. *Structural Safety*, 32(5), 347-356.
35. Ulusoy, H. S., Feng, M. Q., & Fanning, P. J. (2011). System identification of a building from multiple seismic records. *Earthquake Engineering & Structural Dynamics*, 40(6), 661-674.
36. Ozer, E., Feng, M. Q., & Feng, D. (2015). Citizen sensors for SHM: towards a crowdsourcing platform. *Sensors*, 15(6), 14591-14614.
37. Catbas, F. N., Susoy, M., & Frangopol, D. M. (2008). Structural health monitoring and reliability estimation: Long span truss bridge application with environmental monitoring data. *Engineering Structures*, 30(9), 2347-2359.
38. Gomez, H. C., Fanning, P. J., Feng, M. Q., & Lee, S. (2011). Testing and long-term monitoring of a curved concrete box girder bridge. *Engineering Structures*, 33(10), 2861-2869.
39. Morgenthal, G., & Höpfner, H. (2012). The application of smartphones to measuring transient structural displacements. *Journal of Civil Structural Health Monitoring*, 2(3-4), 149-161.
40. Höpfner, H., Morgenthal, G., Schirmer, M., Naujoks, M., & Halang, C. (2013). On measuring mechanical oscillations using smartphone sensors: possibilities and limitation. *ACM SIGMOBILE Mobile Computing and Communications Review*, 17(4), 29-41.
41. Howe, J. (2006). The rise of crowdsourcing. *Wired Magazine*, 14(6), 1-4.

42. Brabham, D. C. (2008). Crowdsourcing as a model for problem solving an introduction and cases. *Convergence: The International Journal of Research into New Media Technologies*, 14(1), 75-90.
43. Albors, J., Ramos, J. C., & Hervás, J. L. (2008). New learning network paradigms: Communities of objectives, crowdsourcing, wikis and open source. *International Journal of Information Management*, 28(3), 194-202.
44. Hammon, D. K. L., & Hippner, H. (2012). Crowdsourcing. *Business & Information Systems Engineering*, 4(3), 163-166.
45. Zhao, Y., & Zhu, Q. (2014). Evaluation on crowdsourcing research: Current status and future direction. *Information Systems Frontiers*, 16(3), 417-434.
46. Schenk, E., & Guittard, C. (2011). Towards a characterization of crowdsourcing practices. *Journal of Innovation Economics & Management*, 7(1), 93-107.
47. Estellés-Arolas, E., & González-Ladrón-de-Guevara, F. (2012). Towards an integrated crowdsourcing definition. *Journal of Information Science*, 38(2), 189-200.
48. Von Hippel, E. (1976). The dominant role of users in the scientific instrument innovation process. *Research policy*, 5(3), 212-239.
49. Corney, J. R., Torres-Sánchez, C., Jagadeesan, A. P., Yan, X. T., Regli, W. C., & Medellin, H. (2010). Putting the crowd to work in a knowledge-based factory. *Advanced Engineering Informatics*, 24(3), 243-250.
50. Rossen, B., & Lok, B. (2012). A crowdsourcing method to develop virtual human conversational agents. *International Journal of Human-Computer Studies*, 70(4), 301-319.
51. Kazman, R., & Chen, H. M. (2009). The metropolis model a new logic for development of crowdsourced systems. *Communications of the ACM*, 52(7), 76-84.
52. Doan, A., Ramakrishnan, R., & Halevy, A. Y. (2011). Crowdsourcing systems on the world-wide web. *Communications of the ACM*, 54(4), 86-96.
53. Wallin, M. W., & Von Krogh, G. (2010). Organizing for Open Innovation: Focus on the Integration of Knowledge. *Organizational Dynamics*, 39(2), 145-154.
54. Ebner, W., Leimeister, J. M., & Krcmar, H. (2009). Community engineering for innovations: the ideas competition as a method to nurture a virtual community for innovations. *R&D Management*, 39(4), 342-356.
55. Wu, W., Tsai, W. T., & Li, W. (2013). An evaluation framework for software crowdsourcing. *Frontiers of Computer Science*, 7(5), 694-709.
56. Boulos, M. N. K., Resch, B., Crowley, D. N., Breslin, J. G., Sohn, G., Burtner, R., Pike, W. A., Jezierski, E., & Chuang, K. Y. S. (2011). Crowdsourcing, citizen sensing and sensor web technologies for public and environmental health surveillance and crisis management: trends, OGC standards and application examples. *International Journal of Health Geographics*, 10(67), 1-29.
57. Fienen, M. N., & Lowry, C. S. (2012). Social. Water—A crowdsourcing tool for environmental data acquisition. *Computers & Geosciences*, 49, 164-169.

58. Heipke, C. (2010). Crowdsourcing geospatial data. *ISPRS Journal of Photogrammetry and Remote Sensing*, 65(6), 550-557.
59. Goodchild, M. F., & Glennon, J. A. (2010). Crowdsourcing geographic information for disaster response: a research frontier. *International Journal of Digital Earth*, 3(3), 231-241.
60. Uden, M., & Zipf, A. (2013). Open building models: towards a platform for crowdsourcing virtual 3D cities. In *Progress and New Trends in 3D Geoinformation Sciences*. Springer: Berlin/Heidelberg, Germany (pp. 299-314).
61. Zhai, Z., Hachen, D., Kijewski-Correa, T., Shen, F., & Madey, G. (2012, January). Citizen engineering: Methods for "crowdsourcing" highly trustworthy results. In *45th Hawaii International Conference on System Science (HICSS)*, Maui, HI, US. (pp. 3406-3415).
62. Kijewski-Correa, T., Su, S., Montestrucque, L., EmNet, L. L. C., & St, E. L. (2014). A Citizen-Centric Health Monitoring Paradigm Using Embedded Self-Locating Wireless Sensor Networks. *Bridges*, 10, 9780784412374-012.
63. Hirth, M., Hoßfeld, T., & Tran-Gia, P. (2013). Analyzing costs and accuracy of validation mechanisms for crowdsourcing platforms. *Mathematical and Computer Modelling*, 57(11), 2918-2932.
64. Goodchild, M. F., & Li, L. (2012). Assuring the quality of volunteered geographic information. *Spatial Statistics*, 1, 110-120.
65. Reilly, J., Dashti, S., Ervasti, M., Bray, J. D., Glaser, S. D., & Bayen, A. M. (2013). Mobile phones as seismologic sensors: Automating data extraction for the iShake system. *Automation Science and Engineering, IEEE Transactions on*, 10(2), 242-251.
66. Zheng, H., Li, D., & Hou, W. (2011). Task design, motivation, and participation in crowdsourcing contests. *International Journal of Electronic Commerce*, 15(4), 57-88.
67. Borst, I. (2010). *Understanding Crowdsourcing: Effects of motivation and rewards on participation and performance in voluntary online activities* (No. EPS-2010-221-LIS). ERIM Electronic Series: Rotterdam, NL.
68. Zichermann, G., & Cunningham, C. (2011). *Gamification by design: Implementing game mechanics in web and mobile apps*. O'Reilly Media, Inc.: Sebastopol, CA, US.
69. Kapp, K. M. (2012). *The gamification of learning and instruction: game-based methods and strategies for training and education*. John Wiley & Sons: New York, NY, US.
70. Ozer, E. *Analysis Report for Structural System Identification and Acceleration Record Manager*. Available online: <http://ekinstitute.com/analiz.html> (accessed on 8 June 2015).
71. Ozer, E. *Design Report for Structural System Identification and Acceleration Record Manager*. Available online: <http://ekinstitute.com/tasarim.html> (accessed on 8 June 2015).
72. Ozer, E. *Implementation Report for Structural System Identification and Acceleration Record Manager*. Available online: <http://ekinstitute.com/gerceklestirim.html> (accessed on 8 June 2015).
73. Ray, J. (2012). *Sams teach yourself iOS 5 application development in 24 hours*. Sams Publishing: Indianapolis, Indiana, US.

74. Allan, A. (2011). *Basic Sensors in iOS: Programming the Accelerometer, Gyroscope, and More*, O'Reilly Media, Inc.: Sebastopol, CA, US.
75. Ozer, E. (2015). *Citizen Sensors for SHM: iPhone Application*. Available online: <https://itunes.apple.com/us/app/citizen-sensors-for-shm/id986036957?mt=8> (accessed on 29 April 2015).
76. Neuburg, M. (2013). *Programming IOS 7*. O'Reilly Media, Inc.: Sebastopol, CA, US.
77. Neuburg, M. (2013). *iOS 7 Programming Fundamentals: Objective-c, xcode, and cocoa basics*, O'Reilly Media, Inc.: Sebastopol, CA, US.
78. Ozer, E. (2011). *Structural system identification and acceleration record manager*. Available online: <http://www.ek institute.com> (accessed on 1 April 2015).
79. Oppenheim, A. V., & Schaffer, R. W. (2009). *Discrete-time signal processing*, Prentice Hall: Upper Saddle River, NJ, US.
80. Welling, L., & Thomson, L. (2003). *PHP and MySQL Web development*. Sams Publishing: Indianapolis, IN, US.
81. Chatzimilioudis, G., Konstantinidis, A., Laoudias, C., & Zeinalipour-Yazti, D. (2012). Crowdsourcing with smartphones. *Internet Computing, IEEE*, 16(5), 36-44.
82. Brincker, R., Zhang, L., & Andersen, P. (2001). Modal identification of output-only systems using frequency domain decomposition. *Smart Materials and Structures*, 10(3), 441.
83. Arias, A. (1970). *A measure of earthquake intensity*, *Seismic Design for Nuclear Power Plants*, R. J. Hansen, Ed., MIT Press: Cambridge, Massachusetts, US.
84. Bachmann, H. (1992). Case studies of structures with man-induced vibrations. *Journal of Structural Engineering*, 118(3), 631-647.
85. Ozer, E. & Feng, M.Q. (2016). Direction-sensitive smart monitoring of structures using heterogeneous smartphone sensor data and coordinate system transformation. *Smart Materials and Structures* (under review).
86. Ozer, E., & Feng, M. Q. (2016). Synthesizing spatiotemporally sparse smartphone sensor data for bridge modal identification. *Smart Materials and Structures*, 25(8), 085007.
87. Ozer, E. & Feng, M.Q. (2016). Use of mobile and participatory pedestrian data for bridge monitoring. *International Journal of Distributed Sensor Networks* (under review).
88. Fan, W., & Qiao, P. (2011). Vibration-based damage identification methods: a review and comparative study. *Structural Health Monitoring*, 10(1), 83-111.
89. Stolz, C., & Neumair, M. (2010). Structural health monitoring, in-service experience, benefit and way ahead. *Structural Health Monitoring*, 9(3), 209-217.
90. Derriso, M. M., DeSimio, M. P., McCurry, C. D., Kabban, C. M. S., & Olson, S. E. (2014). Industrial Age non-destructive evaluation to Information Age structural health monitoring. *Structural Health Monitoring*, 13(6), 591-600.
91. Liu, S. C., Tomizuka, M., & Ulsoy, G. (2006). Strategic issues in sensors and smart structures. *Structural Control and Health Monitoring*, 13(6), 946-957.

92. Gu, H., Zhao, Y., & Wang, M. L. (2005). A wireless smart PVDF sensor for structural health monitoring. *Structural Control and Health Monitoring*, 12(3-4), 329-343.
93. Spencer, B. F., Ruiz-Sandoval, M. E., & Kurata, N. (2004). Smart sensing technology: opportunities and challenges. *Structural Control and Health Monitoring*, 11(4), 349-368.
94. Jeong, M. J., & Koh, B. H. (2009). A decentralized approach to damage localization through smart wireless sensors. *Smart Structures and Systems*, 5(1), 43-54.
95. Taylor, S. G., Farinholt, K. M., Flynn, E. B., Figueiredo, E., Mascarenas, D. L., Moro, E. A., Park, G., Todd, M.D., & Farrar, C. R. (2009). A mobile-agent-based wireless sensing network for structural monitoring applications. *Measurement Science and Technology*, 20(4), 045201.
96. Chen, B., & Liu, W. (2010). Mobile agent computing paradigm for building a flexible structural health monitoring sensor network. *Computer-Aided Civil and Infrastructure Engineering*, 25(7), 504-516.
97. Zhu, D., Yi, X., Wang, Y., Lee, K. M., & Guo, J. (2010). A mobile sensing system for structural health monitoring: design and validation. *Smart Materials and Structures*, 19(5), 055011.
98. OBrien, E. J., & Keenahan, J. (2015). Drive-by damage detection in bridges using the apparent profile. *Structural Control and Health Monitoring*, 22(5), 813-825.
99. Sun, H., & Büyüköztürk, O. (2015). Identification of traffic-induced nodal excitations of truss bridges through heterogeneous data fusion. *Smart Materials and Structures*, 24(7), 075032.
100. Lienhart, W. (2013). Challenges in the analysis of inhomogeneous structural monitoring data. *Journal of Civil Structural Health Monitoring*, 3(4), 247-255.
101. Chatzi, E. N., & Smyth, A. W. (2009). The unscented Kalman filter and particle filter methods for nonlinear structural system identification with non-collocated heterogeneous sensing. *Structural Control and Health Monitoring*, 16(1), 99-123.
102. Cho, S., Giles, R. K., & Spencer, B. F. (2015). System identification of a historic swing truss bridge using a wireless sensor network employing orientation correction. *Structural Control and Health Monitoring*, 22(2), 255-272.
103. Oraczewski, T., Staszewski, W. J., & Uhl, T. (2015). Nonlinear acoustics for structural health monitoring using mobile, wireless and smartphone-based transducer platform. *Journal of Intelligent Material Systems and Structures*, 27(6), 786-796.
104. Zhao, X., Han, R., Ding, Y., Yu, Y., Guan, Q., Hu, W., & Ou, J. (2015). Portable and convenient cable force measurement using smartphone. *Journal of Civil Structural Health Monitoring*, 5(4), 481-491.
105. Han, R., Zhao, X., Yu, Y., Guan, Q., Peng, D., Li, M., & Ou, J. (2016). Emergency Communication and Quick Seismic Damage Investigation Based on Smartphone. *Advances in Materials Science and Engineering*, doi:10.1155/2016/7456182.
106. Han, R., Zhao, X., Yu, Y., Guan, Q., Hu, W., & Li, M. (2016). A Cyber-Physical System for Girder Hoisting Monitoring Based on Smartphones. *Sensors*, 16(7), 1048.

107. Zhao, X., Liu, H., Yu, Y., Zhu, Q., Hu, W., Li, M., & Ou, J. (2016). Displacement monitoring technique using a smartphone based on the laser projection-sensing method. *Sensors and Actuators A: Physical*, 246, 35-47.
108. Kos, A., Tomažič, S., & Umek, A. (2016). Evaluation of Smartphone Inertial Sensor Performance for Cross-Platform Mobile Applications. *Sensors*, 16(4), 477.
109. Jo, H., Sim, S. H., Tatkowski, A., Spencer, B. F., & Nelson, M. E. (2013). Feasibility of displacement monitoring using low-cost GPS receivers. *Structural Control and Health Monitoring*, 20(9), 1240-1254.
110. iPhone 5 Teardown. Available Online: <https://www.ifixit.com/Teardown/iPhone+5+Teardown/10525> (accessed on 4 January 2016).
111. ST Microelectronics. L3G4200D MEMS motion sensor: ultra-stable three-axis digital output gyroscope. Available Online: <http://www.st.com/web/en/resource/technical/document/datasheet/CD00265057.pdf> (accessed on 4 January 2016).
112. ST Microelectronics. LIS331DLH MEMS digital output motion sensor ultra-low-power high performance 3-axes “nano” accelerometer. Available Online: <http://www.st.com/web/en/resource/technical/document/datasheet/CD00213470.pdf> (accessed on 4 January 2016).
113. Asahi Kasei Microdevices. AK8963 3-axis electronic compass. Available Online: <http://www.akm.com/akm/en/file/datasheet/AK8963.pdf> (accessed on 4 January 2016).
114. Lovse, J. W., Teskey, W. F., Lachapelle, G., & Cannon, M. E. (1995). Dynamic deformation monitoring of tall structure using GPS technology. *Journal of Surveying Engineering*, 1(35), 35-40.
115. Nakamura, S. I. (2000). GPS measurement of wind-induced suspension bridge girder displacements. *Journal of Structural Engineering*, 126(12), 1413-1419.
116. Celebi, M. (2000). GPS in dynamic monitoring of long-period structures. *Soil Dynamics and Earthquake Engineering*, 20(5), 477-483.
117. Im, S. B., Hurlebaus, S., & Kang, Y. J. (2011). Summary review of GPS technology for structural health monitoring. *Journal of Structural Engineering*, 139(10), 1653-1664.
118. Chaffin, D. B., Andersson, G., & Martin, B. J. (1999). *Occupational biomechanics*. Wiley: New York, NY, US.
119. Bartlett, R. (2007). *Introduction to sports biomechanics: Analysing human movement patterns*. Routledge: New York, NY, US.
120. Ivancevic, V. G., & Ivancevic, T. T. (2008). *Human-like biomechanics: a unified mathematical approach to human biomechanics and humanoid robotics*. Springer: Dordrecht, Netherlands.
121. Cook, M. V. (2012). *Flight dynamics principles: a linear systems approach to aircraft stability and control*. Butterworth-Heinemann: Woburn, MA, US.
122. Abdel-Ghaffar, A. M., & Scanlan, R. H. (1985). Ambient vibration studies of Golden Gate Bridge: I. suspended structure. *Journal of Engineering Mechanics*, 111(4), 463-482.

123. Golden Gate Bridge Highway and Transportation District. Overview of Golden Gate Bridge Seismic Retrofit Construction Project. Available Online: <http://goldengatebridge.org/projects/retrofit.php> (accessed on 16 January 2016).
124. Farrar, C. R., Park, G., Allen, D. W., & Todd, M. D. (2006). Sensor network paradigms for structural health monitoring. *Structural Control and Health Monitoring*, 13(1), 210-225.
125. Lynch, J. P., & Loh, K. J. (2006). A summary review of wireless sensors and sensor networks for structural health monitoring. *Shock and Vibration Digest*, 38(2), 91-130.
126. Gao, Y., Spencer, B. F., & Ruiz-Sandoval, M. (2006). Distributed Computing Strategy for Structural Health Monitoring. *Structural Control and Health Monitoring*, 13(1), 488-507.
127. Lynch, J. P. (2007). An overview of wireless structural health monitoring for civil structures. *Philosophical Transactions of the Royal Society of London A: Mathematical, Physical and Engineering Sciences*, 365(1851), 345-372.
128. Aygün, B., & Cagri Gungor, V. (2011). Wireless sensor networks for structure health monitoring: recent advances and future research directions. *Sensor Review*, 31(3), 261-276.
129. Prasad, P. (2015). Recent trend in wireless sensor network and its applications: a survey. *Sensor Review*, 35(2), 229-236.
130. Kling, R., Adler, R., Huang, J., Hummel, V., & Nachman, L. (2005). Intel Mote-based sensor networks. *Structural Control and Health Monitoring*, 12(3-4), 469-479.
131. Farhey, D. N. (2006). Integrated virtual instrumentation and wireless monitoring for infrastructure diagnostics. *Structural Health Monitoring*, 5(1), 29-43.
132. Sazonov, E., Krishnamurthy, V., & Schilling, R. (2010). Wireless intelligent sensor and actuator network-a scalable platform for time-synchronous applications of structural health monitoring. *Structural Health Monitoring*, 9(5), 465-476.
133. Salarian, H., Chin, K. W., & Naghdy, F. (2012). Coordination in wireless sensor-actuator networks: A survey. *Journal of Parallel and Distributed Computing*, 72(7), 856-867.
134. Krishnamurthy, V., Fowler, K., & Sazonov, E. (2008). The effect of time synchronization of wireless sensors on the modal analysis of structures. *Smart Materials and Structures*, 17(5), 055018.
135. Brincker, R., Zhang, L., & Andersen, P. (2001). Modal identification of output-only systems using frequency domain decomposition. *Smart Materials and Structures*, 10(3), 441.
136. Peeters, B., & De Roeck, G. (1999). Reference-based stochastic subspace identification for output-only modal analysis. *Mechanical Systems and Signal Processing*, 13(6), 855-878.
137. Vicario, F., Phan, M. Q., Betti, R., & Longman, R. W. (2015). Output-only observer/Kalman filter identification (O3KID). *Structural Control and Health Monitoring*, 22(5), 847-872.
138. Moore, E. Z., Murphy, K. D., & Nichols, J. M. (2013). Optimized sensor placement for damage parameter estimation: Experimental results for a cracked plate. *Structural Health Monitoring*, 12(3), 197-206.

139. He, L., Lian, J., Ma, B., & Wang, H. (2014). Optimal multi-axial sensor placement for modal identification of large structures. *Structural Control and Health Monitoring*, 21(1), 61-79.
140. Cha, Y. J., Raich, A., Barroso, L., & Agrawal, A. (2013). Optimal placement of active control devices and sensors in frame structures using multi-objective genetic algorithms. *Structural Control and Health Monitoring*, 20(1), 16-44.
141. Cheng, M. H., & Heaton, T. H. (2015). Simulating building motions using ratios of the building's natural frequencies and a Timoshenko beam model. *Earthquake Spectra*, 31(1), 403-420.
142. Cheng, M. H., Kohler, M. D., & Heaton, T. H. (2015). Prediction of wave propagation in buildings using data from a single seismometer. *Bulletin of the Seismological Society of America*, 105(1), 107-119.
143. Allan, A. (2012). *Geolocation in IOS*. O'Reilly Media, Inc.: Sebastopol, CA, US.
144. Fazal, S. (2008). *GIS basics*. New Age International: New Delhi, India.
145. Drobnik, O. (2015). *Barcodes with iOS: bringing together the digital and physical worlds*. Manning Publ.: Shelter Island, NY, US.
146. Lathi, B. (1998). *Signal processing and linear systems*. Berkeley Cambridge Press: Carmichael, CA, US.
147. McMahan, D. (2007). *Signals and systems demystified*. McGraw-Hill: New York, NY, USA.
148. Gröchenig, K. (2013). *Foundations of time-frequency analysis*. Springer Science & Business Media: New York, NY, US.
149. Ewins, D. J. (2000). *Modal testing: theory, practice and application*. Research Studies Press, Ltd.: Baldock, Hertfordshire, England.
150. Jarrah, M., Wasseem, W., Othman, M., & Gdeisat, M. (1997). Human body model response to mechanical impulse. *Medical engineering & physics*, 19(4), 308-316.
151. Barauskas, R., & Krušinskienė, R. (2007). On parameters identification of computational models of vibrations during quiet standing of humans. *Journal of Sound and Vibration*, 308(3), 612-624.
152. Hof, A. L. (2007). The equations of motion for a standing human reveal three mechanisms for balance. *Journal of biomechanics*, 40(2), 451-457.
153. Winter, D. A. (1995). Human balance and posture control during standing and walking. *Gait & posture*, 3(4), 193-214.
154. Menegaldo, L. L., de Toledo Fleury, A., & Weber, H. I. (2003). Biomechanical modeling and optimal control of human posture. *Journal of biomechanics*, 36(11), 1701-1712.
155. Fritz, M. (2000). Simulating the response of a standing operator to vibration stress by means of a biomechanical model. *Journal of biomechanics*, 33(7), 795-802.
156. Kiiski, J., Heinonen, A., Järvinen, T. L., Kannus, P., & Sievänen, H. (2008). Transmission of vertical whole body vibration to the human body. *Journal of bone and mineral research*, 23(8), 1318-1325.

157. Matsumoto, Y., & Griffin, M. J. (1998). Dynamic response of the standing human body exposed to vertical vibration: influence of posture and vibration magnitude. *Journal of Sound and Vibration*, 212(1), 85-107.
158. Matsumoto, Y., & Griffin, M. J. (2001). Modelling the dynamic mechanisms associated with the principal resonance of the seated human body. *Clinical Biomechanics*, 16, S31-S44.
159. Kitazaki, S., & Griffin, M. J. (1997). Resonance behaviour of the seated human body and effects of posture. *Journal of biomechanics*, 31(2), 143-149.
160. Mansfield, N. J., & Griffin, M. J. (2002). Effects of posture and vibration magnitude on apparent mass and pelvis rotation during exposure to whole-body vertical vibration. *Journal of Sound and Vibration*, 253(1), 93-107.
161. Kitazaki, S., & Griffin, M. J. (1997). A modal analysis of whole-body vertical vibration, using a finite element model of the human body. *Journal of Sound and Vibration*, 200(1), 83-103.
162. Rützel, S., Hinz, B., & Wölfel, H. P. (2006). Modal description—A better way of characterizing human vibration behavior. *Journal of Sound and Vibration*, 298(3), 810-823.
163. Wei, L., & Griffin, M. J. (1998). Mathematical models for the apparent mass of the seated human body exposed to vertical vibration. *Journal of Sound and Vibration*, 212(5), 855-874.
164. Dieckmann, D. (1958). A study of the influence of vibration on man. *Ergonomics*, 1(4), 347-355.
165. Matsumoto, Y., & Griffin, M. J. (2000). Comparison of biodynamic responses in standing and seated human bodies. *Journal of Sound and Vibration*, 238(4), 691-704.
166. Griffin, M. J. (2001). The validation of biodynamic models. *Clinical Biomechanics*, 16, S81-S92.
167. Nakamura, S. I., & Kawasaki, T. (2006). Lateral vibration of footbridges by synchronous walking. *Journal of Constructional steel research*, 62(11), 1148-1160.
168. Živanović, S., Pavic, A., & Reynolds, P. (2005). Vibration serviceability of footbridges under human-induced excitation: a literature review. *Journal of sound and vibration*, 279(1), 1-74.
169. Zuo, D., Hua, J., & Van Landuyt, D. (2012). A model of pedestrian-induced bridge vibration based on full-scale measurement. *Engineering Structures*, 45, 117-126.
170. Racic, V., Pavic, A., & Brownjohn, J. M. W. (2009). Experimental identification and analytical modelling of human walking forces: Literature review. *Journal of Sound and Vibration*, 326(1), 1-49.
171. Ingólfsson, E. T., Georgakis, C. T., & Jönsson, J. (2012). Pedestrian-induced lateral vibrations of footbridges: a literature review. *Engineering Structures*, 45, 21-52.
172. Reiterer, M., & Ziegler, F. (2006). Control of pedestrian-induced vibrations of long-span bridges. *Structural Control and Health Monitoring*, 13(6), 1003-1027.
173. Brownjohn, J. M. (2001). Energy dissipation from vibrating floor slabs due to human-structure interaction. *Shock and Vibration*, 8(6), 315-323.

174. Ellis, B., & Ji, T. (1997). Human-structure interaction in vertical vibrations. *Proceedings of the Institution of Civil Engineers. Structures and buildings*, 122(1), 1-9.
175. Mayagoitia, R. E., Nene, A. V., & Veltink, P. H. (2002). Accelerometer and rate gyroscope measurement of kinematics: an inexpensive alternative to optical motion analysis systems. *Journal of biomechanics*, 35(4), 537-542.
176. Curone, D., Bertolotti, G. M., Cristiani, A., Secco, E. L., & Magenes, G. (2010). A real-time and self-calibrating algorithm based on triaxial accelerometer signals for the detection of human posture and activity. *IEEE transactions on information technology in biomedicine*, 14(4), 1098-1105.
177. Wong, W. Y., Wong, M. S., & Lo, K. H. (2007). Clinical applications of sensors for human posture and movement analysis: a review. *Prosthetics and orthotics international*, 31(1), 62-75.
178. Qassem, W., Othman, M. O., & Abdul-Majeed, S. (1994). The effects of vertical and horizontal vibrations on the human body. *Medical engineering & physics*, 16(2), 151-161.
179. Liu, W., & Nigg, B. M. (2000). A mechanical model to determine the influence of masses and mass distribution on the impact force during running. *Journal of biomechanics*, 33(2), 219-224.
180. Boileau, P. É., Rakheja, S., & Wu, X. (2002). A body mass dependent mechanical impedance model for applications in vibration seat testing. *Journal of sound and vibration*, 253(1), 243-264.
181. Coermann, R. R. (1962). The mechanical impedance of the human body in sitting and standing position at low frequencies. *Human Factors: The Journal of the Human Factors and Ergonomics Society*, 4(5), 227-253.
182. Bachmann, H., & Ammann, W. (1987). *Vibrations in structures: induced by man and machines*. International Association for Bridge and Structural Engineering: Zürich, Switzerland.
183. Inman, D.J. (2000) *Engineering Vibrations*; Prentice Hall: Upper Saddle River, NJ, USA.
184. Ogata, K. (2010). *Modern control engineering*; Prentice Hall: Upper Saddle River, NJ, USA.
185. Ozer, E. & Feng, M.Q. (2016). Structural reliability estimation with participatory sensing and mobile cyber-physical SHM systems. *Structural Safety* (under review).
186. ASCE (2014), *Seismic Evaluation and Retrofit of Existing Buildings (ASCE/SEI 41-13)*. American Society of Civil Engineers: Reston, Virginia, US.
187. AASHTO (2015), *LRFD Bridge Design Specifications*, American Association of State Highway and Transportation Officials: Washington, DC, US.
188. Brownjohn, J. M. (2007). Structural health monitoring of civil infrastructure. *Philosophical Transactions of the Royal Society of London A: Mathematical, Physical and Engineering Sciences*, 365(1851), 589-622.
189. Farrar, C. R., & Worden, K. (2007). An introduction to structural health monitoring. *Philosophical Transactions of the Royal Society of London A: Mathematical, Physical and Engineering Sciences*, 365(1851), 303-315.

190. Wahbeh, A. M., Caffrey, J. P., & Masri, S. F. (2003). A vision-based approach for the direct measurement of displacements in vibrating systems. *Smart Materials and Structures*, 12(5), 785.
191. Lee, J. J., & Shinozuka, M. (2006). A vision-based system for remote sensing of bridge displacement. *Ndt & E International*, 39(5), 425-431.
192. Feng, D., Feng, M. Q., Ozer, E., & Fukuda, Y. (2015). A vision-based sensor for noncontact structural displacement measurement. *Sensors*, 15(7), 16557-16575.
193. Lasi, H., Fettke, P., Kemper, H. G., Feld, T., & Hoffmann, M. (2014). Industry 4.0. *Business & Information Systems Engineering*, 6(4), 239.
194. Lee, J., Bagheri, B., & Kao, H. A. (2015). A cyber-physical systems architecture for industry 4.0-based manufacturing systems. *Manufacturing Letters*, 3, 18-23.
195. Lee, E. A. (2015). The past, present and future of cyber-physical systems: A focus on models. *Sensors*, 15(3), 4837-4869.
196. Schirner, G., Erdogmus, D., Chowdhury, K., & Padir, T. (2013). The future of human-in-the-loop cyber-physical systems. *Computer*, (1), 36-45.
197. Wu, F. J., Kao, Y. F., & Tseng, Y. C. (2011). From wireless sensor networks towards cyber physical systems. *Pervasive and Mobile Computing*, 7(4), 397-413.
198. Kim, K. D., & Kumar, P. R. (2012). Cyber-physical systems: A perspective at the centennial. *Proceedings of the IEEE*, 100(Special Centennial Issue), 1287-1308.
199. Hu, X., Chu, T., Chan, H., & Leung, V. (2013). Vita: A crowdsensing-oriented mobile cyber-physical system. *Emerging Topics in Computing, IEEE Transactions on*, 1(1), 148-165.
200. Atzori, L., Iera, A., & Morabito, G. (2010). The internet of things: A survey. *Computer networks*, 54(15), 2787-2805.
201. Gubbi, J., Buyya, R., Marusic, S., & Palaniswami, M. (2013). Internet of Things (IoT): A vision, architectural elements, and future directions. *Future Generation Computer Systems*, 29(7), 1645-1660.
202. Gershenfeld, N., Krikorian, R., & Cohen, D. (2004). The Internet of things. *Scientific American*, 291(4), 76.
203. Miorandi, D., Sicari, S., De Pellegrini, F., & Chlamtac, I. (2012). Internet of things: Vision, applications and research challenges. *Ad Hoc Networks*, 10(7), 1497-1516.
204. McKenna, F. (2011). OpenSees: a framework for earthquake engineering simulation. *Computing in Science & Engineering*, 13(4), 58-66.
205. Suh, S. C., Tanik, U. J., Carbone, J. N., & Eroglu, A. (2014). *Applied Cyber-Physical Systems*. Springer: New York, NY, US.
206. Liu, C. H., & Zhang, Y. (2015). *Cyber Physical Systems: Architectures, Protocols and Applications*. CRC Press: Boca Raton, FL, US.
207. Hu, F. (2013). *Cyber-Physical Systems: Integrated Computing and Engineering Design*. CRC Press: Boca Raton, FL, US.

208. Siddesh, G. M., Deka, G., Srinivasa, K. G., & Patnaik, L. M. (2016). *Cyber-Physical Systems: A Computational Perspective*. CRC Press: Boca Raton, FL, US.
209. Ghanem, R., & Shinozuka, M. (1995). Structural-system identification. I: Theory. *Journal of Engineering Mechanics*, 121(2), 255-264.
210. Shinozuka, M., & Ghanem, R. (1995). Structural system identification. II: Experimental verification. *Journal of Engineering Mechanics*, 121(2), 265-273.
211. Chiou, B., Darragh, R., Gregor, N., & Silva, W. (2008). NGA project strong-motion database. *Earthquake Spectra*, 24(1), 23-44.
212. Kircher, C. A., Reitherman, R. K., Whitman, R. V., & Arnold, C. (1997). Estimation of earthquake losses to buildings. *Earthquake spectra*, 13(4), 703-720.
213. Nielson, B. G., & DesRoches, R. (2007). Analytical seismic fragility curves for typical bridges in the central and southeastern United States. *Earthquake Spectra*, 23(3), 615-633.
214. Kramer, S. L. (1996). *Geotechnical Earthquake Engineering*. Prentice Hall: Upper Saddle River, NJ, US.
215. Roeder, C. W., Barth, K. E., & Bergman, A. (2004). Effect of live-load deflections on steel bridge performance. *Journal of Bridge Engineering*, 9(3), 259-267.
216. Nishikawa, K., Murakoshi, J., & Matsuki, T. (1998). Study on the fatigue of steel highway bridges in Japan. *Construction and building materials*, 12(2), 133-141.
217. Billing, J. R. (1984). Dynamic loading and testing of bridges in Ontario. *Canadian Journal of Civil Engineering*, 11(4), 833-843.